Can tidal interactions produce MGC1?

Eric Andersson

Lund Observatory
Lund University

2018-EXA131

Degree project of 60 higher education credits (for a degree of Master)
May 2018

Supervisor: Melvyn B. Davies

Lund Observatory
Box 43
SE-221 00 Lund
Sweden

Abstract

The globular cluster population of large spiral galaxies can be divided into two populations: one population which formed *in-situ* and one which has been assembled through capture of clusters that have been tidally stripped away from other galaxies during close encounters or mergers. In this work, I focus on the globular cluster MGC1, which is orbiting the M31 galaxy. MGC1 is an extremely isolated cluster, located 200 kpc from the M31 centre. Thus, I propose the idea that this cluster was one of those captured from another galaxy. I investigate encounters between dwarf galaxies with masses ranging from $10^7\,M_\odot$ to $10^{10}\,M_\odot$ and the M31 galaxy, using numerical simulations, in which I focus on globular clusters that are tidally stripped away from the dwarf and left on wide orbits in the M31 galaxy. Motivated by the absence of observed tidal features around MGC1, I constrain my encounters such that, afterwards, the dwarf should remain intact and no visible damage should be caused to M31. I find this to be a viable scenario for the origin of MGC1 if M31 has had approximately 20 encounters with dwarf galaxies that do not merge with M31, but rather leave the system post-encounter. Although my results provide a means to produce MGC1, the encounters I simulate do not reproduce the entire observed population of clusters in M31, especially lacking in clusters located closer in. I therefore suggest that these 20 encounters are only a subset of all the encounters that M31 has had in the past.

Populärvetenskaplig beskrivning

Är det möjligt att galaxer kan utbyta enorma samlingar stjärnor utan att vi märker det?

I detta arbete så undersöker jag huruvida dvärg galaxer kan lämna över globulära stjärnhopar till större spiralgalaxer då de kommer mycket nära, genom så kallade tidvatten-krafter. Dessa globulära stjärnhopar består utav hundra tusentals stjärnor vilka är bundna till varandra genom gravitation. Var de kommer ifrån, samt vilken effekt de har på sin omgivning, är än idag inte helt förstått. Vi vet att dessa astrofysiska objekt är mycket gamla och att de förmodligen skapades i gas-moln med mycket hög densitet i ett tidigt stadie av Universum. Trotts att dessa stjärnhopar är relativt stora objekt så hittas de inte enbart i större galaxer utan även i små, så kallade dvärg-galaxer.

Dvärg galaxer är betydligt mindre massiva jämfört med galaxer så som till exempel vår egen Vintergatan. Däremot, så finns det många utav dem. I vårt galaktiska närområde, den Lokala Gruppen, så finns omkring femtio dvärg-galaxer som samverkar med tre något större galaxer Vintergatan, Andomeda och Triangulum galaxen. Observationer visar på att dessa dvärg-galaxer ofta kommer mycket nära de större galaxerna, och i många fall håller de till och med på att bli uppslukade utav dem. Moderna simuleringar visar dessutom att dessa sammanslagningar är en viktig del i uppbyggnaden utav större galaxer. Det finns alltså tydliga bevis på att interaktioner mellan dvärg-galaxer och större spiralgalaxer sker med jämna mellanrum.

Under dessa möten så påverkas dvärggalaxens form genom så kallade tidvattenkrafter. Tidvatten-krafter uppstår på grund utav att gravitation påverkar olika mycket beroende på avstånden mellan de berörda objekten. På samma sätt som vår egen måne flyttar vattenmassor på jorden till den sida av jorden som ligger lite närmare månen, så kan en stor galax sträcka ut formen på de mindre galaxerna om de kommer tillräckligt nära varandra. Är dessa krafter tillräckligt stora så kan delar utav dvärg-galaxen dras från den och hamna i egna banor kring den större galaxen. Vanligvis dras delar utav dvärg-galaxen bort och då bildas stora band utav stjärnor som sträcker sig kring den bana dvärg-galaxen rör sig i. Om stjärnorna är starkt bundna till varandra genom gravitation, så som i globulära stjärnhopar, så kan de överleva interaktionen och bli en del utav spiralgalaxen.

De stjärnhopar som doneras från dvärggalaxen kommer dock skilja sig från den population utav stjärnhopar som formats i spiralgalaxen. Till skillnad från den inhemska populationen så förväntas de till exempel ha mycket vidare banor. Om detta är en gemensam egenskap för alla donerade stjärnhopar så möjliggör detta en metod för att skilja dem från de formats i galaxen. Denna idéen undersöker jag i detta arbete.

Ett objekt som är extra intressant för denna frågeställning är den globulära stjärnhopen MGC1, som tillhör spiralgalaxen Andromeda. Andromeda är den närmsta stora galaxen till Vintergatan och ligger omkring 2.5 miljoner ljusår bort. Den speciella med MGC1 är att den ligger ca 0.65 miljoner ljusår från Andromedas centrum. För att sätta detta i perspektiv så är detta betydligt längre ut än de flesta andra stjärnor i Andromeda, som lig-

ger i en disk kring galaxens centrum med en diameter på ungefär 130 tusen ljusår. Dessa stora avstånd mellan MGC1 och Andromedas centrum gör det mycket troligt att MGC1 kommer ifrån en annan galax som vid något tillfälle donerade MGC1 till Andromeda genom de tidigare nämnda tidvatten-krafterna.

Detta är dock inte uppenbart för MGC1. Mycket noggranna observationer utav MGC1 visar inga som helst tecken på interaktion mellan två galaxer. Tecken som vi associerar till dessa interaktioner, så som ett band av stjärnor, är till synes helt frånvarande. Eftersom detta är ganska besynnerligt så undersöker jag i detta arbete interaktioner mellan dvärg-galaxer och Andromeda som inte lämnar sådana spår och huruvida dessa interaktioner lämnar efter sig stjärnhopar. Jag fokuserar framförallt på stjärnhopar som får omloppsbanor kring Andromeda vilka påminner om den omloppsbana som MGC1 har.

Contents

List of Figures

List of Tables

Chapter 1

Introduction

Globular clusters are astrophysical objects that consist of hundreds of thousands of stars which are gravitationally bound to each other (see Renaud, 2018, for a recent review). These clusters are some of the oldest objects that are known, with ages that are comparable to the age of the Universe. How they are formed is not yet fully understood. Nevertheless, we can assume that they form in gaseous environments, where stars are born. Therefore, for large spiral galaxies, they ought to be constrained to environments where gaseous environments are present, namely the disc of the galaxy.

Since globular clusters are very old, they can be stirred up in dynamical interactions, thus be kicked out of the disc and placed in the halo of the galaxy. This is a reasonable scenario for many of the globular clusters that are observed in the halo, because most of them are still somewhat centrally concentrated. However, for globular clusters further out this mechanism becomes problematic, because the kicks required to place them at these distances would have to be very precise, as to not kick them out of the galaxies entirely.

A mechanism that could explain the existence of these, most remote globular clusters, is to let them be tidally stripped away from other galaxies during encounters, and then captured on wide orbits. This has been suggested as a mechanism that contributes to the overall globular cluster population of various galaxies, see e.g., Searle & Zinn (1978); Abadi et al. (2006). More compelling evidence that this is a viable mechanism, is the Sagittarius dwarf which is believed to have donated multiple globular clusters to the Milky Way in past billion years, see Layden & Sarajedini (2000); Siegel et al. (2007).

One of the most extreme examples of a globular cluster on a wide orbit is the globular cluster MGC1, found in the Andromeda galaxy (hereafter M31). This cluster is currently in a position 200 kpc away from the M31 centre (Mackey et al., 2010a). Furthermore, MGC1 is observed in a location where there is no observable structure, such as tidal streams or dwarf galaxies. In fact, MGC1 is one of the most isolated globular clusters that is known in the Local Group. This particular cluster is the main focus of this project.

MGC1 was first discovered by Martin et al. (2006), who determined its position on the sky given by $\alpha = 0^{\mathrm{h}}50^{\mathrm{m}}42.5^{\mathrm{s}}$ and $\delta = +32^{\circ}54'59.6''$. This gives the MGC1 a projected

distance of 117 kpc from the M31 centre. Mackey et al. (2010a) revisited the MGC1 cluster with deep imaging using the Gemini/GMOS Observatory and determined a distance modulus for the cluster of $\mu = 23.95 \pm 0.06$. Combining the distance modulus and the projected distance from M31 gives MGC1 a radial distance from the M31 galaxy of 200 ± 20 kpc. This makes the MGC1 cluster the most remote globular cluster known in the Local group by some considerable margin. Compared to the second-most distant observed globular cluster in M31, at a galactocentric distance of ≈ 158 kpc (di Tullio Zinn & Zinn, 2013), and the most distant observed globular cluster in the Milky Way, at a Galactocentric distance of ≈ 145 kpc (Laevens et al., 2014), it lies some 50 kpc further out in the halo.

Two groups have, with independent measurements, estimated the radial velocity of the MGC1 cluster. Galleti et al. (2007) found a radial velocity for the cluster of $-312 \pm 17\,\mathrm{km\,s^{-1}}$ using a low resolution spectrum from the Extended Source Catalogue of 2MASS, while Alves-Brito et al. (2009) found a radial velocity of $-354.7 \pm 2.2\,\mathrm{km\,s^{-1}}$ for MGC1 using a high resolution spectrum from the Keck telescope. Although these radial velocities are a few sigma away from each other, they both coincide with the systematic velocity of the M31 galaxy ($\sim -300\,\mathrm{km\,s^{-1}}$, see, e.g. van der Marel et al. (2012), translated into heliocentric velocity). The radial velocity relative to M31 ($\approx -50\,\mathrm{km\,s^{-1}}$) is well within the escape velocity of the M31 galaxy, see e.g. Chapman et al. (2007), which implies that MGC1 is very likely a genuine member of the M31 galaxy.

In order to determine the origin of the MGC1, it is worthwhile to investigate its metallicity and age. Mackey et al. (2010a) performed a photometric analysis of the clusters from which they obtained (g, r) and (g, i) colour-magnitude diagrams (CMD) for its stellar population. From these results they determined the existence of a steep red-giant-branch, a well populated horizontal branch extending to the blue and the presence of RR Lyrae stars. They concluded that this is indicative of a very old, metal-poor stellar population, providing a cluster age of more than 10 Gyr.

Martin et al. (2006) determined the a metallicity of the cluster at [Fe/H] ≈ -1.3, by fitting isochrones to the CMD that they obtained while observing the MGC1. Using high resolution spectroscopy, Alves-Brito et al. (2009) found a similar metallicity of the MGC1 at [Fe/H] $= -1.37 \pm 0.15$. Controversially, Mackey et al. (2010a) derived a significantly lower metal abundance for the cluster, at a reported value of [Fe/H] $= -2.3$.

Although the mentioned authors disagree regarding its metal abundance, there does not seem to be any disagreement regarding the old age of the cluster. The old age of the MGC1 cluster is not something suprising. In fact, most globular clusters are believed to have formed early in the Universe, around redshifts of $z \approx 3 - 6$ or ~ 12 Gyr ago. This has been observed both in the Milky Way cluster population (see, e.g., Forbes et al., 2015; Leaman et al., 2013), and in the M31 cluster population (see, e.g., Strader et al., 2009).

With regards to the old age of globular clusters, they are believed to be an integrated part in the evolution of galaxies, see e.g.,Brodie & Strader (2006); Renaud et al. (2017) or Renaud (2018) for a review. In the successful Λ-cold-dark-matter cosmological model galaxies are build up through a hierarchical assembly of smaller galaxies (see, e.g, Abadi

et al., 2006; Bullock & Johnston, 2005; Font et al., 2006a). The merger events will bring with them globular clusters that together with those that form *in-situ* build up the total population of globular clusters.

There are other indications of a twofold build-up of the globular cluster population. In fact, the globular cluster population of large spiral galaxies show a colour bimodality: for the Milky Way (see Harris, 1996) there is a population of blue clusters, with a metallicity peak at [Fe/H] ≈ -1.5, have an extended distribution in space, while another population of red clusters, with a metallicity peak at [Fe/H] ≈ -0.5, are more centrally concentrated (see Brodie & Strader, 2006, for a review). It has been suggested that this bimodality could arise if the blue population has an accretion origin, while the red population has formed *in-situ*, see, e.g., Côté et al. (1998); Tonini (2013); Renaud et al. (2017). It is worth to note that MGC1 has a metallicity which is consistent with the blue, accreted populations.

The M31 globular cluster population (which is of particular interest for this project) have been carefully studied by several works. The most ambitious project to study the extended structure of M31 to date is the Pan-Andromeda-Archaeological-Survey (PAndAS), (see, e.g., Martin et al., 2006; Ibata et al., 2007; McConnachie et al., 2008). This survey focused on exploring the halo of M31 out to a projected radius of $\sim 150\,\mathrm{kpc}$ and the halo of its neighbouring galaxy, M33, out to a projected radius of $\sim 50\,\mathrm{kpc}$. Mackey et al. (2010b) used the a sample of outer globular clusters from this survey and compared their spatial correlation to dwarf galaxies and tidal features, such as stellar streams. Using a Monte-Carlo approach they found a significant spatial association between these objects. The likelihood they estimated for this association to be due to chance alignment was below 1%. This is a key result in favour of the idea that globular clusters are donated to large galaxies, by tidally stripping them away from smaller galaxies and capturing them.

However, the aforementioned mechanism is also problematic for the MGC1, due to its extreme isolation. Resolved images of MGC1 does not appear to include any features associated to tidal interaction. Moreover, the structure of MGC1 is extremely extended, with a luminous radius that could extend as far as 900 pc (Mackey et al., 2010a). This is a significant fraction of the clusters tidal radius, thus one expects that this cluster has spent quite some time in isolation.

This brings me to the main hypothesis of this project, which can be posed as the following question:

Is it possible for a globular cluster to be tidally stripped away from a dwarf galaxy during an encounter with M31 that does not tidally strip the dwarf galaxy or cause visible damage to the M31 disc, after which it is captured on a wide enough orbit for us to observe it 200 kpc away from M31, thus appearing as MGC1?

To test this hypothesis I developed a program that simulates encounters between dwarf galaxies and M31. By integrating trajectories of globular clusters, modelled as test-particles, in the potential fields of the involved galaxies, I can determine whether clusters initially bound to the dwarf can be moved to M31. The M31 potential is given by a static, axisymmetric, three component model, while the dwarf galaxy uses a spherically symmetric potential with a centre defined by the position of the dwarf galaxy. The dwarf galaxy position is determined by tracking its trajectory in the M31 potential through numerical integration. In order to determine whether the encounter causes visible damage to either the dwarf galaxy or M31, I used an analytical description of the tidal radius to check the extent of tidal strain.

Report structure

The report is structured in the following way:

In Chapter 2, I give an overview of the models that were used for this project. Firstly, in Section 2.1 and 2.2, I describe the models used for the potential field, with a focus on models from Bekki et al. (2001) and Geehan et al. (2006). I then describe how trajectories evolve in these models in Section 2.3. Lastly, in Section 2.4, I re-derive an analytic expression of the tidal radius based on work done by Read et al. (2006).

In Chapter 3, I go through a simulation of a single encounter in which 1000 different globular cluster trajectories were tested. Here I describe how I estimate the likelihood of producing a cluster similar to MGC1. Moreover, I investigate what properties one might expect for such a cluster before the encounter.

In Chapter 4, I expand the investigation and look at various dwarf galaxy encounters to determine how the likelihood of producing an MGC1-like cluster depend on the trajectory of the dwarf galaxy. This analysis was restricted to trajectories where the dwarf galaxy comes in from a distance of at least 500 kpc, thus leaving the M31 system after the encounter.

In Chapter 5, I discuss and explore the scientific implications and predictions that the results of my simulations provide. To guide the reader through this chapter I included boxes that summarize the major findings.

Finally, in Chapter 6, I summarise the entire work and point out both the major results as well as conclusions that I make based on my investigation. This summary is somewhat detailed, and repeats much of the work in the previous chapters. This is intentional and aimed toward reader that does not want to read the entire work. Much of this chapter can be skipped by readers who read the entire thesis.

Chapter 2

Motions in galactic potentials

In this section I describe the models that were used to estimate the gravitational potential fields of the galaxies that are included in my simulations. The simulations include two galaxies, the M31 galaxy and a smaller galaxy (referred to as the dwarf galaxy). The M31 galaxy is a large spiral galaxy located $\sim 785\,\mathrm{kpc}$ from the Sun (McConnachie et al., 2005), which makes it the closest neighboring spiral galaxy of the Milky Way. The dwarf galaxy, which is assumed to be the original host of the MGC1 cluster in this thesis, is modeled with the assumption that its mass is distributed spherically symmetrically. This implies that the potential field will also be spherically symmetric. In contrast to the M31 galaxy, we do not have any evidence of what the properties for this galaxy are. The only traces that we have of this galaxy is the MGC1 cluster, which was discovered by Martin et al. (2006) and later investigated in detail by Mackey et al. (2010a). Since the properties of the dwarf galaxy are unknown it is essential that the model can easily be modified so that various dwarves can be tested and compared.

2.1 The M31 galaxy

The gravitational potential, $\Phi(r)$, of a galaxy is directly proportional to its mass distribution according to

$$\Phi(r) = \frac{GM(r)}{r^2}, \tag{2.1}$$

where r is the radial position in the potential field, G is the Newtonian gravitational constant and $M(r)$ is the mass distribution. This expression is straightforward to implement numerically if the mass distribution is spherically symmetric, however, this is seldom the case. The M31 galaxy is known to have a morphological structure of a disc with multiple spiral arms, see e.g. Simien et al. (1978) (and references therein). It is also known to have an extended halo consisting mainly of dark matter. The extended halo can be considered to be spherically symmetric with a density that decreases with increasing radius.

The exact mass-profile of M31 has been debated and it is not yet known which of M31 and the Milky Way is the most massive galaxy in the Local Group. Braun (1991)

investigated the kinematic structure of the inner parts of M31 through observations of emission from neutral hydrogen gas. The authors found a radial velocity profile for the M31 which corresponded to a mass of $2.0 \pm 0.1 \times 10^{11}\, M_{\odot}$ enclosed within 28 kpc. However, the aim of this project is to investigate interactions between the M31 and smaller galaxies where the separation can be large, thus we need a model where we can probe the outer potential field. In previous work on estimation of the mass of the Milky Way it has been shown that outer globular clusters and satellite galaxies are good tracers of the Galactic mass (see, e.g. Kochanek, 1996; Little & Tremaine, 1987; Wilkinson & Evans, 1999). Similar estimates have been made for the M31 galaxy, as well (see, e.g. Evans et al., 2000; Watkins et al., 2010). By using observed radial velocities of discrete sources in M31, such as satellite galaxies, globular clusters and halo stars, Watkins et al. (2010) found the mass enclosed within 300 kpc of M31 to be $M_{300,\mathrm{M31}} = 1.4 \pm 0.4 \times 10^{12}\, M_{\odot}$. It should be noted that for this mass estimate, Watkins et al. (2010) assumed that the distribution of these objects were isotropic.

In this work I consider a potential field for M31 which is divided into three different parts, namely a bulge, a disc and an extended halo. In such a potential we can solve the acceleration of a body with only three computations for each considered dimension. This is a simplification which relieves the computational demand that is needed when I integrate the trajectories of objects. Similar methods have been used in previous studies of the M31, see e.g., Bekki et al. (2001); Font et al. (2006b); Geehan et al. (2006). In the following sections I describe how each of these aforementioned parts are modelled.

Bulge

The Hernquist potential

The central region of most spiral galaxies hosts a large number of tightly packed stars, which are distributed in such a way that they create a spherical over-density, see e.g., Binney & Tremaine (1987). This region is referred to as the bulge and in our model it is one of the three potential components. Hernquist (1990) found a simple analytic formula that well describe the potential of this component as function of radius, r:

$$\Phi_{\mathrm{b}}(r) = -\frac{GM_b}{r_b + r}, \tag{2.2}$$

where M_b is the total mass of the region and r_b is a scale length which smooths the potential, thus preventing a singularity at the center. The potential is physical in the sense that as $r \to \infty$, the $\Phi_b \to 0$. The parametrization used for the bulge potential is given in Table 2.1.

The Hernquist potential is derived from a density distribution

$$\rho_b = \frac{M_b}{2\pi}\frac{r_b}{r}\frac{1}{(r + r_b)^3},$$

which is an approximation made to fit the de Vaucouleurs profile (de Vaucouleurs, 1948). The de Vaucouleurs profile is an empirically estimated relation between the observed luminosity distribution and the projected radius, which for bulges scales as $L(r) \propto r^{1/4}$.

Disc

The Miyamoto-Nagai potential

The visible matter in the M31 galaxy has a very clear disc-like structure. This disc component arises due to conservation of angular momentum in the material that builds up the galaxy during its formation. The model for this potential uses a cylindrically symmetric coordinate system, with R being the radial coordinate in the plane of the disc and z being the vertical coordinate perpendicular to this plane. Miyamoto & Nagai (1975) showed that this cylindrically symmetric potential, free of singularities for all R and z, can be written accordingly,

$$\Phi_{\mathrm{d}}(R,z) = -\frac{GM_d}{\sqrt{R^2 + (a + \sqrt{z^2 + b^2})^2}}, \tag{2.3}$$

where M_d is the mass of the disc component and a, b are scaling parameters. The ratio b/a can be interpreted as the flatness of the disc where a b/a of unity gives a spherically symmetric potential and as $b/a \to 0$ the disc becomes increasingly flattened. The density of the Miyamoto-Nagai disc can be solved from the Poisson equation giving

$$\rho_d(R,z) = \frac{b^2 M_d}{4\pi} \frac{aR^2 + \left(a + 3\sqrt{z^2 + b^2}\right)\left(a + \sqrt{z^2 + b^2}\right)^2}{\left(R^2 + \left(a + \sqrt{z^2 + b^2}\right)^2\right)^{5/2} (z^2 + b^2)^{3/2}}, \tag{2.4}$$

which gives a non-negative density in all space. In order to fit the Miyamoto-Nagai potential to the M31 disc I use parameters originally estimated by Bekki et al. (2001), which are listed in Table 2.1

The exponential disc

It was observed by Walterbos & Kennicutt (1987) that the mass distribution of the M31 disc can be described with an exponentially decreasing surface density. The potential field for such a potential was derived by Binney & Tremaine (1987) and the expression they derived is given by

$$\Phi_{\mathrm{d,exp}}(R,z) = -2\pi G \Sigma_0 R_d^2 \int_0^\infty \frac{J_0(kR) e^{-k|z|}}{(1 + (kR_d)^2)^{3/2}} \mathrm{d}k, \tag{2.5}$$

where Σ_0 is the central surface density, R_d is the scale length of the disc and $J_0(x)$ is the Bessel function of first kind. Such a potential could be solved numerically, however, it sets a large computational demand on simulations. For this reason it is preferable to use the Miyamoto-Nagai disc if one can afford this approximation.

Halo

The last of the three components that we consider for the M31 potential field model is the extended halo. The extended halo was introduced by Freeman (1970) as a mass component for spiral galaxies to explain the behavior where their rotational velocity remained constant to a very large radius, although the luminous mass of the galaxy should give a rotational curve which decreases with radius. This discrepancy meant that either the theory of gravity was incomplete or there where some invisible mass in which the luminous galaxy was embedded. Freeman (1970) suggested that the latter was the better solution. The existence of this extended "dark matter" halo has been augmented by a large number of studies, see e.g., Broeils (1992); Rubin et al. (1980) or de Swart et al. (2017) for a review.

The logarithmic potential

One of the models I considered in this work for the extended halo is a spherically symmetric logarithmic potential model which was suggested by Binney (1981), given by,

$$\Phi_{\mathrm{h,log}}(r) = \frac{1}{2} V_h^2 \ln(r_h^2 + r^2), \tag{2.6}$$

where V_h is the rotational velocity, and r_h is a scale length. The values for the parameters which give a fit to the M31 potential where estimated by Bekki et al. (2001) and are given in Table 2.1.

Bajkova & Bobylev (2017) investigated how this model compared to other models and concluded that the major problem with this potential field is the monotonic increase in rotational velocity. This becomes a problem for my simulations since I will handle the motions of dwarf galaxies which effectively approaches the system from an infinite distance. To relieve this issue I introduce a cut-off at some radius r_{cut} where the halo is assumed to end. Outside this distance the halo potential will assume a point-mass potential. This gives a halo potential model,

$$\Phi_h(r) = \begin{cases} \frac{1}{2} V_h^2 \ln(r_h^2 + r^2) + \Phi_0 & \text{if } r < r_{\mathrm{cut}} \\ \frac{GM_{\mathrm{h}}}{r} & \text{if } r > r_{\mathrm{cut}} \end{cases}, \tag{2.7}$$

where M_{h} is the mass of the extended halo. Also note that I have added a potential field Φ_0 to the potential field within the cut-off radius. This is a freedom that we have due to the fact that potential energy is defined relative to some arbitrary point. Usually this point is chosen such that the potential energy is zero at infinity, however, this cannot be the case for a logarithmic field due to its monotonic increase with radius. I will explain later how I use this to my advantage.

I discussed earlier that the mass of the M31 galaxy is not easily determined, yet it is necessary for this formulation of the halo potential. To determine the mass of the halo I considered M31 to have a mass enclosed within 300 kpc of $M_{300} = 1.4 \times 10^{12}\, M_\odot$. To determine the portion of the total mass that belongs to the halo I integrated the densities of the bulge and disc components over a spherical volume with a 300 kpc radius. This gave

$M_{\rm h} = M_{300} - (M_{\rm b,300} + M_{d,300}) = 1.4 \times 10^{12}\,M_\odot - (9.16 \times 10^{10}\,M_\odot + 6.3 \times 10^{10}\,M_\odot) = 1.24 \times 10^{12}\,M_\odot$.

In order to have a physical transition in the potential field when an object passes the boundary located at $r_{\rm cut}$ I require that the following conditions are satisfied:

$$\left[\Phi_h(r < r_{\rm cut}) = \Phi_h(r > r_{\rm cut})\right]_{r=r_{\rm cut}}, \tag{2.8}$$

$$\left[\nabla\Phi_h(r < r_{\rm cut}) = \nabla\Phi_h(r > r_{\rm cut})\right]_{r=r_{\rm cut}}. \tag{2.9}$$

The condition given in Equation 2.9 sets a constraint on the cut-off radius, $r_{\rm cut}$, according to

$$\frac{V_h^2 r_{\rm cut}}{r_{\rm cut}^2 + r_h^2} = \frac{GM_h}{r_{\rm cut}^2}$$

$$\Rightarrow \quad r_{\rm cut} = 155.08\,{\rm kpc}, \tag{2.10}$$

where I used the value $G = 4.300912722\,{\rm kpc(km/s)^2}\,M_\odot$, and parameters as they are given in Table 2.1. From the condition given in Equation 2.8 we can simply scale the potential by setting the value for Φ_0 in Equation 2.7 according to

$$\Phi_0 = -\frac{GM_h}{r_{\rm cut}} - \frac{1}{2}V_h^2 \ln(r_{\rm cut}^2 + r_h^2) = -2.08993 \times 10^5\,({\rm km/s})^2. \tag{2.11}$$

This gives a potential field which is continuous and smooth for all r.

The Navarro-Frenk-White potential

Another model that approximates the extended halo potential of larger galaxies was formulated by Navarro et al. (1996). In their work they investigated the density distribution of dark matter halos that naturally arise in Λ cold dark matter (ΛCDM) simulations. For a review on simulating the ΛCDM universe see e.g. Springel et al. (2006). The Navarro-Frenk-White (NFW) density profile that they obtained is given by

$$\rho_{\rm NFW}(r) = \frac{\rho_c \delta}{(r/r_h)(1 + r/r_h)^2}, \tag{2.12}$$

where ρ_c is the critical density of the Universe, δ is a dimensionless parameter and r_h is a characteristic radius. The critical density is a function of the Hubble constant, $\rho_c = 277\,h^2\,M_\odot\,{\rm kpc}^3$, which for this work was assumed to be $h = H_0/(100\,{\rm km/s/Mpc} = 0.71$.

The potential field which arises in the NFW profile is given by

$$\Phi_{\rm NFW}(r) = -\frac{4\pi G\delta\rho_c r_h^3}{r} \ln\left(\frac{r + r_h}{r_h}\right). \tag{2.13}$$

Compared to the logarithmic potential field described previously this density profile does not suffer from a monotonically increasing rotational velocity, but rather goes to zero as r goes to infinity. This implies that, compared to the logarithmic halo potential, the NFW profile does not require a cut-off radius. This is an advantage for this profile.

2.2 The dwarf galaxy

In each simulation there will be a dwarf galaxy on a trajectory that at some point gives it a close encounter with the M31 galaxy. Unlike the M31 galaxy the dwarf galaxy does not have an observationally constrained mass, however, there are some indications as to what the mass might be, given that it was the original host for MGC1. Spitler & Forbes (2009) suggested that there is a linear scaling relation between the total halo mass, $M_{\rm tot}$, of a galaxy (dark matter halo plus the baryonic components) and its globular cluster population $M_{\rm GCs}$. They found this empirical trend to be independent of galaxy type and environment, however, due to the limitation in available data the relation cannot be confirmed for smaller galaxy masses. Other works confirmed this trend, see e.g. Baumgardt et al. (2010); Harris et al. (2017) or Renaud (2018) for a review. Harris et al. (2017) determined a quantitative relation by introducing a scaling law,

$$\nu_M \equiv \frac{M_{\rm GCs}}{M_{\rm tot}}, \quad \langle \nu_M \rangle = 2.9 \times 10^{-5}, \tag{2.14}$$

for which they found a scatter in ν_M of ± 0.28 dex.

The mass of MGC1 was estimated by Mackey et al. (2010a) to be $2.02 \times 10^5\, M_\odot$. If we assume that MGC1 was the only globular cluster in the dwarf galaxy then we obtain a minimum mass total mass for it of $\approx 7 \times 10^9\, M_\odot$, although this is a very uncertain estimate. Firstly, there is no way of telling whether MGC1 was alone in its original galaxy. There are many indications that contradict this. Observational data from Local group dwarf galaxies reveal that most dwarf galaxies host populations of multiple globular clusters (see, e.g., van den Bergh, 2006; Colucci & Bernstein, 2011). In a work by Zepf & Ashman (1993) the authors defined a quantity T, which is the number of globular clusters per $10^9\, M_\odot$ of galaxy stellar mass. They found that this quantity was of the order of a few for galaxies with stellar mass of $10^9\, M_\odot$ and increased slightly for more massive galaxies. For a review on the subject I refer the reader to Brodie & Strader (2006). For the dwarf galaxies the masses are typically dominated by dark matter, hence the stellar mass for the dwarfs that I simulate is probably rather small. When stating assumptions about the number of globular clusters in dwarf galaxies later in this report, this should be taken into consideration.

Because of the uncertainty in the relation between globular cluster mass and host galaxy mass, especially for dwarf galaxies, I digress from choosing a specific dwarf galaxy mass. In this work I will instead select a set of different dwarf galaxy masses and present results for each mass. For this project I look only at dwarf galaxies as original hosts of MGC1, with and upper mass limit chosen at $10^{10}\,{\rm M}_\odot$.

The Plummer model

The encountering galaxy in our simulations is assumed to be spherically symmetric galaxy which has a significantly smaller mass compared to M31. The potential of such a galaxy can be modelled using a Plummer potential, see Plummer (1911). This potential was originally created to fit the potential field of globular clusters and was later adapted to a

range of object including the central region of large disc galaxies and spherical galaxies. It is a good model for dwarf galaxies since it is cored which is typical for dwarf galaxies, see, e.g., Genina et al. (2018).

The Plummer model is derived from the Lane-Embden equation (Lane, 1870). By assuming a polytropic index of 5 one can find a spherically symmetric potential according to

$$\Phi_{\rm plum} = \frac{GM_{\rm plum}}{\sqrt{r_{\rm plum}^2 + r^2}}. \tag{2.15}$$

$M_{\rm plum}$ is the total mass of the galaxy and $r_{\rm plum}$ is a scale radius that sets the core radius of the dwarf galaxy. From dimensional analysis and the assumption that the density and the potential field are related via a polytrope, we can obtain the corresponding density profile of the Plummer model,

$$\rho_{\rm plum}(r) = \frac{3M_{\rm plum}}{4\pi r_{\rm plum}^3}\left(1 + \frac{r^2}{r_{\rm plum}^2}\right)^{-5/2}. \tag{2.16}$$

It is worthwhile to mention that half-light radius for the plummer potential is approximately $1.3\, r_{\rm plum}$.

2.3 Motions in potential fields

As was mentioned previously we define the gravitational potential field as a scalar field associated with the mass distribution of an object, see Equation 2.1. We now look at the gravitational acceleration a body experiences due to some mass, given by

$$\boldsymbol{a}(\boldsymbol{r}) = -\frac{GM}{|\boldsymbol{r}|^3}\boldsymbol{r}, \tag{2.17}$$

where M is the mass of a point located at the origin of the vector $\boldsymbol{r}$. Because the acceleration of an object is a linear property we can generalize the the expression given in Equation 2.17 to a set of point-masses m_i at arbitrary positions $\boldsymbol{r}_i$, which gives

$$\boldsymbol{a}(\boldsymbol{r}) = \sum_i \frac{Gm_i}{|\boldsymbol{r}_i - \boldsymbol{r}|^3}(\boldsymbol{r}_i - \boldsymbol{r}). \tag{2.18}$$

Because the potential field is also a linear property a direct consequence of this is the Poisson's equation for gravity,

$$\boldsymbol{a}(\boldsymbol{r}) = -\boldsymbol{\nabla}\Phi(\boldsymbol{r}), \tag{2.19}$$

where $\boldsymbol{\nabla}$ is the gradient operator and $\Phi(\boldsymbol{r})$ is the sum of all potential fields that are relevant to consider for the body. In our case these potential fields consists of the aforementioned M31 and dwarf galaxy components.

Table 2.1: Values used for the parameters determining the potential field of the M31 galaxy and the dwarf galaxy. Values for the M31 potential in the left column are taken from Bekki et al. (2001), while the values on the right side are taken from Geehan et al. (2006). In this particular work I used the parameters from Geehan to model the M31 galaxy. The dwarf galaxy masses, given by $M_{\rm plum}$, that where used in this projects are listed in the table as well. The characteristic radii $r_{\rm plum}$ is given for each mass respectively. The dwarf galaxy parameters are compared to properties of observed dwarf galaxies (Mateo, 1998) in Figure 4.3.

	Bekki et al. (2001)	**Geehan et al. (2006)**
Bulge	$M_b = 9.2 \times 10^{10}\, M_\odot$	$M_b = 3.3 \times 10^{10}\, M_\odot$
	$r_b = 0.7\,\mathrm{kpc}$	$r_b = 0.61\,\mathrm{kpc}$
Disc	$M_d = 1.3 \times 10^{11}\, M_\odot$	$M_d = 1.03 \times 10^{11}\, M_\odot$
	$a = 6.5\,\mathrm{kpc}$	$a = 6.43\,\mathrm{kpc}$
	$b = 0.26\,\mathrm{kpc}$	$b = 0.265\,\mathrm{kpc}$
Halo	$V_h = 186\,\mathrm{km\,s^{-1}}$	$\delta = 27 \times 10^4$
	$r_h = 12\,\mathrm{kpc}$	$\rho_c = 136\, M_\odot\,\mathrm{kpc}^3$
		$r_h = 8.18\,\mathrm{kpc}$
Dwarf	$M_{\rm plum} = [10^7, 10^8, 10^9, 10^{10}]\, M_\odot$	
	$r_{\rm plum} = [0.2, 0.4, 0.6, 0.8]\,\mathrm{kpc}$	

One interesting property which is commonly used to describe the extent of a potential field is the orbital velocity that an object must have in order to stay in a circular orbit. We will refer to this as rotational velocity, v_c. This velocity is obtained by comparing the centripetal acceleration for a particle on a circular orbit to the gravitational acceleration it experiences. This gives a magnitude for the rotational velocity according to

$$v_c = \sqrt{-r\nabla\Phi(r)}. \tag{2.20}$$

In Figure 2.1 I have plotted the rotational velocity for the different components of the M31 potential along a radial axis R which lies in the plane of the M31 disc using parameters from Bekki et al. (2001) (top plot) and Geehan et al. (2006) (bottom plot). The model from Bekki et al. (2001) uses a Hernquist bulge, Miyamoto-Nagai disc and a logarithmic halo, while Geehan et al. (2006) uses a Hernquist bulge, exponential disc and NFW halo. In addition to the models, the figure also includes the observed rotational velocity of the M31 system from Braun (1991) and Kent (1989). Braun (1991) obtained the measurements by investigating the kinematics of spiral arms in the M31 galaxy. To do so they investigated the emission from neutral gas present in these spiral arms. Kent (1989) used a similar method but looked only at emission from HII gas. As was also noted by Geehan et al. (2006) the model from Bekki et al. (2001) overestimates the rotational velocity, and therefore also the depth of the potential field, especially in the outer parts of the galaxy. This is likely due to the fact that the bulge potential is significantly deeper,

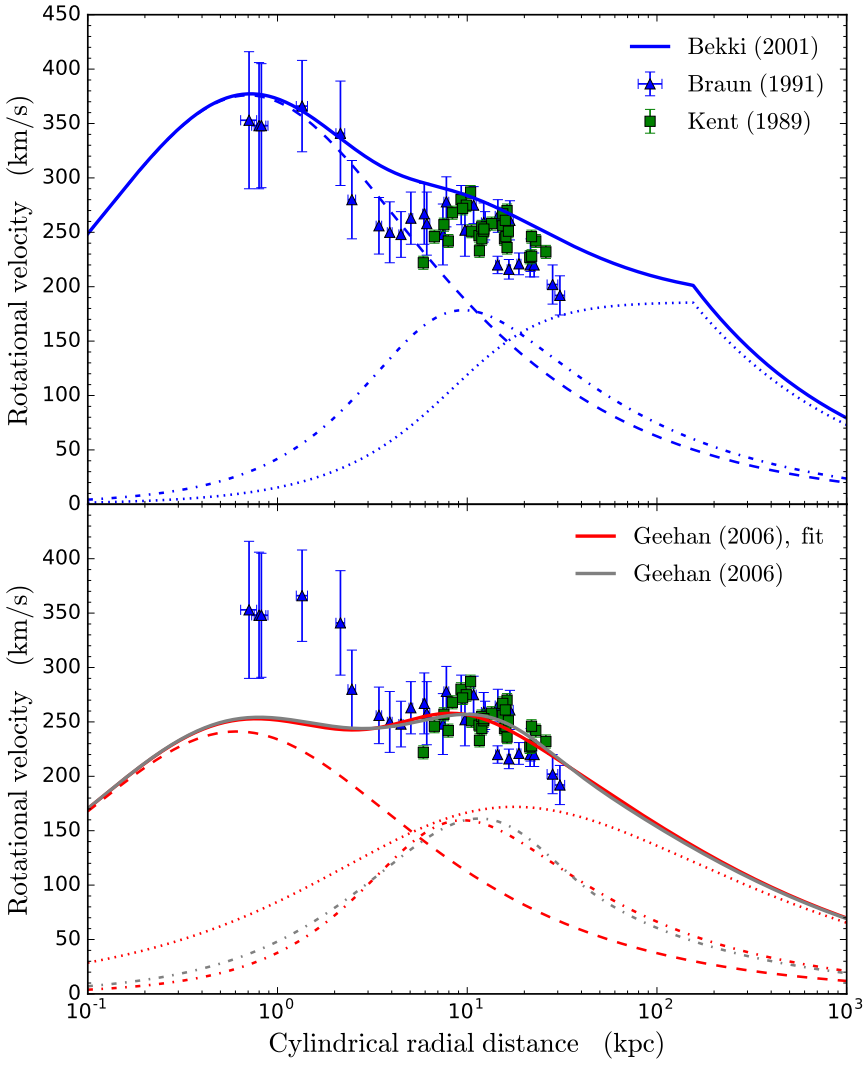

Figure 2.1: Rotational velocity of the M31 galaxy as function of radial distance, R, in the plane of the disc. The top plot shows the rotational velocity of the potential model by Bekki et al. (2001), while the bottom plot shows the rotational velocity of both the Geehan et al. (2006) potential. The bottom plot also includes a Geehan et al. (2006) model in which the disc was fitted to a Miyamoto-Nagai disc. The marks indicate measured values of the rotation velocity from Kent (1989) (green squares) and Braun (1991) (blue triangles). Both plots includes the individual components of the potential field where bulge, disc and halo are given by dashed, dotted-dash and dotted lines respectively. In the bottom plot I also include the exponential disc profile (gray, dot-dash line) for comparison to the fitted Miyamoto-Nagai disc profile.

arguably to account for the large values in rotational velocity observed by (Braun, 1991) in the inner regions.

In Section 2.1 I discussed the computational demand of using a exponential disc profile. Geehan et al. (2006) used an exponential profile in their approximation of the M31 potential field, however, for the purpose of this work I consider the Miyamoto-Nagai profile to be a good enough approximation of the potential field. I therefore modified their model by fitting a MN potential to their disc component, using this instead. The bottom plot of Figure 2.1 shows the two rotational velocity profiles, both the disc (dotted-dashed line) and for the total potential (solid line). The difference is very small, of only a few km/s, where the two potentials differ the most. The trajectory of the dwarf galaxy in the encounters that I later simulate will mostly be affected by the halo potential, hence this difference was not considered to be essential. It is worth noting that the program that was developed to simulate encounters, which will be described in Chapter 3, includes both mentioned potential models and it is therefore up to the user to decide what model to use. For all simulations used in this project I used the potential model from Geehan et al. (2006).

I will now derive the acceleration of a test-particle in the potential field used in our simulations. Due to how our experiment is set up it is preferable to use a Cartesian coordinate system, (x, y, z). The coordinates are defined such that x and y are perpendicular to each other and lie in the plane of the M31 disc while z is perpendicular to this plane. The origin of this coordinate system is located at the center of the M31 potential. The conversions from the spherically symmetric and cylindrically symmetric coordinates used in Section 2.1 are $r = \sqrt{x^2 + y^2 + z^2}$ and $R = \sqrt{x^2 + y^2}$ respectively. The acceleration that an object would obtain in the M31 potential field is the sum of the acceleration from all its components. Solving Equation 2.19 for the bulge and disc component gives:

$$\boldsymbol{a}_b(x, y, z) = -\frac{GM_\mathrm{b}}{r\left(r_\mathrm{b} + r\right)^2}\left(x\hat{\boldsymbol{x}} + y\hat{\boldsymbol{y}} + z\hat{\boldsymbol{z}}\right), \tag{2.21}$$

$$\boldsymbol{a}_d(x, y, z) = -\frac{GM_\mathrm{d}}{\left(\left(a + \sqrt{b^2 + z^2}\right)^2 + R^2\right)^{3/2}}\left(x\hat{\boldsymbol{x}} + y\hat{\boldsymbol{y}} + \frac{z(a + \sqrt{b^2 + z^2})}{\sqrt{b^2 + z^2}}\hat{\boldsymbol{z}}\right). \tag{2.22}$$

For the logarithmic halo we need to take into consideration that the potential field is splitted, nevertheless we can solve Equation 2.19 for both components separately and find

$$\boldsymbol{a}_h(x, y, z) = -\frac{V_\mathrm{h}^2}{r_\mathrm{h}^2 + r^2}\left(x\hat{\boldsymbol{x}} + y\hat{\boldsymbol{y}} + z\hat{\boldsymbol{z}}\right), \quad r < r_\mathrm{cut} \tag{2.23}$$

$$\boldsymbol{a}_h(x, y, z) = -\frac{GM_h}{r^3}\left(x\hat{\boldsymbol{x}} + y\hat{\boldsymbol{y}} + z\hat{\boldsymbol{z}}\right), \quad r > r_\mathrm{cut} \tag{2.24}$$

The last M31 potential field component that we consider is the NFW profile. Solving Equation 2.17 by inserting Equation 2.13 gives:

$$\boldsymbol{a}_\mathrm{NFW}(x, y, z) = -4\pi G\delta\rho_c\left(\frac{r_c}{r}\right)^3\left[\ln\left(\frac{r_c + r}{r_c}\right) - \frac{r}{r_c + r}\right]\left(x\hat{\boldsymbol{x}} + y\hat{\boldsymbol{y}} + z\hat{\boldsymbol{z}}\right). \tag{2.25}$$

For the dwarf galaxy we need to take into account that its potential field, given in Equation 2.15, is defined with r positioned at the center of the potential. Since the dwarf will move around in the simulation it is useful to define a coordinate such that its origin moves with the position of the dwarf galaxy. I defined this as $r_{\rm rel} = r - r_s$, where r_s is the position of the dwarf galaxy with respect to the center of the M31 potential and r is the position of the object in question. This gives acceleration of a object due to the dwarf galaxy given by

$$\boldsymbol{a}_p(x, y, z) = -\frac{GM_p}{\left(r_{\rm p}^2 + r_{\rm rel}^2\right)^{3/2}}\left((x - x_s)\hat{\boldsymbol{x}} + (y - y_s)\hat{\boldsymbol{y}} + (z - z_s)\hat{\boldsymbol{z}}\right), \tag{2.26}$$

where the subscript s implies the position of the dwarf galaxy.

I will later divide different types of trajectories into different subsets of orbits. They way I do this is by giving each dwarf galaxy either a hyperbolic, a parabolic or a bound orbit. The orbital type will be defined by what the total energy is if the dwarf were to be placed at infinity. They are defined accordingly:

$$E_{\rm tot}(r \to \infty) = \begin{cases} > 0 & \text{hyperbolic} \\ 0 & \text{parabolic} \\ < 0 & \text{bound.} \end{cases} \tag{2.27}$$

The total energy is conserved throughout the entire trajectory and the potential energy is easily obtained from the potential field of the M31 galaxy for any position. Therefore, it is possible to obtain a initial velocity for any given orbital type as function of initial position.

2.4 Analytic description of tidal interactions between potential fields

Analytic formula for the tidal radius

A body is subject to tides if the forces applied to it differ for different positions on the body. One common example of this is when a body of some non-negligible size feels the gravitational force from some other massive object, henceforth referred to as the source. Gravitational force is a function of distance from the source so the force on the side pointing toward the source will be larger than that on the far-side of the object. If the body is flexible it will cause the body to be stretched. This stretching is the cause of the tidally stripping away stellar objects from satellite galaxies.

It is interesting to investigate an analytical description of the tidal force, we will derive what is referred to as tidal radius, r_t. Comparable to the Roche lobe (see, e.g., Eggleton, 1983), the tidal radius is the distance from a body subjected to the tidal force outside which the gravitational force of the source is large enough to strip objects from the body. In contrast to the Roche lobe, the tidal radius depends on the orbital properties of both

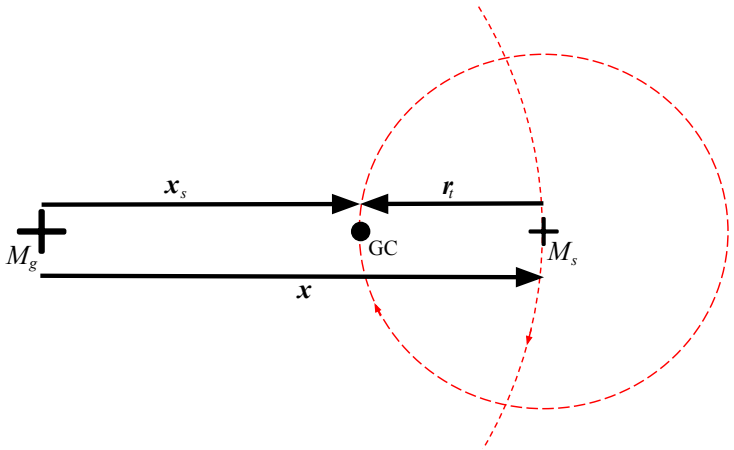

Figure 2.2: Coordinate system used when deriving the tidal radius of a satellite galaxy in orbit around a larger galaxy. The coordinate system is fixed at the position of the mass, M_g, and is rotating with angular velocity $\Omega = \Omega(t)$ such that the smaller mass, M_s, remains stationary in time. The black dot shows the position of a globular cluster at the tidal radius.

the body and the objects which are subject to being stripped away. To derive this tidal distance we will closely follow the derivation of Read et al. (2006).

Consider the geometrical description given in Figure 2.2. We define the coordinate system such that has its origin at $x = 0$, that is the position of the left cross, which is henceforth refereed to as major galaxy. This galaxy has a mass M_g. The right cross is a satellite galaxy with mass M_s, which is orbiting the major galaxy with angular momentum Ω, and this satellite hosts a globular cluster (GC) which is orbiting with an angular momentum Ω_s. The frame of reference is rotating with an angular velocity that corresponds to $\Omega(t) = \Omega$, hence the satellite remains stationary in time. The equation of motion for the satellite galaxy is given by

$$\ddot{\boldsymbol{x}} + \dot{\boldsymbol{\Omega}} \times \boldsymbol{x} + 2\boldsymbol{\Omega} \times \dot{\boldsymbol{x}}_s + \boldsymbol{\Omega} \times (\boldsymbol{\Omega} \times \boldsymbol{x}) + \nabla \Phi_g(\boldsymbol{x}) = 0, \tag{2.28}$$

where $\boldsymbol{x}$ the position of the satellite, $\boldsymbol{x}_s$ is the position of the globular cluster and $\nabla \phi_g$ is the gradient of the major galaxy potential. In this expression we consider the globular cluster to be a test-particle, hence neglecting its mass. Note that we use the convention where $\dot{\boldsymbol{x}}$ implies the time derivative of $\boldsymbol{x}$. A detailed derivation of the equation of motion for a rotating frame of reference is given in Appendix A. In a similar fashion we find the equation of motion for the GC, given by

$$\ddot{\boldsymbol{x}} + \dot{\boldsymbol{\Omega}} \times \boldsymbol{x}_s + 2\boldsymbol{\Omega} \times \dot{\boldsymbol{x}}_s + \boldsymbol{\Omega} \times (\boldsymbol{\Omega} \times \boldsymbol{x}_s) + \nabla \Phi_g(\boldsymbol{x}_s) + \nabla \Phi_s(\boldsymbol{r}_t) = 0, \tag{2.29}$$

where $\Phi_s(\boldsymbol{r}_t)$ is the gravitational potential of the satellite galaxy at the position of the GC. We assume that this GC is positioned exactly at the tidal radius $\boldsymbol{r}_t$.

We want to derive an expression of the tidal radius and therefore search for a solution where the GC is unbound from both potentials. This limit is given by the condition

$$\ddot{\boldsymbol{r}}_t = \ddot{\boldsymbol{x}}_s - \ddot{\boldsymbol{x}} = 0. \tag{2.30}$$

Without the loss of generality, two new terms are defined, one term $\boldsymbol{F}$ for the potential fields and one term $\boldsymbol{F}_f$ describing the forces due to the rotation of the reference system,

$$\begin{aligned} \boldsymbol{F} &= \nabla\Phi_g(\boldsymbol{x}) - \nabla\Phi_g(\boldsymbol{x}_s) - \nabla\Phi_s(\boldsymbol{r}_t), \\ \boldsymbol{F}_f &= -\dot{\boldsymbol{\Omega}} \times \boldsymbol{r}_t - \boldsymbol{\Omega} \times (\boldsymbol{\Omega} \times \boldsymbol{r}_t) - 2\boldsymbol{\Omega} \times (\boldsymbol{\Omega}_s \times \boldsymbol{r}_t). \end{aligned} \tag{2.31}$$

It is straightforward to find that substituting Equations 2.28 and 2.29 into Equation 2.30 gives

$$\boldsymbol{F} + \boldsymbol{F}_f = 0. \tag{2.32}$$

This condition provides a way to calculate the tidal radius in a very general sense, however, it is not straightforward to compute.

To simplify we search for the smallest radii $\boldsymbol{r}_t$ where the GC is stripped. Firstly, we can maximize the effect that the host has on the GC by only considering orbits which are coplanar. With such an orbit the space velocity of the GC will add up (or subtract) to that of the satellite. For a GC on a prograde orbit the velocities add up and the tidal radius is minimized, while a retrograde orbit will cause the velocities to be subtracted, binding the GC more tightly to the dwarf galaxy, thus increasing the tidal radius. We will find it useful to define a factor α which describes the orbit of the GC,

$$\alpha = \begin{cases} 1, & \text{prograde} \\ 0, & \text{radial} \\ -1, & \text{retrograde.} \end{cases} \tag{2.33}$$

To get some intuition on how the tidal stripping depends on the α-factor consider the case where a co-planar orbit of the GC is purely radial, that is $\alpha = 0$. If the GC is positioned as is shown in Figure 2.2 with these conditions it will be at rest in the rotating reference system at the tidal radius. Now if the orbital speed of the GC in its satellite orbit increases slightly (creating a prograde orbit) it implies an increased centripetal acceleration of the GC which makes it less bound to the satellite. Furthermore, the orbital speed of the GC around the larger galaxy will decrease, thus with the same analogy make it more bound to the major galaxy. The result is inevitably that the GC is moved outside the tidal radius, r_t and thus becomes tidally stripped away from the satellite. With the same reasoning you find that the opposite is true for a retrograde orbit. We therefore expect GC's on prograde orbits to be more easily stripped away.

It is now possible to obtain a simple formula to describe the tidal interactions of the encounter. The interesting force is that in the direction of $\boldsymbol{x}$. In the limit where the GC is not bound to neither the major galaxy or the satellite we obtain

$$\boldsymbol{F} \cdot \hat{\boldsymbol{x}} + \boldsymbol{F}_f \cdot \hat{\boldsymbol{x}} = 0. \tag{2.34}$$

For readability we solve the two scalar products individually. starting with

$$\boldsymbol{F}\cdot\hat{\boldsymbol{x}} = \left.\frac{\mathrm{d}\Phi_g}{\mathrm{d}x}\right|_x - \left.\frac{\mathrm{d}\Phi_g}{\mathrm{d}x}\right|_{|x-r_t|} + \left.\frac{\mathrm{d}\Phi_s}{\mathrm{d}r}\right|_{r_t}, \tag{2.35}$$

where it should be noted that the radial direction pointing away from the satellite is $\hat{\boldsymbol{r}} = -\hat{\boldsymbol{x}}$. By assigning functions describing the mass distributions, $M_g(x)$ and $M_s(r)$, for the major galaxy and the satellite respectively, we can solve the derivatives in Equation 2.35 obtaining an expression for $\boldsymbol{F}\cdot\hat{\boldsymbol{x}}$ which explicitly depend on the set-up parameters, x and r_t,

$$\boldsymbol{F}\cdot\hat{\boldsymbol{x}} = \frac{GM_g(x)}{x^2} - \frac{GM_g(x-r_t)}{(x-r_t)^2} + \frac{GM_s(r_t)}{r_t^2}. \tag{2.36}$$

The second term can be solved to find

$$\begin{aligned}\boldsymbol{F}_f\cdot\hat{\boldsymbol{x}} = -\underbrace{(\dot{\boldsymbol{\Omega}}\times\boldsymbol{r}_t)\cdot\hat{\boldsymbol{x}}}_{=0} &-(\boldsymbol{\Omega}\times(\boldsymbol{\Omega}\times\boldsymbol{r}_t))\cdot\hat{\boldsymbol{x}} - 2(\boldsymbol{\Omega}\times(\boldsymbol{\Omega}_s\times\boldsymbol{r}_t))\cdot\hat{\boldsymbol{x}}\\ &= -\Omega^2 r_t - 2\alpha\Omega\Omega_s r_t,\end{aligned} \tag{2.37}$$

where we introduced $\Omega = |\boldsymbol{\Omega}|$. Note that the α-factor introduced earlier comes in here as well. We have now arrived at a general, fully analytic, description of the tidal radius, r_t.

The tidal radius of point-mass potentials

There is an especially simple case in which we let the potentials of both the host galaxy and satellite galaxy be point mass potentials. Using the equations derived in the previous section, although now assuming point-masses rather than mass functions, we have the following:

$$\frac{GM_g}{x^2} - \frac{GM_g}{(x-r_t)^2} + \frac{GM_s}{r_t^2} - \Omega^2 r_t - 2\alpha\Omega\Omega_s r_t = 0, \tag{2.38}$$

where M_g is the mass of the major galaxy and M_s is the mass of the satellite galaxy.

The solution to Equation 2.38 is not trivial since the angular velocity of the system is a function of time, $\Omega = \Omega(t)$. In addition to this, we also consider the orbit of the GC around the satellite which gives an additional term Ω_s. The angular velocity, Ω_s, of the GC orbiting a point mass is obtained through Kepler's third law,

$$GM_s = \Omega_s^2 r_t^3 \quad \Leftrightarrow \quad \Omega_s = \sqrt{\frac{GM_s}{r_t^3}}. \tag{2.39}$$

To find the time-dependence of the angular velocity Ω we investigate how the system changes in order to conserve energy. The orbital position of the satellite can be constrained by $x_p < x < x_a$, where x_p is the pericentre and x_a is the apocentre of the orbit. Given that

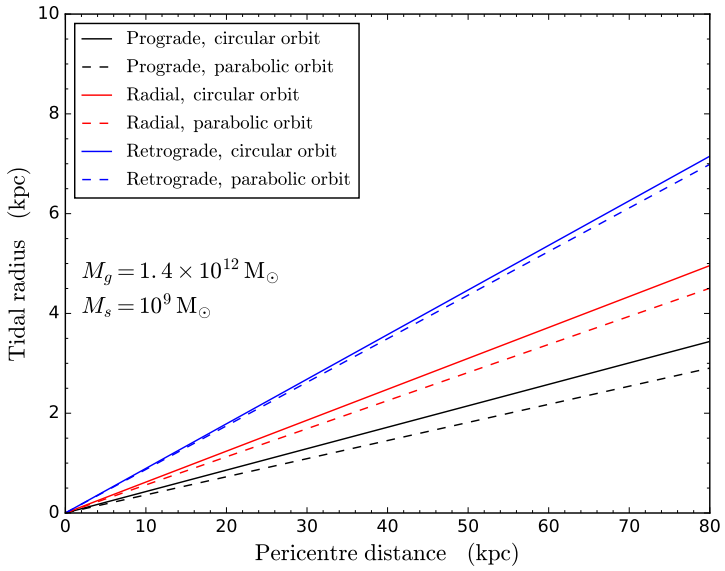

Figure 2.3: Tidal radius at the pericentre of the encounter as a function of the pericentre distance, see Equation 2.44. The plot shows results for a dwarf galaxy modelled as a point mass with total mass of $10^9\,M_\odot$ encountering a $1.4 \times 10^{12}\,M_\odot$ mass galaxy. It also shows the difference in tidal radius depending on prograde ($\alpha = 1$), radial ($\alpha = 0$) and retrograde ($\alpha = -1$) orbits. To illustrate the effect of the GC eccentricity, the plot includes two extremes, parabolic ($e = 1$) orbit and circular ($e = 0$) orbit.

the satellite has a conserved total specific energy E and conserved total specific angular momentum, J, we can obtain the relation

$$E = \frac{1}{2}\frac{J^2}{x_a^2} + \Phi_g(x_a) = \frac{1}{2}\frac{J^2}{x_p^2} + \Phi_g(x_p). \tag{2.40}$$

Exercising some algebra on Equation 2.40 gives us an expression for the total angular momentum,

$$J^2 = \frac{2x_p^2 x_a^2(\Phi_g(x_p) - \Phi_g(x_a))}{x_p^2 - x_a^2} = 2GM_g\frac{x_a x_p^2 - x_p x_a^2}{x_p^2 - x_a^2} = \frac{2GM_g x_p x_a}{x_p + x_a} \tag{2.41}$$

From the relation between angular momentum and angular velocity we find

$$\Omega(t)^2 = \frac{J^2}{x(t)^4} = \frac{2GM_g x_p x_a}{x^4(x_p - x_a)} = \frac{GM_g}{x^4}a(1-e^2) = \frac{GM_g}{x^4}\Lambda \tag{2.42}$$

where we define the semi-major axis $a = \frac{x_p + x_a}{2}$ and eccentricity of orbit $e = \frac{x_p - x_a}{x_p + x_a}$. To simplify later calculations we also define $\Lambda = a(1-e^2)$.

By substituting the expression for angular velocity of the GC (Equation 2.39) and the expression for the frame angular velocity (Equation 2.42) into Equation 2.38 we obtain an

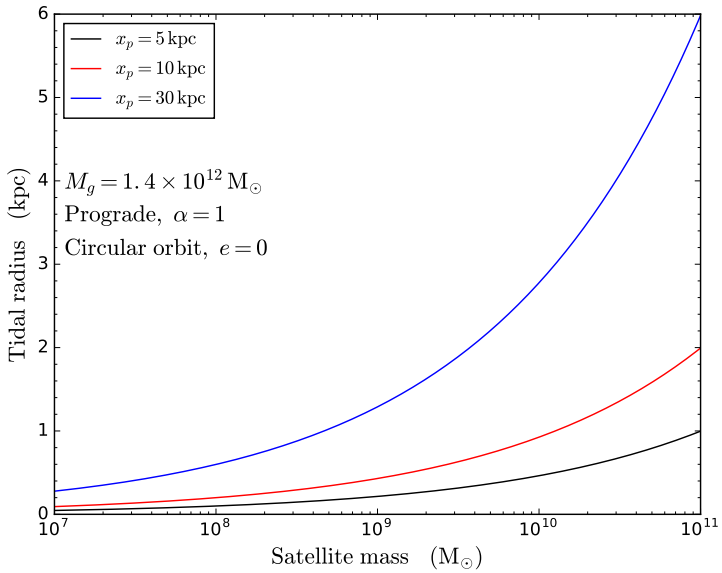

Figure 2.4: Tidal radius at the pericentre of the encounter as a function of dwarf galaxy mass. The M31 has an assumed mass of $1.4 \times 10^{12}\,M_\odot$ and the orbits in the dwarf galaxy are assumed to be circular ($e = 0$) and prograde. The plots shows tidal radius for three different encounter pericentres to illustrate their differences.

equality that sets the tidal radius. Read et al. (2006) showed that r_t can be approximated with

$$r_t \simeq \left(x^4 \frac{M_s}{M_g} \Lambda \right)^{1/3} \left(\frac{\sqrt{\alpha^2 + 1 + 2x\Lambda} - \alpha}{\Lambda + 2x} \right)^{2/3} . \tag{2.43}$$

As is mentioned by Read et al. (2006) this expression agrees with that of some special cases (see, e.g., King, 1962). Since the tidal radius strongly depends on the separation between the major galaxy and the satellite, we will strip away the innermost globular clusters at the pericentre of the satellite trajectory. At this position the tidal radius reduces to

$$\begin{aligned} r_t &\simeq \left(x_p^4 \frac{M_s}{M_g} \frac{2x_a x_p}{x_a + x_p} \right)^{1/3} \left(\frac{\sqrt{\alpha + 1 + 2x_p \frac{2x_a x_p}{x_a + x_p}} - \alpha}{\frac{2x_a x_p}{x_a + x_p} + 2x} \right)^{2/3} \\ &= x_p \left(\frac{M_s}{M_g} \right)^{1/3} \left(\frac{1}{1+e} \right)^{1/3} \left(\frac{\sqrt{\alpha^2 + 1 + \frac{2}{1+e}} - \alpha}{1 + \frac{2}{1+e}} \right)^{2/3} . \end{aligned} \tag{2.44}$$

Figures 2.3 and 2.4 shows how the tidal radius depends on the various parameters. In Figure 2.3 it becomes apparent that the tidal radius is smaller for prograde orbits, implying that it is easier to tidally strip an object on a prograde orbit. The opposite is true for retrograde orbits. We also find that the tidal radius only depends marginally on the eccentricity of the satellite orbit for a given pericentre distance.

Chapter 3

Tidal stripping during a close encounter

In this chapter I investigate the the outcome of a single encounter between a dwarf galaxy, with a total mass $M_s = 10^9\,M_\odot$ (this mass is the same as the mass-parameter, $M_{\rm plum}$, used in the Plummer model, see Equation 2.15), and the M31 galaxy. I will explain the details of a single encounter and investigate the different populations of clusters that will be used when I later investigate the likelihood of producing MGC1-like clusters for a large set of encounters. I used the model from Geehan et al. (2006) for the M31 potential and the Plummer model for the dwarf galaxy (both described in Chapter 2) to simulate the encounter in this chapter. A detailed description of the numerical set-up is given in Section 3.1.

To provide an understanding of a specific encounter I will investigate how the orbital properties of the globular clusters change after the encounter. I will in particular look at three different populations of clusters. The first population consists of clusters that are stripped away from the dwarf galaxy and captured on orbits around M31; these are referred to as **Captured** clusters. Cluster that are not tidally stripped away, but remain on orbits bound to the dwarf galaxy after the encounter are referred to as **Retained** clusters and clusters which are stripped away and left unbound from both the dwarf and M31 are referred to as **Unbound** clusters. There is a sub-population of clusters in the captured population which I refer to as **MGC1-like** clusters. MGC1-like clusters are captured clusters that after the encounter ($t > 0$) return to M31 in such a way that they are located 200 kpc away from the M31 centre at least two times. I require them to be at this position two times within the time of the simulation, since the they will be on trajectories similar to the dwarf galaxy the first time they pass the 200 kpc. (Mackey et al., 2010a) concluded that the observed MGC1 cluster is not associable to any dwarf galaxy, which implies that the if the cluster was donated to M31 from another galaxy they no longer remain on similar orbits.

3.1 Numerical simulation of an encounter

The program

To simulate an encounter between a dwarf galaxy and M31 I used a program [1] written by myself in C++ language. A detailed description of how the code is used is available in the `git`-repository where it is stored. Following is an overview of how the program is built.

The program uses numerical integration to evolve the trajectories of the dwarf galaxy and a set of globular clusters initially bound to the dwarf galaxy. This gives the program a traditional *N-body* style, although gravitational forces are computed from the potential fields of the two galaxies. The program intentionally does not treat interactions between the globular clusters so that every encounter can be simulated include a large set of them. Initializing a large enough set of globular clusters with some random distribution means that we can compare the number in one of the previously mentioned populations to the total number of initiated globular clusters and thus gain insight as to what is the likelihood is of obtaining a cluster in that given population. This fraction can then be compared to the real cluster population of a dwarf galaxy to estimate how this population would change if the dwarf galaxy would have an encounter with a large galaxy, such as M31.

The program works in a Cartesian coordinate system in the reference-frame of the M31 galaxy, thus giving a static potential throughout the simulation. The dwarf galaxy potential will be moving in the M31 potential, therefore, we need to consider the relative position between it and the globular clusters which are affected by it. For a given dwarf galaxy position the potential is static.

To integrate the trajectories of the dwarf galaxy and the clusters the program solves the ordinary differential equations (ODE) that defines the evolution of their phase-space coordinates. These ODE's are given by

$$\begin{aligned} \frac{\mathrm{d}x}{\mathrm{d}t} &= v_x, & \frac{\mathrm{d}y}{\mathrm{d}t} &= v_y, & \frac{\mathrm{d}z}{\mathrm{d}t} &= v_z, \\ \frac{\mathrm{d}v_x}{\mathrm{d}t} &= a_x, & \frac{\mathrm{d}v_y}{\mathrm{d}t} &= a_y, & \frac{\mathrm{d}v_z}{\mathrm{d}t} &= a_z, \end{aligned} \tag{3.1}$$

where (x, y, z, v_x, v_y, v_z) are the conventional Cartesian phase-space coordinates. The accelerations, a, are computed from the equations derived in Chapter 2 for each indexed coordinate. The program is equipped with two different numerical schemes for solving ODE's. The first integration scheme is a traditional fourth-order Runge-Kutta(Runge, 1895) integrator that was implemented in a straight forward manner. The second integrator is also a variation of the Runge-Kutta integration scheme known as the Runge-Kutta Cash-Karp scheme. This integrator which was developed by Cash & Karp (1990) uses six function evaluations per integration to simultaneously solve a fourth and fifth order accurate integration. By comparing the difference between the two one can estimate the error of the fourth order integration and thereafter adapt the time-step to provide a constant

[1] The code is available for download on GitHub,
`https://github.com/ericander/Galactic-Potential-Particle-Integrator.git`

accuracy. The implementation of this integration scheme is not as simple as for the fourth-order Runge-Kutta, so a detailed description of this algorithm is provided in Appendix B. A detailed description of both integration methods are also available in Numerical Recipes in C[2].

The program consists of two different versions, one which has a more traditional way of reading in initial conditions and one which is specifically designed for the simulations used in this project. The traditional version of the program will search for initial conditions for both the dwarf galaxy and the globular clusters in a file where all the initial conditions are listed, which then are integrated to trace the trajectories of all moving objects. The second version of the program will instead look only for initial conditions for the dwarf galaxy. The program then assumes that the dwarf galaxy lies at the pericentre of its trajectory and will integrate it out to a given distance, r_0. When the dwarf galaxy reaches this position it turns the dwarf trajectory around and initializes the population of globular clusters in the dwarf galaxy. In this way it is possible to set up a set of encounters in which we can control the distribution of pericentre distances, a parameter which we showed in Chapter 2 is very sensitive to the tidal radius. This particular method also gives a straight forward way of defining $t = 0$ as the time when the dwarf galaxy is located at its closest approach. The method will integrate the dwarf galaxy trajectory for a given amount of time after this moment.

Initial globular cluster population

In each simulated encounter I give the dwarf galaxy a population of independent globular clusters from a random sampling function. The point is to use a large enough sample so that a comparison between the number of clusters that is found in each of the different populations (mentioned previously) after the encounter and the initial number of clusters provides an estimate of the likelihood of finding a cluster in a given population. The random sampling function that was used gives a population of globular clusters distributed uniformly within a shell surrounding the dwarf galaxy. The inner radius of this shell is limited by the fact that the dwarf galaxy should not be able to tidally strip clusters, while the outer radius is limited by some decided value. The orbit of each cluster is set to initially give them a circular orbit in the dwarf.

I used a modified version of an algorithm from Muller (1959) to position the clusters. The algorithm places particles uniformly on the surface of a sphere, for which I select a radius given by

$$r_{\rm GC} = \sqrt{\mathrm{U}(r_{\rm min}^2, r_{\rm max}^2)}, \tag{3.2}$$

where $\mathrm{U}(\mathrm{x}_1, \mathrm{x}_2)$ is a uniform distribution between x_1 and x_2. This produces a shell of globular clusters between radii $r_{\rm min}$ and $r_{\rm max}$. The Muller (1959) algorithm utilises the normal distribution to generate points, which makes it an efficient and simple method. A property of the N-dimensional normal distribution is that any realisation of it is has

[2]For information about Numerical Recipes in C visit `http://numerical.recipes/`

a constant probability on the surface of an N-dimensional sphere with the centre on the distribution mean and radius equal to its standard deviation. Following this, the algorithm generates 3 random variables (x, y, z) from a normal distribution, $\mathcal{N}$, which are then re-normalised to the radius of the cluster orbit according to

$$\boldsymbol{r}_{\mathrm{GC}} = \frac{r_{\mathrm{GC}}}{\sqrt{x^2 + y^2 + z^2}} \begin{bmatrix} x \\ y \\ z \end{bmatrix}. \tag{3.3}$$

The minimum and maximum initial orbital distances for the set of globular clusters is set by two conditions. As already mentioned, the globular clusters cannot be allowed to be tidally shredded by the dwarf galaxy itself. This puts a condition on the minimum orbital distance, $r_{\mathrm{min,GC}}$, inside which stars start to be removed from the cluster. To determine this distance I used the Roche lobe which is defined as the region where the gravitational potential is dominated by an orbiting satellite. A formula that approximates the radius of the Roche lobe was determined by Eggleton (1983) and it is expressed as

$$r_L = \frac{0.6q^{2/3} + \ln\left(1 + q^{1/3}\right)}{0.49q^{2/3}}, \quad q = \frac{M_1}{M_2}, \tag{3.4}$$

where r_L is expressed in units of orbital distance, M_1 is the mass of the orbiting object and M_2 is the mass of the object around with M_1 is orbiting. For our particular case M_1 is the mass of the globular cluster which I assume to have a mass of $M_{\mathrm{GC}} = 10^5\, M_\odot$ while M_2 is the mass of the dwarf galaxy M_{s}. We are interested in the minimum orbital distance for which r_L does not exceed the size of the globular cluster, which was assumed to have a size of 0.1 kpc. Setting $r_L = 0.1\,\mathrm{kpc}/r_{\mathrm{GC,min}}$ and inverting Equation 3.4 gives

$$r_{\mathrm{GC,min}} = \frac{0.6q^{2/3} + \ln\left(1 + q^{1/3}\right)}{0.49q^{2/3}} \cdot 0.1\,\mathrm{kpc}, \quad q = \frac{M_{\mathrm{GC}}}{M_{\mathrm{s}}} \tag{3.5}$$

.

I choose the maximum radial distance such that the globular cluster does not become tidally stripped by the M31 galaxy before coming within a decided distance, again using Equation 3.4. I choose this distance to be 200 kpc for all simulations in this project. This will give the globular cluster population in the dwarf galaxy, which is initiated 500 kpc from M31, some time to randomise before stronly affected by tidal forces. For the M31 I used the mass $M_{\mathrm{M31}} = 1.4 \times 10^{12}\, M_\odot$. This gives

$$r_{\mathrm{GC,max}} = \frac{0.49q^{2/3}}{0.6q^{2/3} + \ln\left(1 + q^{1/3}\right)} \cdot 200\,\mathrm{kpc}, \quad q = \frac{M_{\mathrm{s}}}{M_{\mathrm{M31}}}. \tag{3.6}$$

The orbital velocity of each globular cluster was set to be the rotational velocity of the dwarf galaxy. In order to determine the orientation of the orbit I, for each globular cluster, generated an orthogonal coordinate system $(\hat{e}_x, \hat{e}_y, \hat{e}_z)$, where $\hat{e}_z$ points in the radial direction of the dwarf galaxy. The direction of the velocity was then set to be

Table 3.1: Initial conditions for the dwarf galaxy and the four globular clusters with different outcomes shown in Figure 3.1

	x_0 (kpc)	y_0 (kpc)	z_0 (kpc)	$v_{x,0}$ ($\mathrm{km\,s^{-1}}$)	$v_{y,0}$ ($\mathrm{km\,s^{-1}}$)	$v_{z,0}$ ($\mathrm{km\,s^{-1}}$)
Dwarf	−246.86	434.81	0.0	4.11	−86.51	0.0
Captured	−246.70	424.41	3.07	1.75	−80.97	18.89
Retained	−244.01	242.50	−4.64	−3.45	−81.02	−16.72
Unbound	−256.19	431.19	8.63	10.97	−103.13	0.45
MGC1-like	−246.83	432.59	11.52	−6.01	−70.64	3.08

in the plane of $\hat{e}_x, \hat{e}_y$ shifted some angle ϕ away from $\hat{e}_x$. The angle was drawn from a uniform distribution between 0 and 2π. This will generate a sample where the probability of prograde and retrograde orbit is equally likely. The orbital velocity can then be set by

$$\boldsymbol{v}_{\mathrm{GC}} = v_{GC} \times (\sin(\phi)\hat{e}_x, \cos(\phi)\hat{e}_y, \hat{e}_z), \tag{3.7}$$

where $v_{GC} = v_{\mathrm{s,c}}$. $v_{\mathrm{s,c}}$ is the rotational velocity of the dwarf galaxy.

3.2 Capturing MGC1-like clusters

We are interested in investigating if it is possible to capture a globular cluster that has been tidally stripped away from a dwarf galaxy during a close encounter and then leave it on an orbit which could make it resemble the MGC1 cluster. In order to do so I set up an encounter between a dwarf galaxy, modelled with a Plummer potential using $M_s = M_{\mathrm{plum}} = 10^9\,M_\odot$ (henceforth I refer to dwarf galaxy mass as M_s, which is the same as total mass or mass parameter of Plummer model) and characteristic radius, $r_{\mathrm{plum}} = 0.6\,\mathrm{kpc}$. The dwarf galaxy trajectory was set up in such a way that it would only move in the x, y-plane, that is the plane of the M31 disc. The dwarf galaxy trajectory was initiated with a pericentre of $r_p = 78.1\,\mathrm{kpc}$ with a velocity of $v_0 = 260.5\,\mathrm{km/s}$. This gives a elliptical orbit for the dwarf galaxy around M31. It was then integrated out and given a population of 1000 globular clusters. Table 3.1 shows the coordinates of the dwarf galaxy when the globular clusters where initiated. The table also includes initial conditions of 4 selected globular clusters.

Figure 3.1 shows the trajectories of the dwarf galaxy and four selected globular clusters. The clusters were selected such that there is one example from each of the different cluster populations, i.e., one cluster tidally stripped away and captured by M31 (Captured), one cluster which remained bound to the dwarf galaxy throughout the encounter (Retained), one cluster which was unbound from both galaxies (Unbound) and one cluster which was captured by M31 on an orbit which places it at the orbital distance of MGC1 at least once after the encounter (MGC1-like). The trajectory of the dwarf (red dashed line) shows how it passes the M31 galaxy, and although it is bound, does not return to M31 within a

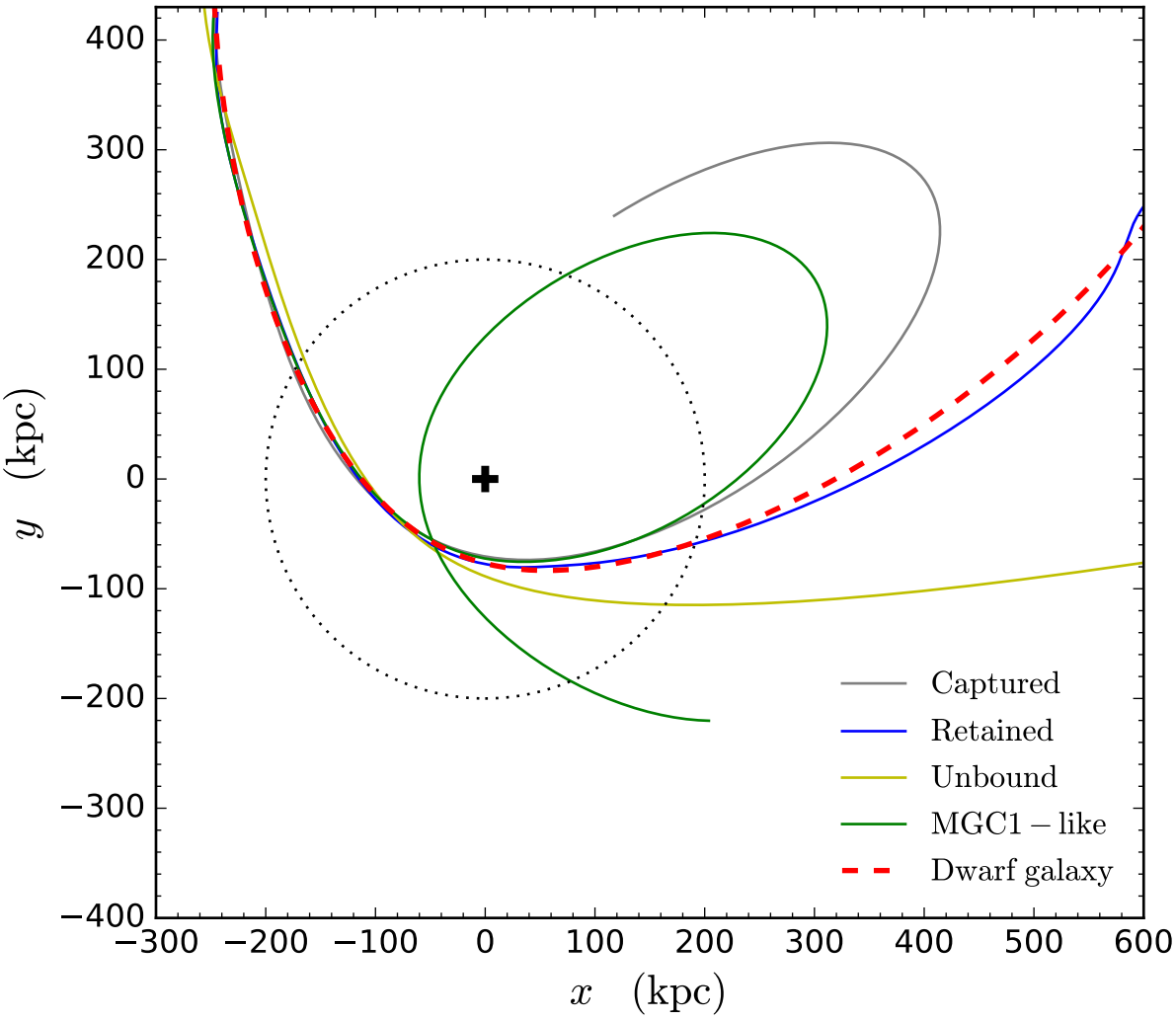

Figure 3.1: Trajectories in the orbital plane of the dwarf galaxy for a dwarf galaxy (chosen to be in plane of the M31 disc) and four globular clusters (see legend for labels). The globular clusters, originally bound to the dwarf galaxy, were picked from the three different populations: clusters that where stripped away from the dwarf and bound to M31 (Captured); clusters that remained bound in the dwarf galaxy throughout the entire simulation (Retained); clusters left unbound to either potential fields (Unbound); clusters in the Captured population that were placed at the current orbital position of MGC1 at least two times after the encounter (MGC1-like). The M31 galaxy is positioned at the origin of the plot (+). The red dotted line marks a 200 kpc radius, which corresponds to the distance between M31 and the observed MGC1.

Table 3.2: Number of cluster in each population in the encounter shown in Figure 3.2.

Total	Captured	Retained	Unbound	MGC1-like
1000	540	425	35	199

Hubble time. At the start of the trajectory (upper left in Figure 3.1) it is clear that the globular clusters are orbiting the dwarf galaxy. During the encounter tidal forces change the orbits of the globular clusters.

The left part of Figure 3.2 shows the distances between all objects in the simulation and M31. The figure uses the same colour coding as in Figure 3.1 for the cluster populations. The black dashed line marks the orbital separation between M31 and MGC1. This means that all MGC1-like clusters (green lines) pass through this line at least twice after the encounter, which happens at $t = 0$. The first time is when leaving M31 after the encounter. I neglected counting clusters passing the 200 kpc line the first time as MGC1-like, as they are easily associated with the dwarf galaxy.

The right hand side of Figure 3.2 shows a histogram of the number of clusters at each position at the end of the encounter. Note that the horizontal axis is logarithmic. The vertical axis of this plot is the same as for the left plot which means that the height of a bin in the histogram corresponds to the number of lines which hit it at $t = 12\,\mathrm{Gyr}$, i.e, the end of the simulation. The number of clusters in each population is given in Table 3.2. We find that roughly half of the clusters are stripped away from the dwarf galaxy during this particular encounter. We also find that about 20 % of the clusters end up being MGC1-like.

3.3 Properties of the cluster populations

It is interesting to investigate the orbital properties of the different cluster populations during the encounter to see whether there are any patterns that could give away the outcome already during the encounter. The tidal radius, which was described in Chapter 2 (see Equation 2.44), is one parameter that is especially interesting. Firstly, we expect that clusters which are stripped away from the dwarf galaxy should reside outside this radius. Secondly we expect that clusters are more easily stripped if they are on prograde orbits, compared to retrograde orbits.

Figure 3.3 shows the position of all clusters projected on the orbital plane of the dwarf galaxy, which is the same as the xy-plane in the simulated coordinate system, at $t = 0$ in the simulation. The dwarf galaxy trajectory (position) is marked in the plot with the black dashed line (black plus). The background of the plot gives the strength of the potential field that the dwarf galaxy and clusters move in. The M31 galaxy is positioned at $(0, 0)$ off the plot. The different tidal radii of the dwarf galaxy are illustrated with the red circles.

The clusters, marked with coloured circles according to what cluster population they end up in at the end of the simulation, show a few interesting features. Firstly, one should

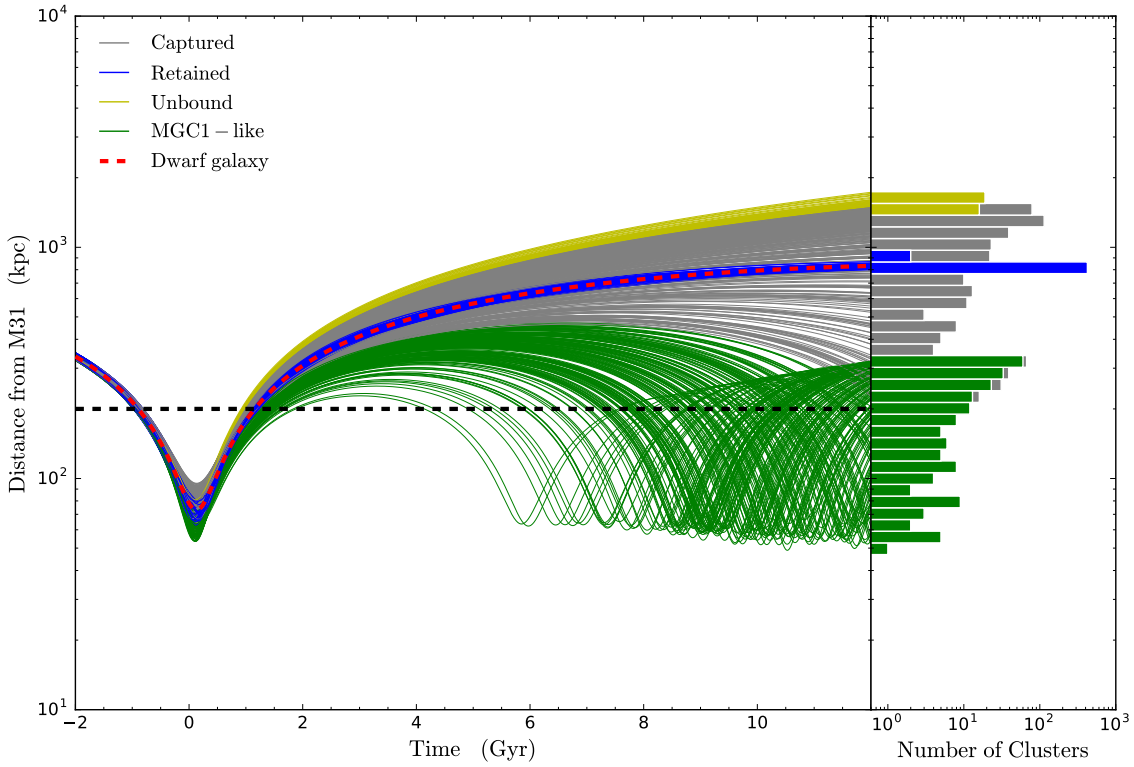

Figure 3.2: **Left:** Distance from M31 as function of time in a simulated encounter. The red dashed line shows the trajectory of the dwarf galaxy, while the thin lines show the trajectory of all globular clusters in the simulation. See legend for labels. The dwarf has its closest approach at $t = 0$. The black dashed line marks a distance of 200 kpc which corresponds to the observed distance between M31 and MGC1. **Right:** Histogram which gives the number of clusters at different bins of distance from M31 at the end of the simulation ($t = 12$ Gyr). The y-axis has the same scale as the left plot which implies that the height of each bin is directly proportional to the number of lines that hits that bin. The colours correspond to the fraction of clusters in the different populations as is given in the legend.

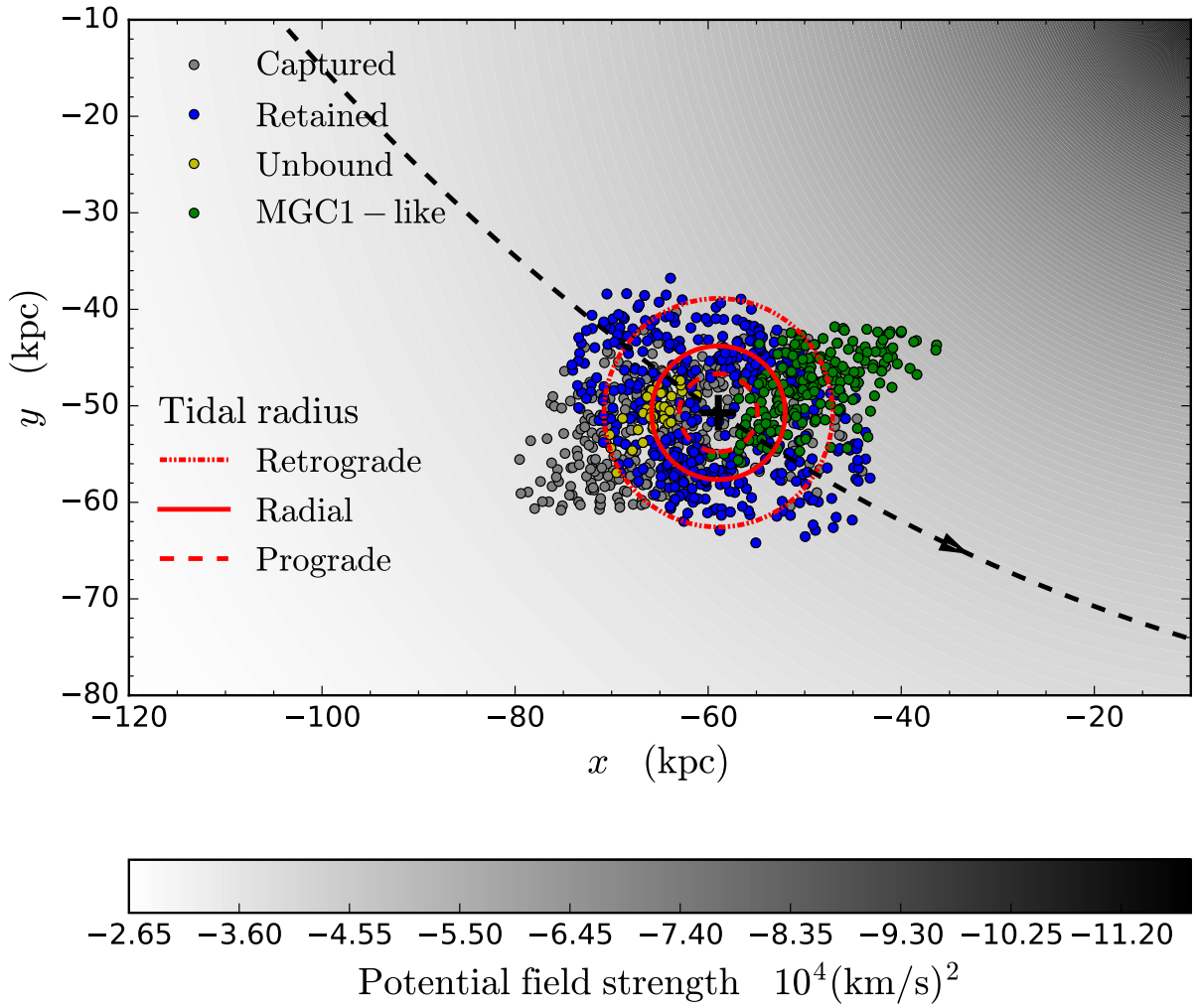

Figure 3.3: The spatial distribution of the globular clusters in the orbital plane of the dwarf galaxy when the dwarf galaxy is at its closest approach (i.e., $t = 0$). The black dashed line shows the trajectory of the dwarf galaxy before (upper left) and after (bottom right) the encounter. The clusters are colour-coded according to what population they ended up in after the encounter (see legend for labels). The background shows the total potential field strength from the M31 galaxy and the dwarf galaxy in units $10^4(\mathrm{km/s})^2$. The red lines (dot-dashed, filled, dashed) shows circles with radius given by the tidal radius (given by Equation 2.44) for retrograde, radial and prograde orbits respectively.

notice that the different populations are not randomly distributed in the plot but rather form groups. The retained clusters (blue) form an elliptical shape elongated along the trajectory of the dwarf galaxy. The majority of the clusters that are eventually stripped away from the dwarf are grouped together in a similar elliptical shape, but with a larger elongation. Furthermore, this elliptical shape is oriented with an offset from the direction of the trajectory. This elongated shape is especially prominent if considering only the unbound and MGC1-like clusters, which in some sense could be considered the extremes of the outcomes.

It should be noted that if one projects the separation between the retained clusters and the dwarf galaxy onto a line parallel with the direction between the dwarf galaxy and the M31 centre, all retained clusters fall within the tidal radius of retrograde orbits. This is not an obvious feature since the tidal radius formula derived in Chapter 2 depends on the assumption that both the M31 and the dwarf galaxy are point masses, which is not true in this case. Similarly, one would expect that all clusters that eventually are stripped away were to be located outside the prograde tidal radius, i.e, the tightest tidal radius. This is not the case, as multiple clusters within this radius were stripped away in the encounter. We find that the innermost clusters in the unbound and MGC1-like populations are positioned slightly further out compared to the captured and retained populations. It is expected that they should be located further out compared to the retained clusters. Focusing on the captured cluster, we would expect these to be placed outside the tidal radius, however, this is not the case. There are many clusters located well within the innermost tidal radius (prograde) which are stripped away in the encounter. This could hint that the distribution of mass (compared to the assumed point-mass potentials) is not negligible. This assumption especially breaks down close to the dwarf where the deviation from the point-mass assumption is largest.

Now focusing again on the elongated shapes that are clearly visible in the different groups in Figure 3.3. It is interesting to further investigate from where this originates. Figure 3.4 shows the same plot, however, now the cluster markers have been colour coded depending on whether the clusters are on prograde (top plot) or retrograde orbits (bottom plot). We find a clear correlation between the two different shapes and retrograde versus prograde orbits. First we consider only the retrograde (right plot) that reside on the top right side of the dwarf galaxy trajectory, i.e., within the orbit of the dwarf. As the dwarf moves closer toward the M31 galaxy these clusters will feel a gravitational force pulling them along their orbit around the dwarf galaxy. This will place the clusters in front of the dwarf galaxy, which can catch up to them as it pulls them in again. If we instead look at the clusters on the lower left side of the dwarf trajectory, i.e., outside the dwarf orbit, we find the opposite effect. The retrograde clusters will have their orbital velocity decelerated while ahead of the dwarf and as they move behind the dwarf they will be pulled to tighter orbits. This effect gives the retrograde cluster tighter orbits in the direction perpendicular to the dwarf trajectory, thus producing the elongated shape. After the encounter they are relaxed of this shape and the group return to a shape comparable to the original one, although a few clusters have diffused out to larger orbits. It would be interesting to see if multiple encounters could cause the retrograde globular cluster population to significantly

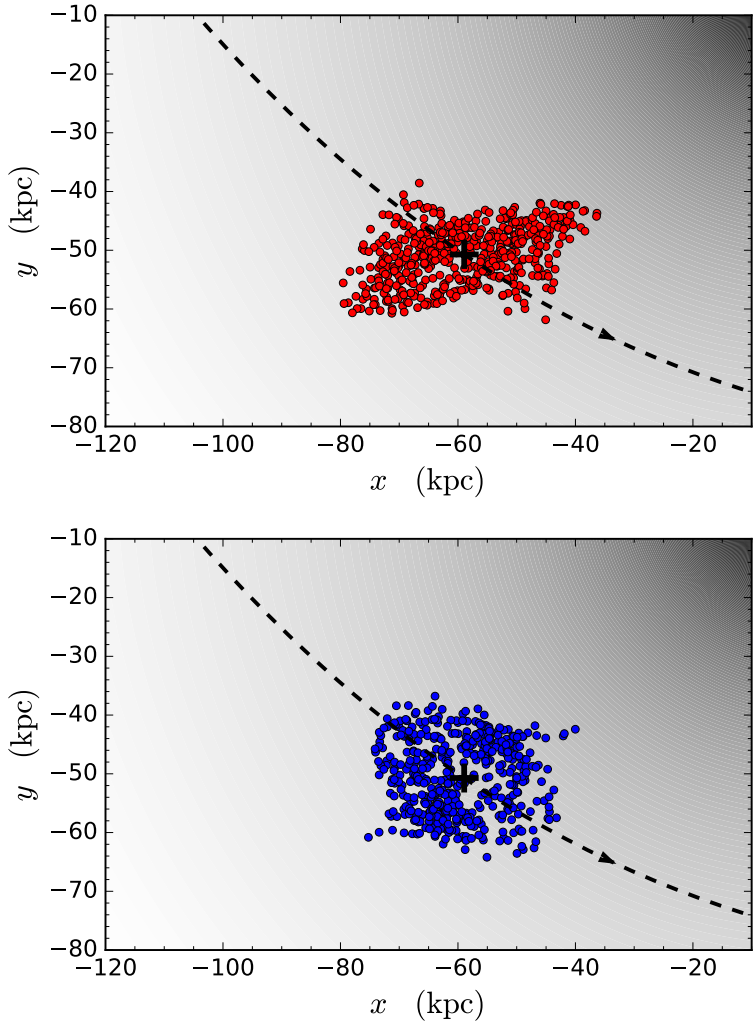

Figure 3.4: Top (bottom) plot shows the position of all prograde (retrograde) clusters when the dwarf is at the pericentre, i.e, $t = 0$. Axis and background is the same as in Figure 3.3.

diffuse the distribution.

Now focusing on the prograde population. The effect for these clusters will be opposite to that on the retrograde clusters as their orbital velocity around the dwarf is accelerated while outside the dwarf trajectory and decelerated as they are inside the trajectory. In contrast to what happens to the retrograde group this stretches the shape in the direction perpendicular to the dwarf trajectory. This effect is what eventually causes the prograde clusters to be tidally stripped away from the dwarf galaxy.

Since tidally stripping clusters away from the dwarf galaxy during an encounter has shown to depend strongly on whether their orbit is prograde or retrograde this was investigated further. To quantify to what degree a cluster is prograde or retrograde I used the scalar product between the normalized specific angular momentum vector of the dwarf orbit around M31 and all the normalized specific angular momenta of the clusters orbiting the dwarf galaxy,

$$\hat{\mathbf{J}}_s \cdot \hat{\mathbf{J}}_c = \frac{\mathbf{r}_s \times \mathbf{v}_s}{|\mathbf{r}_s \times \mathbf{v}_s|} \cdot \frac{\mathbf{r}_c \times \mathbf{v}_c}{|\mathbf{r}_c \times \mathbf{v}_c|}. \tag{3.8}$$

I indexed the dwarf galaxy with s and the cluster with a c. If a cluster has a prograde orbit in the plane of the dwarf galaxy orbit then this scalar product will be 1, while the same for a retrograde orbit would be -1. Depending on the offset from a co-planar orbit this value will have a value between 0 and either -1 or 1. An orbit where the orbital planes are perpendicular to each other the orbital orientation would be 0.

Figure 3.5 shows a histogram with fractions of clusters as function of the orbital orientation, quantified with the measure in Equation 3.8, for each of the cluster populations. We find clear evidence that retrograde clusters are less likely to be stripped away, while in contrast prograde clusters are more likely to be stripped away. We also find that for this particular encounter the unbound clusters are exclusively prograde. Nevertheless, it is important to note that this holds for this particular encounter and whether clusters are unbound from the system or not depends on several factors, where one of the most important factors is how bound the dwarf galaxy is to M31 in the first place.

One should however note that the likelihood of producing an MGC1-like cluster is larger for prograde clusters. Other than the fact that this encounter has a significant chance of leaving behind an MGC1-like cluster ($\sim$ 20%), this set of encounter parameters is not special and could represent an average encounter. Therefore, it might be a good idea to obtain a sense of whether clusters are retrograde or prograde when observing them in satellite galaxies.

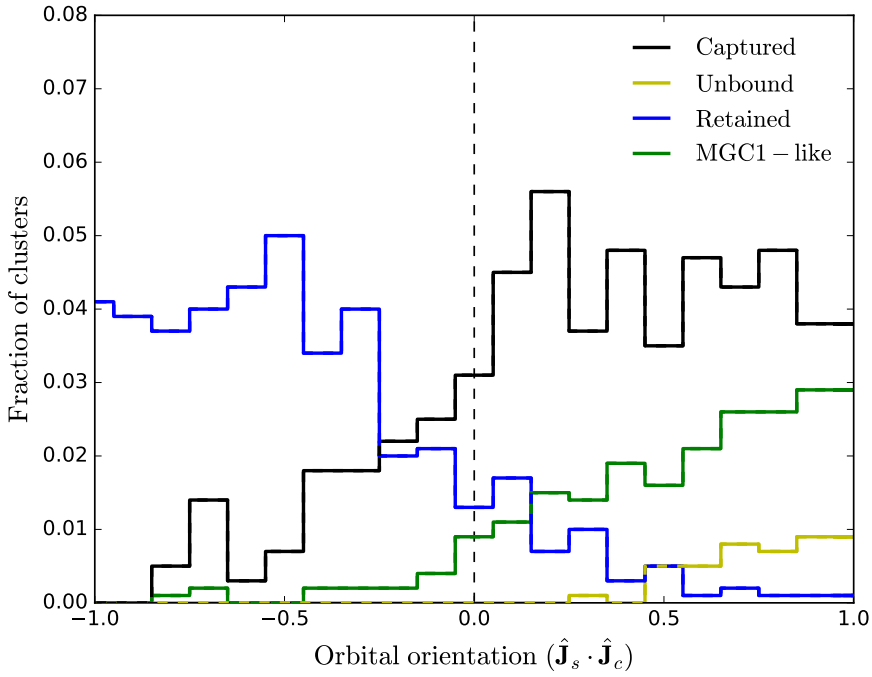

Figure 3.5: Histogram showing the fraction of clusters in different cluster populations for different orbital orientations, as is given by the scalar product between the normalized directions of the orbital planes (i.e., the directions of the specific orbital angular momentum for the dwarf galaxy orbit around M31 ($\hat{\mathbf{J}}_s$) and that of the cluster orbit around the dwarf galaxy ($\hat{\mathbf{J}}_c$)). A positive orbital orientation implies a prograde orbit for a given cluster, while a negative orbital orientation implies a retrograde orbit. An orbital orientation of zero implies a radial orbit, i.e., perpendicular orbital planes.

Chapter 4

Population of captured globular clusters

In this chapter I investigate how the likelihood of producing MGC1-like clusters depends on the dwarf galaxy parameters. The dwarf galaxy was modelled as a spherically symmetric Plummer model (see Section 2.2) in all simulations, for which I changed the mass and characteristic radius, see Equation 2.15. Through initial experimentation I found that the important characteristics of the dwarf galaxy trajectory can be described by specific total orbital energy and distance to M31 at closest approach (pericentre distance). I refer to an encounter as a simulation in which a dwarf galaxy, starting at some initial distance, r_0, with a population of globular cluster, moves along its trajectory passing the M31 galaxy after which it is integrated for 12 Gyr. The time at which the dwarf galaxy is positioned at the pericentre is defined as $t = 0$.

I remind the reader again that the globular cluster populations were divided into 3 groups and 1 subgroup after the encounter: **Captured** clusters, which end up on orbits bound to M31; **Retained** clusters, which remain bound to the dwarf galaxy; **Unbound** clusters, which end up unbound from either galaxies; **MGC1-like** clusters, which are clusters in the Captured population that have orbital properties that resemble those of MGC1. Details on each group is described extensively in Chapter 3. In addition to these groups I investigate my encounters with the separation to M31 versus time plot for all simulated trajectories (see, e.g., Figure 3.2). This plot is referred to as the SVT plot.

4.1 Dwarf galaxy initial conditions

In order to give a sense of how the probability of producing a MGC1-like cluster depends on the dwarf galaxy properties, I simulated different sets of encounters. Each encounter in a set had an unique trajectory, but the dwarf galaxy potential used, as well as the initial globular cluster population, was identical. Every set of encounters included a large number of encounters, which required an automated way of selecting initial conditions for these encounters. In this section I describe the process that I used to select these initial

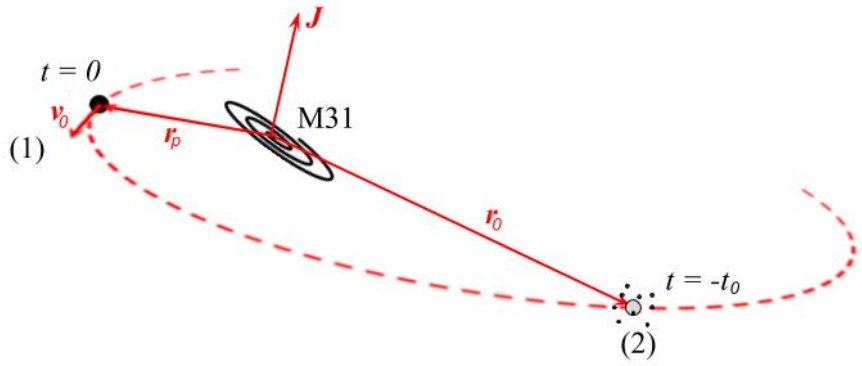

Figure 4.1: Geometric description of the parameters that determine the initial conditions for the dwarf galaxy in a encounter. The dwarf galaxy (black dot/circle) is initiated at location (1) at position $\boldsymbol{r}_p$ with velocity $\boldsymbol{v}_0$ and then integrated to a distance r_0 away from M31. At this location (2) the velocity of the dwarf is flipped and a globular cluster population is added. The time, t_0, that the integration takes is recorded and used to define the time-line as being $t = 0$ at the point of closest approach.

conditions. A geometric description of the variables that were used for this process is shown in Figure 4.1. The description of how each individual encounter was simulated, as well as how the initial globular cluster population was generated, is provided in Section 3.1.

The first step in selecting dwarf galaxy initial conditions was to select the position of the dwarf galaxy when it was at the closest approach to M31. Throughout this work this position is referred to as the pericentre position and it also defines $t = 0$ in the simulation. To obtain this position I generated a random point on a spherical shell through a method developed by Muller (1959). The procedure Muller (1959) used to select the random position on the shell is described in Section 3.1. The radius of this sphere was drawn between 0 and 120 kpc in such a way that pericentre positions were uniformly distributed within a sphere with a radius of the maximum pericentre distance, i.e, scales as r^2. A useful property of the trajectory at this position is that the direction of the trajectory is perpendicular to the radial direction with respect to M31.

After selecting a position I determined a velocity for the dwarf galaxy. The magnitude of this velocity is set by the total specific orbital energy of the dwarf. This energy was selected uniformly in a range which varied for different sets of encounters. With this energy selected, the velocity was readily available from the following equation:

$$E = \frac{1}{2}v_0^2 + \Phi(\boldsymbol{r}_p) \quad \Rightarrow \quad v_0 = \sqrt{2E + 2\Phi(\boldsymbol{r}_p)}. \tag{4.1}$$

The direction of the velocity was generated by randomly selecting the direction of the orbital vector (same the normalized angular momentum vector) and then taking the cross

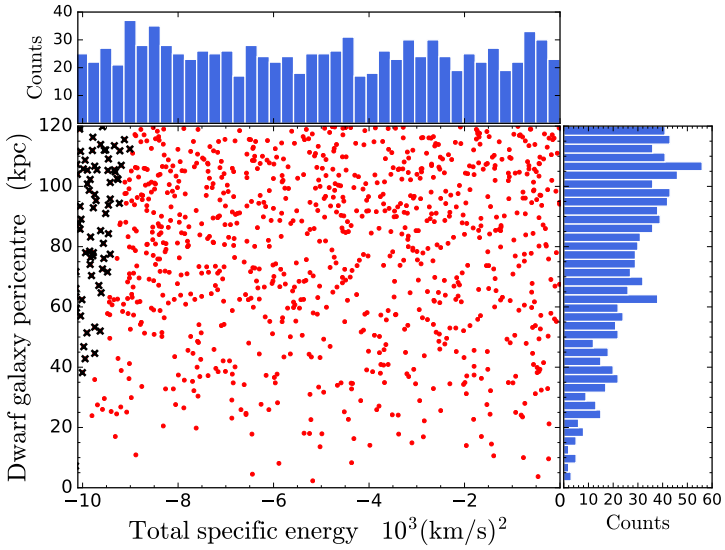

Figure 4.2: Distribution of dwarf galaxy total specific orbital energy as a function of dwarf galaxy pericentre. Red marks show a sample of dwarf galaxies generated with the sampling algorithm. Black crosses show encounters which were terminated due to not reaching r_0 within a Hubble time. The histograms show the counts in each parameter, i.e., the distribution of each initial condition.

product,

$$\boldsymbol{v}_0 = v_0 \left[\hat{\boldsymbol{J}} \times \frac{\boldsymbol{r}_p}{|\boldsymbol{r}_p|} \right] . \tag{4.2}$$

$\hat{\boldsymbol{J}}$ was generated in a similar way as $\boldsymbol{r}_p$, but instead using a unit sphere.

When the dwarf galaxy position and velocity had been selected the dwarf was integrated to some initial distance, r_0, where the direction of the trajectory was reversed. The time it took to integrate the dwarf to this position was recorded and used as a benchmark for setting $t = 0$ of the simulation. A globular cluster population was added to the dwarf galaxy and the encounter was simulated until $t = 12\,\mathrm{Gyr}$.

As an example, Figure 4.2 shows a sample of initial conditions for a typical set of encounters. The x-axis, including the histogram with the corresponding axis, shows the distribution in the total specific energy, while the y-axis shows the distribution in pericentre distances. Taking into account the Poisson noise that is present in any randomly generated sample, we find that there is no preferred energy. The distribution of pericentre distances appears weighed toward larger values, because the selection method picks random points homogeneously within the given range. A larger radii implies a sphere with larger surface area which means that more points have to be picked to obtain the homogeneous distribution.

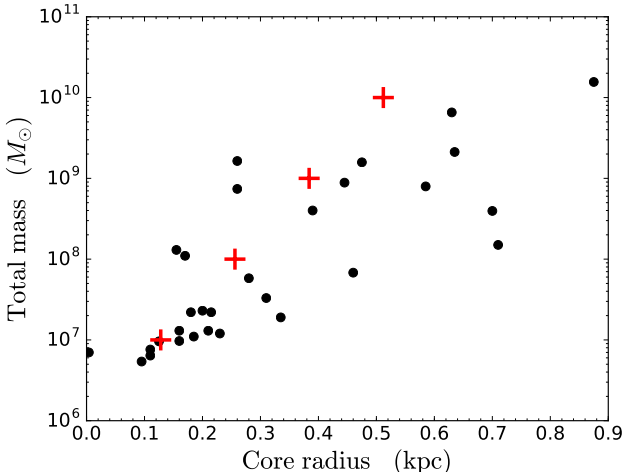

Figure 4.3: Total mass as function of core radius (characteristic radius) for observed local group galaxies (see Mateo, 1998). The core-radius corresponds to the radius where the mass drops to approximately half of the total mass. The core radius of the models used for the simulated dwarf galaxies have been plotted (core radius is $\approx 0.64\, r_{\rm plum}$). Observations are marked with black dots and parameters used in this work are marked with red crosses.

4.2 Encounter properties and their relation to the produced globular cluster population

We are interested in investigating whether there are any clear trends that relate the fraction of MGC1-like clusters and the properties that describe certain dwarf galaxy trajectories. In order to do so I produced a large set of simulations comparable to the one described in Chapter 3. The model used for the M31 galaxy for all simulations was the one fitted to the Geehan et al. (2006) model (see Chapter 2 for details). I focused on four different dwarf galaxy models, all modelled by a Plummer model. The parameters are given in Table 4.1 or plotted as red crosses in Figure 4.3. This figure also includes the same paramters for a sample of observed Local Group dwarf galaxies (black dots), obtained from Mateo (1998). For each galaxy I simulated 500 encounters, each with a unique total specific energy (defining its velocity at $t = 0$) and pericentre distance. For all simulations I choose an initial distance $r_0 = 500\,$kpc, which implies that we limit the total specific energy of the dwarf galaxy to be $> \Phi(r_0) \sim -10000\,(\mathrm{km/s})^2$. The dwarf galaxy would otherwise not have enough kinetic energy to reach this distance, even if travelling purely in the radial direction. This means that dwarf galaxies in the lower end of the energy distribution might not reach the initial position. The black crosses shown in Figure 4.2 are encounters in which the dwarf failed to reach r_0 within a Hubble time. These encounters were not simulated.

For each encounter I used a globular cluster sample of 1000 independent clusters in order to obtain a statistically robust estimate of the MGC1-like fraction. These samples were distributed according to the method explained in Section 3.1, in which the radial

Table 4.1: Limits within which globular clusters are distributed for different dwarf galaxy masses. The inner limit is set to prohibit the tidal stripping of the globular cluster by the dwarf galaxy (see Equation 3.5), while the outer limit is set so that the globular clusters are not tidally stripped before having some time to fully randomise in the dwarf (see Equation 3.6)

Mass	Scale-radius	$r_{\min}$	$r_{\max}$
$M_\odot$	kpc	kpc	kpc
10^7	0.2	0.13	3.9
10^8	0.4	0.38	8.27
10^9	0.6	0.76	17.7
10^{10}	0.8	1.19	37.94

extent of the clusters depend on the mass of the dwarf galaxy. The radial limits are shown in Table 4.1.

In this section I will discuss different sets of encounters. Each set of encounters is a group of simulations in which all dwarf galaxies have the same potential model, same globular cluster population and total specific energy restricted to be within a given range. The properties that vary in a specific set of encounters is that each dwarf galaxy trajectory is unique. That implies different pericentre distances, selected in the entire pericentre range considered, and different orbital orientations for the incoming dwarf. The energy bins were defined to have 10 different energy bins within the range going from very bound orbits ($E = -9000\,(\mathrm{km/s})^2$) to parabolic orbits ($E = 0\,(\mathrm{km/s})^2$). Each bin has a width of $1000\,(\mathrm{km/s})^2$ and the centre of each bin is given in Table 4.2. This table also includes information about the resulting number of clusters in each globular cluster population.

It is worth discussing the total specific energy, which is used frequently throughout this chapter. The total specific energy is the sum of the potential energy and kinetic energy per unit mass. This is a conserved quantity which is directly related to the velocity a particle have if it would be moved to infinity. The reason for using this quantity rather than the mentioned velocity is because it is well defined even for bound orbits, in contrast to the velocity at infinity which would take a non-physical (imaginary) value. To put the quantity in context consider the space that we use for it. The simplest case is when the total specific energy is zero, which would result in a parabolic trajectory. This is the upper limit that is considered for all but one dwarf galaxy mass. The other limit is that when the dwarf galaxy has exactly enough kinetic energy to reach the position r_0. For our potential field such a trajectory has a total specific energy of $\sim -10^4\,(\mathrm{km/s})^2$.

Dependence on dwarf total specific energy

There is a clear trend between the total specific energy of the incoming dwarf galaxy and the fraction of MGC1-like clusters that is produced in the encounter. This trend appears for all dwarf galaxy masses, see Figures 4.4 and 4.5. Figure 4.4 shows that for the masses

Table 4.2: Energy bins that were used to divide up the encounters. Each bin has a width of $10^3\,(\mathrm{km/s})^2$ and the centre of each bin is shown in the energy row.

Name	E0	E1	E2	E3	E4	E5	E6	E7	E8	E9
Energy $10^3\,(\mathrm{km/s})^2$	−9	−8	−7	−6	−5	−4	−3	−2	−1	0
$\boldsymbol{M_s = 10^7\,M_\odot}$										
Encounters	22	57	46	45	55	46	40	47	44	50
Clusters	22000	57000	46000	45000	55000	46000	40000	47000	44000	50000
Captured	14637	34951	26518	24649	31039	25323	21306	26455	21335	15272
Retained	7363	22049	19482	20351	23961	20677	18694	20451	21451	24578
Unbound	0	0	0	0	0	0	0	94	1214	10150
MGC1-like	7479	11541	565	20	4	0	0	0	0	0
f_{mean}	0.34	0.202	0.012	0.0	0.0	0.0	0.0	0.0	0.0	0.0
$\boldsymbol{M_s = 10^8\,M_\odot}$										
Encounters	20	56	53	52	44	47	39	52	42	45
Clusters	20000	56000	53000	52000	44000	47000	39000	52000	42000	45000
Captured	13492	32767	30178	29258	24428	24383	19714	22660	14034	11758
Retained	6508	23233	22819	22714	19509	22496	18782	26299	19932	22503
Unbound	0	0	3	28	63	121	504	3041	8034	10739
MGC1-like	6734	14093	9517	2954	483	99	37	22	4	0
f_{mean}	0.337	0.252	0.18	0.057	0.011	0.002	0.001	0.0	0.0	0.0
$\boldsymbol{M_s = 10^9\,M_\odot}$										
Encounters	13	44	40	53	43	46	49	46	56	47
Clusters	13000	44000	40000	53000	43000	46000	49000	46000	56000	47000
Captured	8254	26069	23479	28327	20635	18895	16559	13811	14788	11211
Retained	4667	17630	15951	23278	19841	20457	24065	22191	28238	23986
Unbound	79	301	570	1395	2524	6648	8376	9998	12974	11803
MGC1-like	3876	11897	9977	11080	7084	5571	2602	1153	515	231
f_{mean}	0.298	0.27	0.249	0.209	0.165	0.121	0.053	0.025	0.009	0.005
$\boldsymbol{M_s = 10^{10}\,M_\odot}$										
Encounters	8	33	25	45	32	42	33	25	25	20
Clusters	8000	33000	25000	45000	32000	42000	33000	25000	25000	20000
Captured	4047	13764	8797	15017	9776	12155	9024	6281	5331	4192
Retained	2604	14197	11780	20864	14842	19748	15238	12460	14021	11292
Unbound	1349	5039	4423	9119	7382	10097	8738	6259	5648	4516
MGC1-like	1392	4991	3765	7406	5508	7277	5521	4068	3422	2659
f_{mean}	0.174	0.151	0.151	0.165	0.172	0.173	0.167	0.163	0.137	0.133

$10^7\,M_\odot$, $10^8\,M_\odot$, $10^9\,M_\odot$ the MGC1-like fraction steadily decreases with increasing total specific energy, while for the $10^{10}\,M_\odot$ dwarf this is shown in Figure 4.5. The rate of this decrease appears to scale with the mass of the dwarf galaxy where lower mass gives a faster decrease with increasing total specific energy. This is the reason for using a larger range of total specific energies for the dwarf galaxy with largest mass.

There are two reasons for this trend. Firstly, due to the fact that there are clusters on wider orbits in the larger mass galaxies these tend to increase the number of clusters which are stripped away during the encounter, see Table 4.2. Although, this allows more clusters to end up on orbits separated from the dwarf galaxy, it does not necessarily give them MGC1-like orbits. On the contrary, clusters that initially have wide orbits in the dwarf tend to be stripped away and left on orbits similar to that of the dwarf, therefore not returning to M31 within the simulated time.

The second reason believed to contribute to this trend is the interplay between gravitational forces from M31 and the dwarf galaxy at $t = 0$. As was shown in Chapter 3, if a cluster is on a prograde orbit interior of the dwarf galaxy trajectory, and subsequently tidally stripped away from the dwarf galaxy, then the dwarf galaxy will exert a gravitational force on the clusters as it is leaving the dwarf potential. This gravitational tug will reduce the kinetic energy of the cluster, which in turn implies that if the clusters is captured by M31 it will be more strongly bound to the M31 potential compared to if the cluster retains a large portion of its kinetic energy. For the encounters that I test this will in most cases increasing the likelihood of giving it a MGC1-like orbit. This effect is stronger for more massive dwarf galaxies, since the gravitational tug from them is larger. This effect becomes even more clear if we instead consider the clusters that end up in the unbound population. The gravitational tug is much stronger for more massive dwarf galaxy, which increases the *catapult effect* that converts the potential energy from the dwarf potential into kinetic energy, eventually throwing the clusters out of the system.

Now focusing on Figure 4.5, which shows the MGC1-like fraction as function of total specific energy for the $10^{10}\,M_\odot$ dwarf galaxy, for which I considered not only bound orbits but hyperbolic encounters as well. I found that for the sets of encounters simulated for this dwarf galaxy, the fraction of MGC1-like clusters plateaus at ~ 0.17 for the energy bin E7 ($-2 \times 10^3\,(\mathrm{km/s})^2$), and then even decreases for more bound trajectories. It is unclear whether this trend could show up in sets of encounters with smaller mass galaxies if lower total specific energies were considered. Because of the fact that most clusters that are stripped tend to end up on orbits similar to the original host orbit we would expect a steep increase in MGC1-like fraction around the total specific energy of the MGC1-cluster.

Since the proper motions for this cluster is not known it is difficult to estimate what this energy would be, nevertheless, we can constrain it with some assumptions. If the MGC1-cluster would be on a circular orbit then its total specific energy would be $\sim -12.8 \times 10^3\,(\mathrm{km/s})^2$. Additionally, we are biased to observing it when it is located at its apocenter position simply due to the fact that this is where it will spend most of its time. We can also consider the fact that it has an extremely remote position, although it is still likely bound to M31, which increases this bias even more. If it is the case that it is at the apocenter position then the mentioned energy is an upper limit for the total specific energy of MGC1.

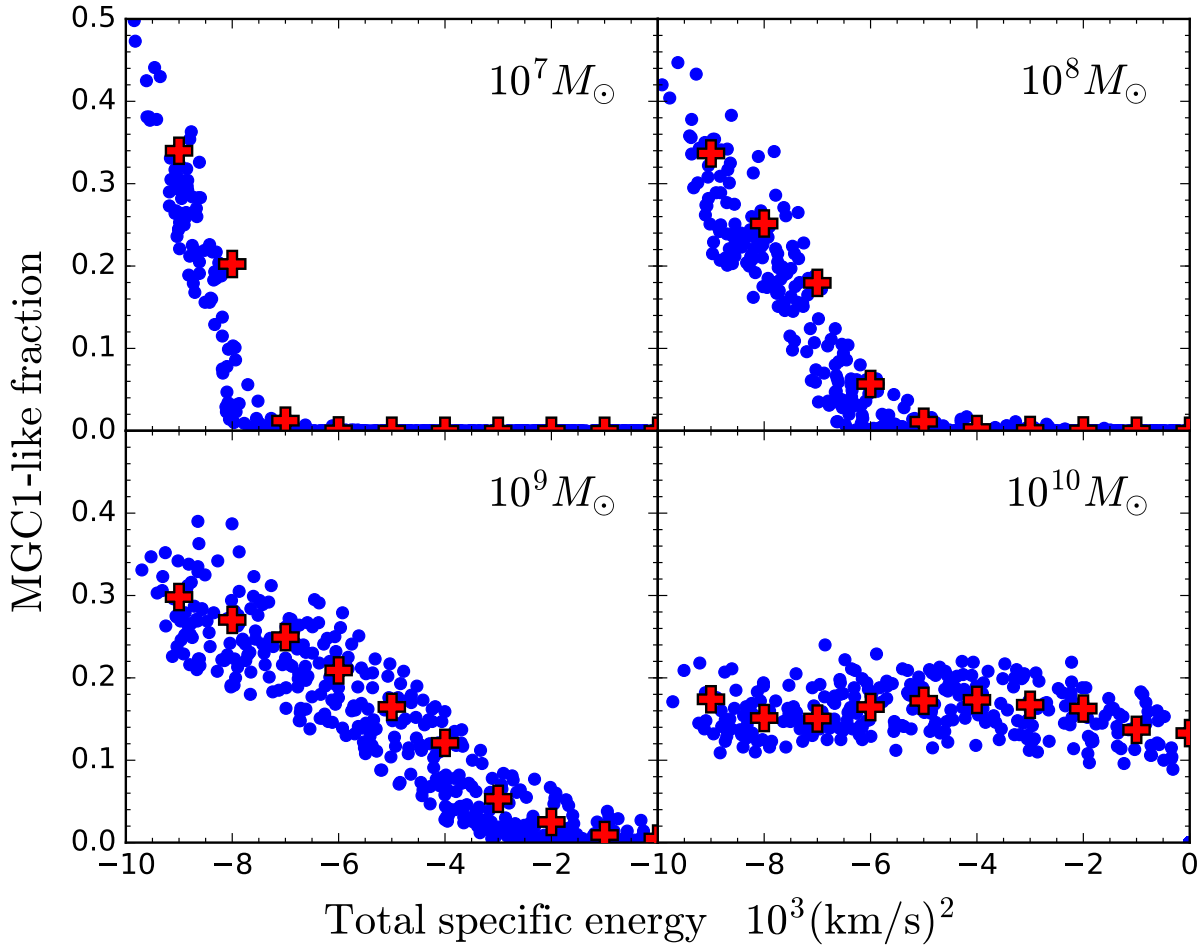

Figure 4.4: Plots showing fraction of MGC1-like clusters as function of dwarf galaxy total specific energy. Red plus-signs shows the mean for all clusters in a specific energy bin. Each energy bin is defined in Table 4.2

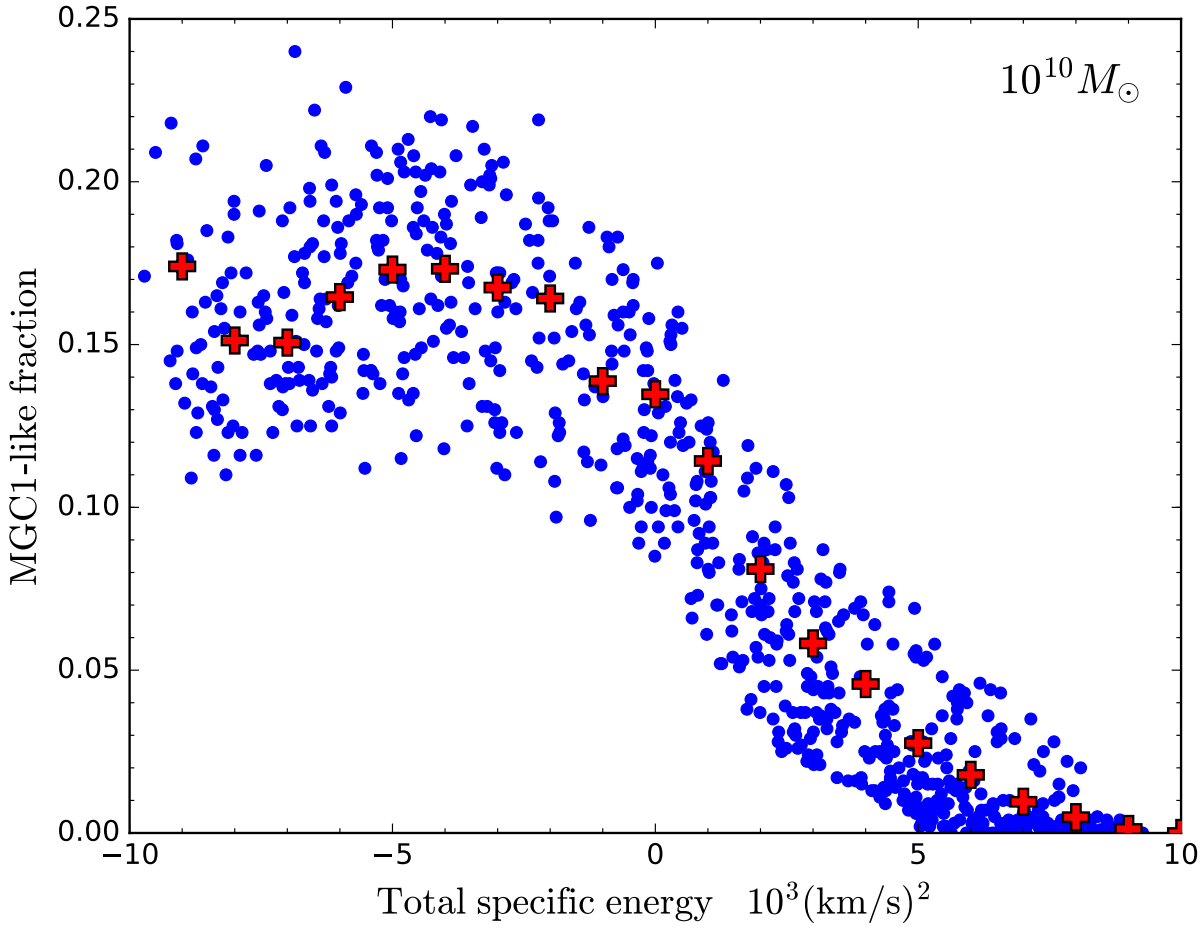

Figure 4.5: Same as lower right plot in Figure 4.4, however, now including encounters with a hyperbolic dwarf trajectory, i.e., total specific orbital energy larger than 0. Red plus-signs show the mean for all clusters in a specific energy bin. Each energy bin is defined in Table 4.2 and 4.3.

It would be interesting to explore if there is a peak around this point for all dwarf galaxy masses.

Another interesting feature in the $10^{10}\,M_\odot$ dwarf galaxy is that the number of MGC1-like clusters and the number of unbound clusters is surprisingly similar for the energy bins at the ends of the energy distributions, compared to all other dwarf galaxy masses. This can be seen by comparing the numbers in Table 4.2.

Dependence on dwarf pericentre

In Chapter 2 I showed the derivation of an expression for the tidal radius, see Equation 2.44 (see also Read et al., 2006). We found in this equation that the tidal radius should scale linearly with the pericentre distance. If we assume that the fraction of MGC1-like clusters

Table 4.3: Energy bins that were used for the hyperbolic encounter with a $10^{10}\,M_\odot$ dwarf galaxy. Each bin has a width of $10^3\,(km/s)^2$ and the centre of each bin is shown in the energy row. The last row shows the mean of the MGC1-like fraction in the bin.

Name	E10	E11	E12	E13	E14	E15	E16	E17	E18	E19
Energy $10^3\,(km/s)^2$	0	1	2	3	4	5	6	7	8	9
$\boldsymbol{M_s = 10^{10}\,M_\odot}$										
Encounters	42	37	52	51	58	59	52	62	48	9
Clusters	42000	37000	52000	51000	58000	59000	52000	62000	48000	9000
Captured	9465	7489	10161	10138	10331	10045	8012	8808	5973	889
Retained	21329	20679	29100	26907	32119	33164	30134	36714	29763	6231
Unbound	11206	8832	12739	13955	15550	15791	13854	16478	12264	1880
MGC1-like	4798	2999	3028	2333	1600	1053	498	301	59	0
$f_{\rm mean}$	0.114	0.081	0.058	0.046	0.028	0.018	0.01	0.005	0.001	0.0

scales with the fraction of the number of clusters that are stripped away from the dwarf galaxy then we could expect a linear relation between the fraction of MGC1-like clusters and pericentre distance for a given energy bin. In Figures 4.6 and 4.7 I have plotted the MGC1-like fraction as function of pericentre distance and colour-coded the energy bins according to the labels shown in the legend of the two figures. Note that the vertical axes have logarithmic scale, thus not showing encounters where the MGC1-like fraction is zero. In the figures I also include a line for each energy bin, which is a linear fit to the data. The fitting method used was a simple least-squares fit. I find that the trends give the best fit for larger mass galaxies in the energy bins which have the smallest value in total specific energy. The reason for this is that in encounters with smaller numbers of clusters becoming MGC1-like the statistical noise increase. For the set of encounters with the $10^{10}\,M_\odot$ dwarf galaxy, I include the hyperbolic trajectories (marked with stars and squares). The energy bins and encounter numbers are listed in Table 4.3.

To understand the difference between encounters in which the dwarf galaxy pericentre are similar, while the fraction of MGC1-like cluster differ significantly I selected two encounters for each dwarf galaxy mass. The selected encounters all have a pericentre distance of approximately 60 kpc. For these encounters I show the SVT plot for all the selected clusters in Figure 4.8, where the left plots show the encounters with small MGC1-like fraction and right plots show the large MGC1-like fraction. Note that for all different masses the difference in MGC1-like fraction depends on how bound the dwarf galaxy is to M31, as was shown in Figures 4.6 and 4.7.

What we learn from the plots shown in Figure 4.8 is that the mass of the dwarf galaxy plays an important role in the orbits of the captured clusters. Larger dwarf galaxies change the orbit of the captured clusters significantly compared to the smaller mass galaxies. For the $10^9\,M_\odot$ and $10^{10}\,M_\odot$ mass dwarf galaxies the gravitational tug is larger during the encounter so orbits change more significantly. We see this both in the fact that these type of encounters throw more clusters out of the system but also in the distribution of captured clusters. These captured clusters have orbits which are more bound to M31 compared to

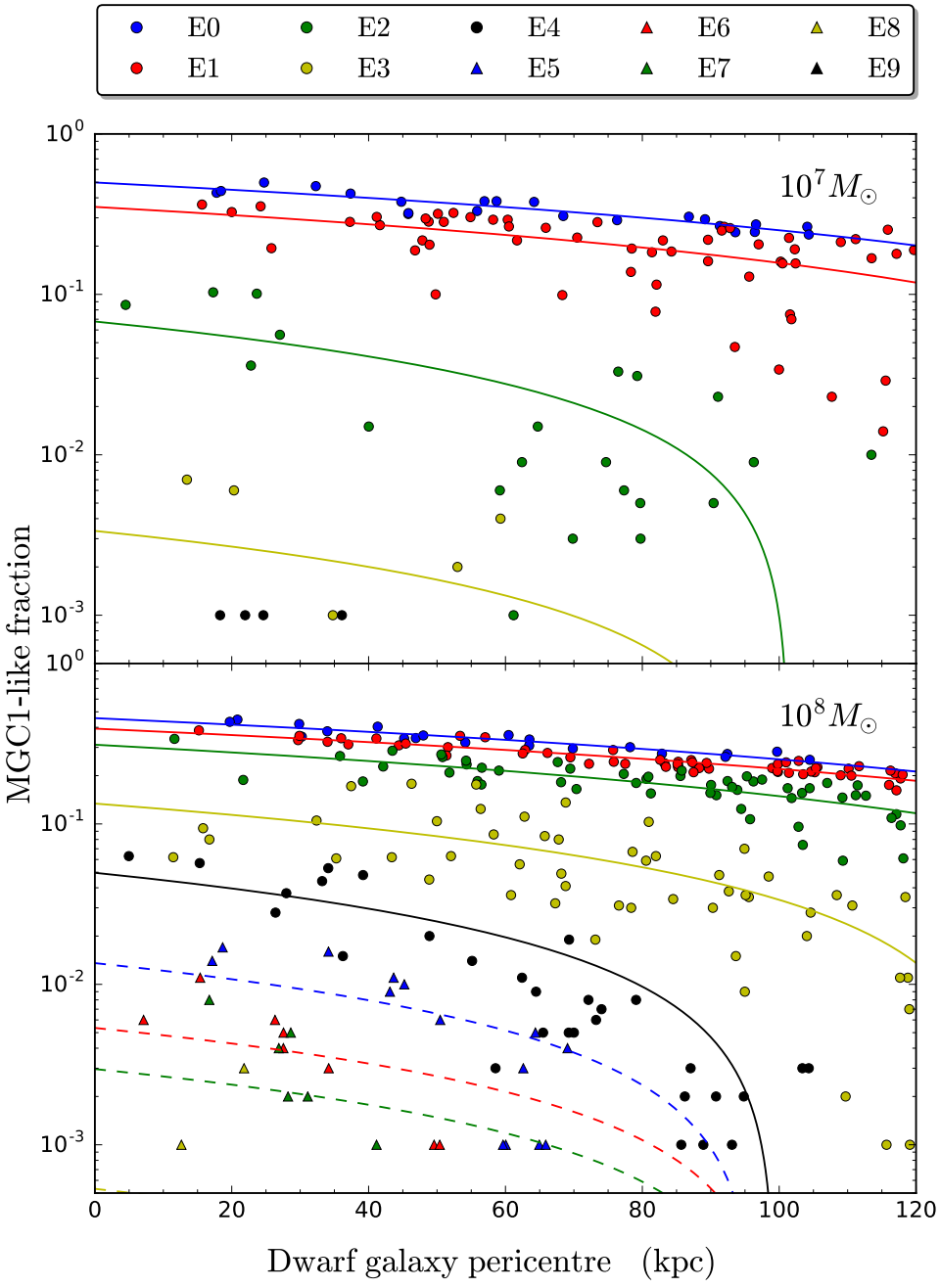

Figure 4.6: Plot of MGC1-fraction as function of dwarf galaxy pericentre distance for dwarf galaxy mass of $10^7\,M_\odot$ (top) and $10^8\,M_\odot$ (bottom). The data was binned in energy bins (see Table 4.2 for bin definitions) and coloured according to legend. A line was fitted to the data in each bin to highlight the correlation between MGC1-like fraction and pericentre distance for a given energy. Lines are coloured in the same colour as markers, where filled lines correspond to dots and dashed lines correspond to triangles.

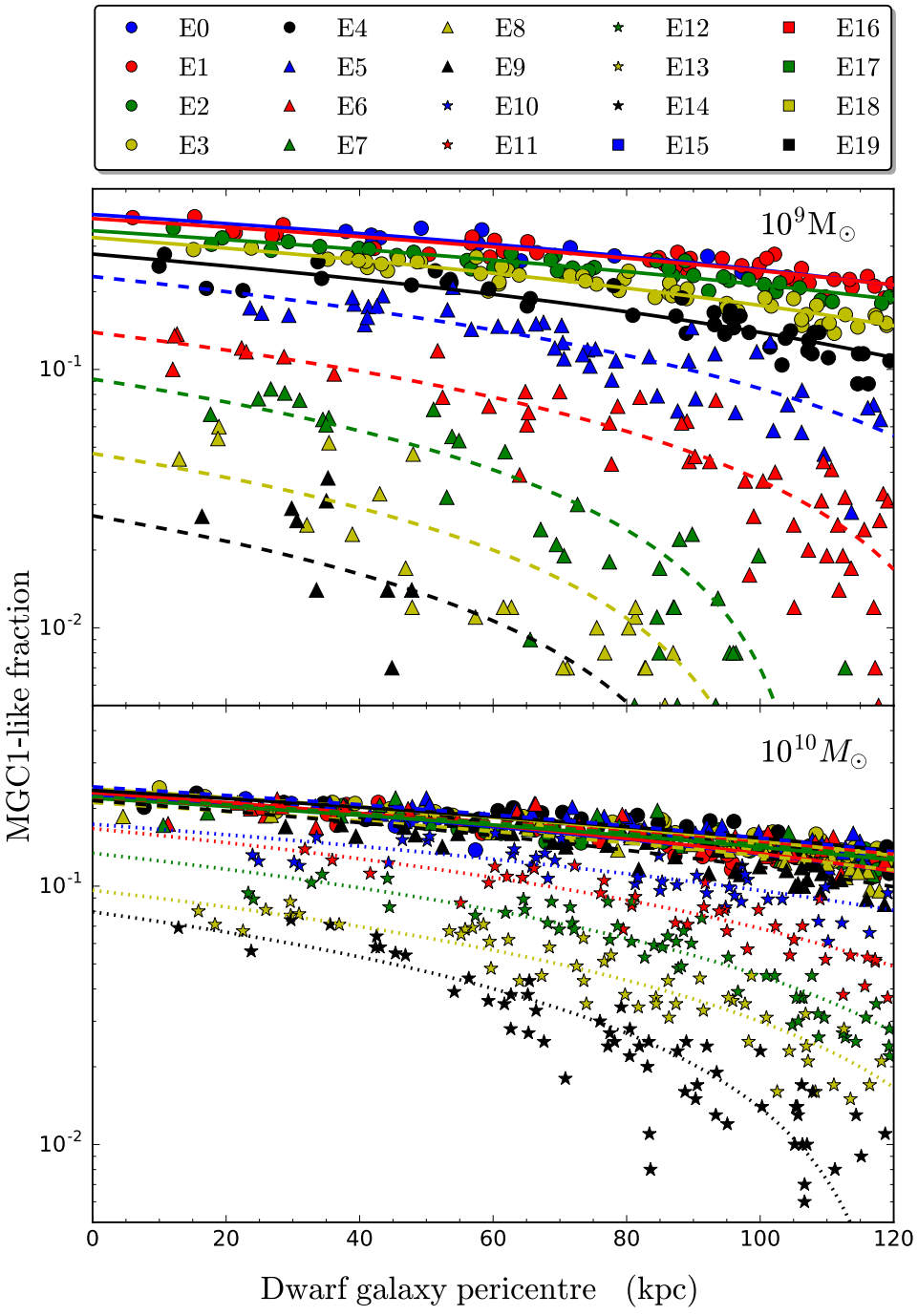

Figure 4.7: Plot is the same as Figure 4.6 but for dwarf galaxy masses $10^9\,M_\odot$ (top) and $10^{10}\,M_\odot$ (bottom). Note that some bins (squares) does not show up in the plot, due to MGC1-like fraction of zero.

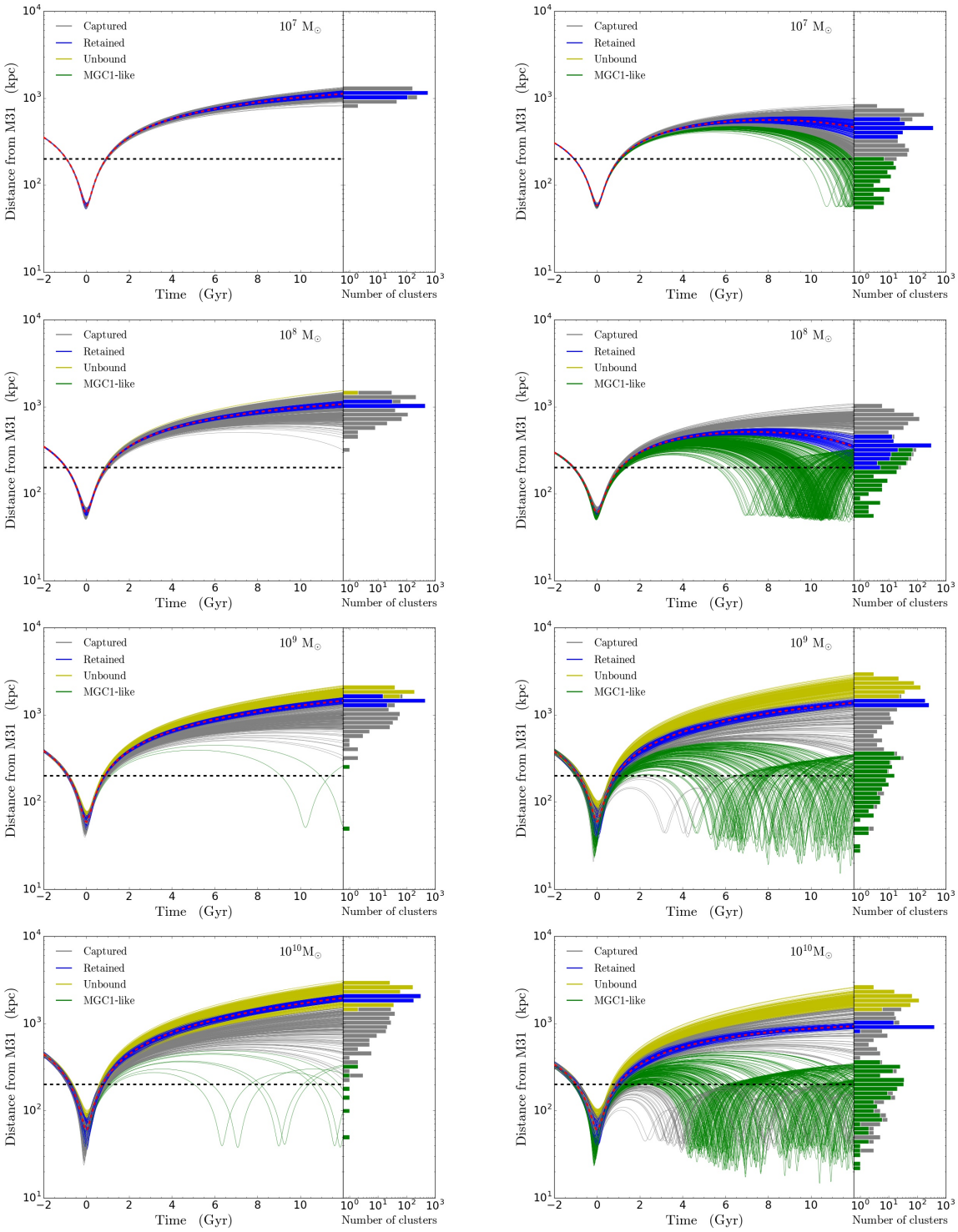

Figure 4.8: Plots showing separation between M31 and all clusters as function of time (SVT) for 8 different encounters, all with a dwarf pericentre distance of ~ 60 kpc. Plots are the same as for Figure 3.2. Each row includes two encounters with the same dwarf galaxy potential, but selected as to have one encounter with a small MGC1-like fraction (left) and one with large MGC1-like fraction (right).

the captured clusters in the lower mass dwarf galaxies. For the $10^{10}\,M_\odot$ dwarf galaxy there is even a population of clusters which are too bound to reach the 200 kpc distance, which implies that they do not count as MGC1-like clusters. This, in combination with retaining more clusters, is the reason for fewer MGC1-like clusters.

Dependence on dwarf trajectory orientation

An important property that we are interested in exploring is whether the trajectory orientation of the incoming dwarf galaxy will affect the likelihood of producing MGC1-like clusters. This could be the case due to the asymmetry of the M31 potential close to the galaxy, which arises due to the fact that the galaxy has a disc. This is interesting to explore because if the effect is negligible, we would expect that all outer clusters that are accreted should not show any preferred orbital direction. This would be a clear contrast to the globular clusters that have been formed *in-situ*, as these clusters would preferably orbit in the direction of the disc rotation. The reason for this is that they form from material in the galactic disc, and thus obtain the orbital properties of this material. This could reveal an observable dichotomy between accreted and *in-situ* globular clusters.

Figure 4.9 shows the direction of the orbit (i.e. the normal to the orbital plane) for all $10^9\,M_\odot$ encounters. The fraction of MGC1-like clusters is plotted as a colour gradient on each marker. Firstly, it is worth noting that the distribution of these orbital directions are homogeneous on the projected sphere, which indicate that there is no preferred direction in our initial conditions. Secondly we find that there is no obvious trend between the fraction of MGC1-like clusters and this direction. This was investigated for all sets of encounters and no such trend was found for any of them. This is an interesting result which I will investigate more thoroughly in Chapter 5.

4.3 Likelihood of producing MGC1 for different sets of encounters

I have shown how the fraction of MGC1-like clusters depends on different encounter properties. I will now go one step further and investigate what the actual number of MGC1-like clusters could be for different types of dwarf galaxies. In Chapter 2, it was mentioned that there is a known empirical relation between the mass one expects to find in globular clusters for a given galaxy mass, see Equation 2.14. However, as has been noted by several authors before (see, e.g., Renaud, 2018, for a review), lower mass galaxies in the Local Group deviate from this relation. If we look at the dwarf galaxies with known globular cluster populations in the Local Group this becomes very clear. In Figure 4.10, I plot the number of globular clusters as function of host galaxy mass from the clusters observed by Mateo (1998). I also show the relation which was estimated in Equation 2.14 in this figure. The figure shows that the relation underestimates the number of globular clusters for almost all low mass galaxies.

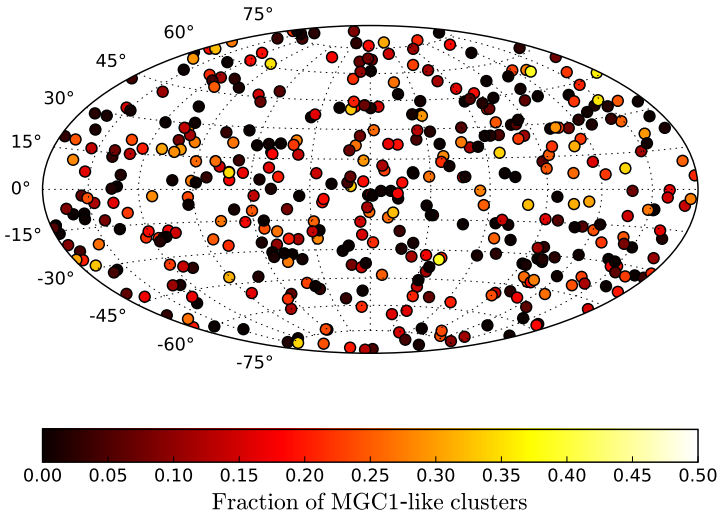

Figure 4.9: The distribution in dwarf galaxy orbital vectors for the set of encounters with $10^9\,M_\odot$ dwarf galaxies. The markers are colour-coded with the fraction of MGC1-like clusters. The distribution, both in position and colour, is similar for all sets of encounters. Note that the roughly homogeneous distribution of incoming dwarfs serves as a sanity-check to show isotropy in incoming trajectories for the method of selecting initial conditions.

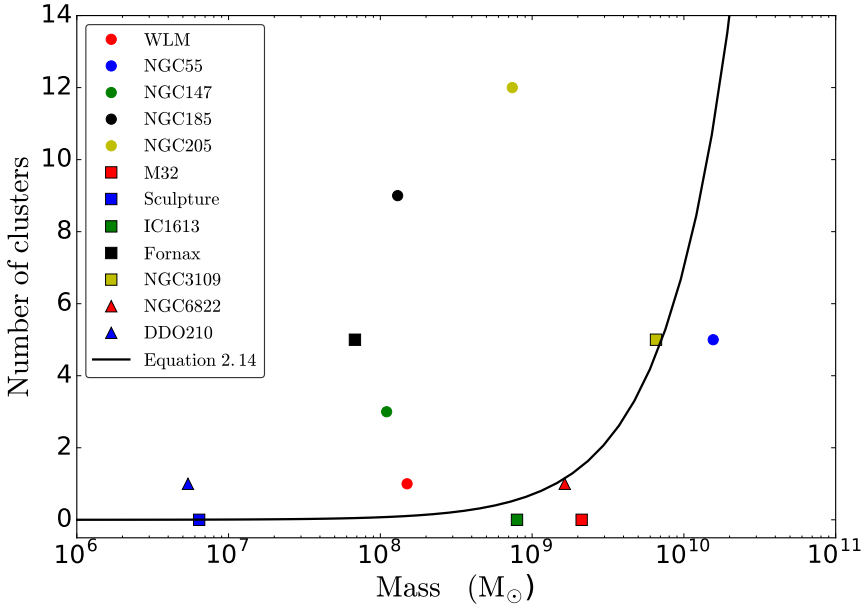

Figure 4.10: Observed number of clusters in Local Group dwarf galaxies from Mateo (1998) as function of the dwarf galaxy mass. The line shows the empirical relation (Equation 2.14) found in larger galaxies and galactic groups, see Renaud (2018) for a review.

If one assumes that this is a property linked to the formation of globular clusters this discrepancy could come from the fact that smaller mass galaxies are more sensitive to tidally stripping away their cluster populations. If we assume that for my simulated dwarf galaxies the number of such encounters are very limited then this effect could be minimized. In Figure 4.11 I show the expected number of MGC1-like clusters for all encounters that I have simulated, assuming the relation in Equation 2.14. To compare with the known properties of the Local Group I created the same plot but now assuming that each dwarf galaxy hosts 5 globular clusters before the encounter. It should be noted that this is a very crude approximation.

If we assume that the number of clusters can be approximated by Equation 2.14 (shown in Figure 4.11) we find that the number of MGC1-like clusters per encounter is significantly larger in encounters with the large mass galaxies. This is due to the fact that they host more globular clusters to begin with. If we on the other hand look at clusters where I assumed a constant number of globular clusters regardless of dwarf galaxy mass we find an interesting trend. For the smallest mass galaxies the number of MGC1-like clusters peak for the most bound dwarf galaxies. Furthermore, when the mass of the dwarf galaxy increases the number of clusters remains constant up to a certain specific total energy before decreasing with a similar gradient as for the lower mass galaxies.

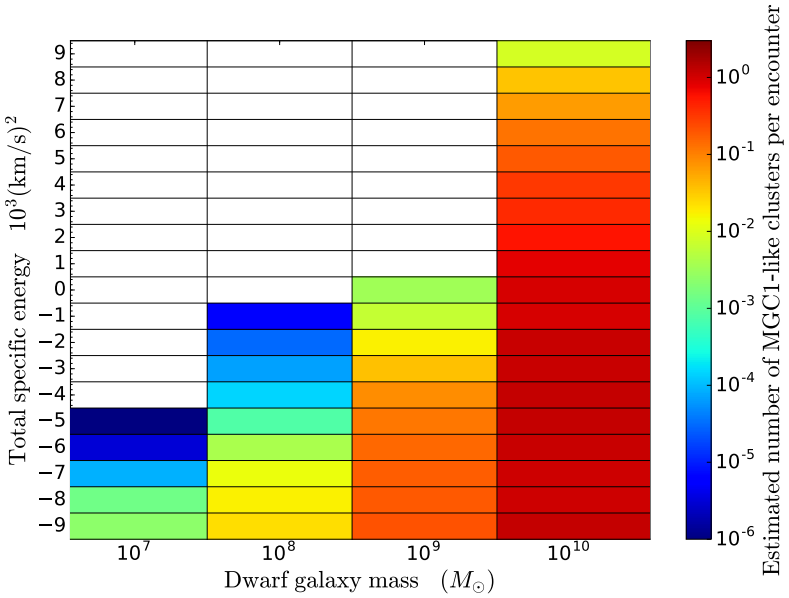

Figure 4.11: Expected number of MGC1-like clusters per encounter colour-coded on binned set of encounters characterized by dwarf galaxy mass and total specific orbital energy. The number of globular clusters for a given dwarf galaxy mass was estimated using Equation 2.14 and a globular cluster mass of $10^5\,M_\odot$ per cluster. The white area shows a region in which the MGC1-fraction is zero for all encounters.

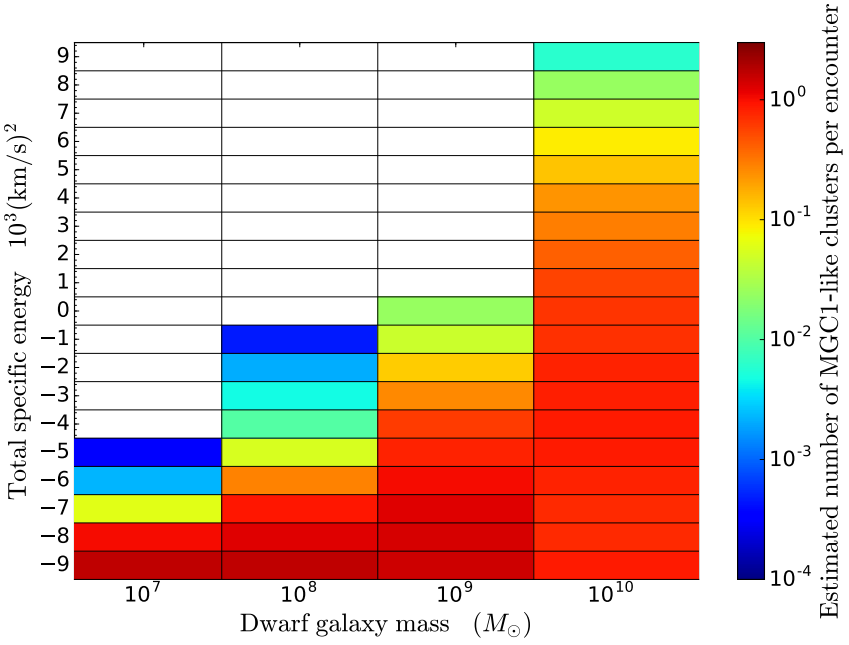

Figure 4.12: Same plot as Figure 4.11 but assuming that each dwarf galaxy hosts 5 globular clusters. This is motivated by observations of the Local Group galaxies. The white area shows a region in which the MGC1-fraction is zero for all encounters.

Chapter 5

Discussion

In this chapter I will discuss in detail what my results imply for the accreted cluster population in a large spiral galaxy, especially focusing on M31 and the globular cluster MGC1. This is to give my work a broader context, provide predictions to compare to observations and discuss where my model does not work. Key points in this chapter are summarised in boxes at the end of sections in order to guide the reader.

5.1 Isotropic distribution in captured globular clusters

I showed in Chapter 4 that the fraction of MGC1-like clusters does not depend on the orbital orientation of the dwarf galaxy, see Figure 4.9. This could imply that the clusters that are tidally stripped away from the dwarf galaxy and captured by M31 do not show a preferred orbital direction, i.e., their orbital direction is isotropically distributed. To show that this is the case for our clusters I investigated whether captured clusters in my simulation had co-rotational or counter-rotational orbits in the M31 galaxy. It should be recognised that, although the model used for the M31 potential has a disc, it is static and thus do not have any rotation, so this statement relies on the assumption that any orbital motion in M31 does not change the orbits of the clusters. Whether this is the case should be investigated in the future, although it is now beyond the scope of this project. I also made the assumption that dwarf galaxies that have close encounters with M31 do not have any preferred incoming direction, that is they approach the main galaxy from isotropically distributed directions. Figure 5.1 shows a histogram of number of clusters, being either on co-rotating or counter-rotating orbits, at different distances from M31 for all captured clusters within 300 kpc at the end of the simulation for all 500 encounters using a dwarf galaxy mass with mass $10^9\,\mathrm{M}_\odot$. The rotation of M31 was chosen such that the normal to the rotating plane is in the direction of the z-axis. The plot clearly shows that there is no preference for obtaining either co-rotating or counter-rotating orbits for the captured clusters. This was the case for all sets of encounters, including looking at only MGC1-like clusters.

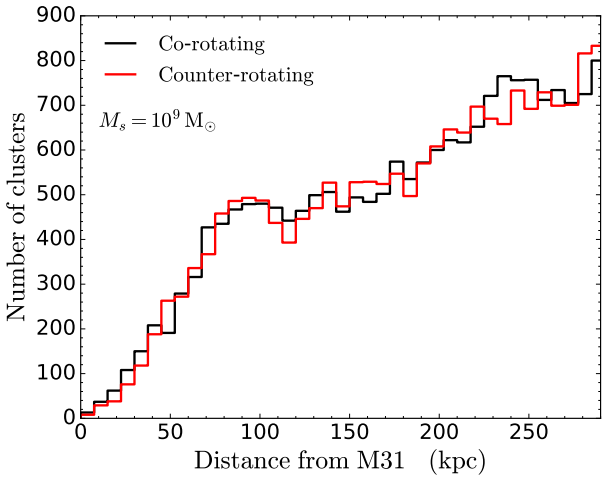

Figure 5.1: Comparison between co-rotating and counter-rotating clusters in the simulated encounters. Plot shows the number of clusters as a function of binned distances for clusters with co-rotating orbits (black line) and counter-rotating orbits (red-line). The rotation-axis of the M31 galaxy was chosen to point in the positive direction to its $z-axis$. Positions and orbital properties were taken at the end of the simulations ($t = 12\,\mathrm{Gyr}$) for all encounters using a $10^9\,\mathrm{M}_\odot$ dwarf galaxy.

If we on the other hand look at clusters that have formed in the M31 galaxy, henceforth referred to as *in-situ* clusters, there should be a trend where these clusters preferably are found on co-rotating orbits. This trend originates from the fact that the material from which they are formed follows the rotation pattern of the host galaxy. Without significant scattering this trend should remain, at least to some degree. I now assume that all the *in-situ* clusters orbit in co-rotation with the M31 rotation curve, in other words, the scalar product between the orbital axis and the z-axis in the M31 reference frame is always positive. In Figure 5.2 I plotted the position of 300 confirmed M31 globular clusters with measured radial velocity. Their position is plotted with respect to the M31 centre which has a right ascension of $\alpha = 0^{\mathrm{h}}42^{\mathrm{m}}44.31^{\mathrm{s}}$ and a declination of $\delta = +41°16'9.4''$ (J2000). The data was obtain from the M31 Revised Bologna Clusters and Candidates Catalog (Version 5), see Galleti et al. (2006) and Galleti et al. (2014). The radial velocities in the data were provided to the catalogue by Galleti et al. (2006). By comparing this to the M31 systematic velocity, $v_{\mathrm{M31}} = 301\,\mathrm{km/s}$, (van der Marel et al., 2012), each mark in the plot could be color-coded with blue if a given cluster is moving toward us with respect to the M31 systematic velocity (Approaching) or red if a cluster is moving away from us with respect to the M31 systematic velocity (Receding). Figure 5.2 also includes the positions and velocities for some of the satellite galaxies (Mateo, 1998) in M31. These were coloured in the same way as the globular clusters.

Following up on the investigation of distinguishing captured and *in-situ* clusters, I divided the observed clusters in Figure 5.2 into two populations. I divided M31 into two different sides, with the split along the z-axis (see dashed line in Figure 5.2). Also note

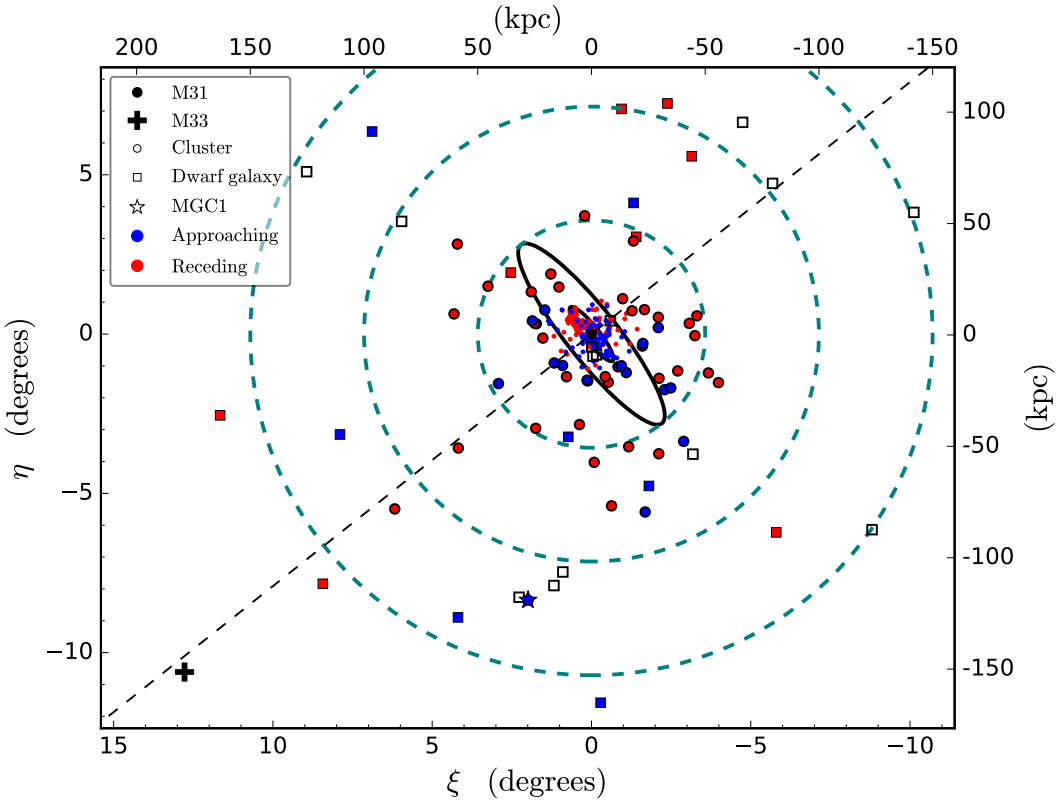

Figure 5.2: Observed relative position of globular clusters and dwarf galaxies to the M31. Marker size for the innermost globular clusters have been reduced for visibility. Objects are coloured in blue if the are approaching in the reference frame of M31 and likewise in red if they are receding. Clusters and galaxies with unknown radial velocity were left unfilled. All the data points come from the M31 Revised Bologna Clusters and Candidates Catalog (Version 5), see Galleti et al. (2006) and Galleti et al. (2014). In the figure I have marked out the positions of M31 (black dot), the M33 galaxy (black cross) and the MGC1 cluster (star coloured according to colour-code). The dashed line shows the split that divides the M31 galaxy along the polar axis ($z - axis$). It should be noted that in this plot the rotational axis of M31 points toward the bottom left. The black ovals show the projection of two circles in the plane of the M31 galaxy with radii of 15 kpc and 50 kpc. The teal dashed lines show circles with projected radii of 50 kpc, 100 kpc and 150 kpc

Table 5.1: The observed number of clusters with known radial velocities in regions surrounding the M31 galaxy, orbiting in either co-rotating orbits (A) or counter-rotating orbits (B) with respect to the rotation of the M31 disc. The three different distance bins correspond to: BIN1; clusters within the ellipse given by the projection of a 15 kpc radius circle. BIN2; clusters between the inner ellipse and an ellipse given by the projection of a 50 kpc radius circle. BIN3; All clusters outside the outer ellipse. For clarification, each bin is plotted in Figure 5.2. If assuming that all *in-situ* clusters have co-rotating orbits then these two groups can be used to determine the number of clusters that have been captured from other galaxies during encounters. Errors are assumed Poisson noise in the data.

Name	Co-rotating	Counter-rotating	Accreted	*In-situ*	Fraction of *in-situ*
	A	B	$2 \cdot$ B	A $-$ B	(A $-$ B)/(A $+$ B)
BIN1	141 ± 11.9	43 ± 6.6	86 ± 13.2	98 ± 13.6	0.533 ± 0.08
BIN2	51 ± 7.1	28 ± 5.3	56 ± 10.6	23 ± 8.9	0.291 ± 0.12
BIN3	22 ± 4.7	15 ± 3.9	30 ± 7.8	7 ± 6.1	0.189 ± 0.17

that the figure includes two black ellipses. These are the projections of two circles with radii of 15 kpc and 50 kpc which lie in the plane of the M31 disc. These two ellipses were used to divided the globular clusters into different populations.

The M31 galaxy has a rotation axis which points toward the bottom left of the plot, i.e., the rotation is receding on the upper left side and approaching on the lower right side of Figure 5.2. This implies that clusters marked as approaching (blue) are on co-rotating orbits on the lower right side of the dashed line and on counter-rotating orbits on the upper left side of the dashed line. The opposite is true for the receding clusters (red).

Now we have a way of determining whether observed clusters are on co-rotating or counter-rotating orbits. To simplify I will refer to the population of co-rotating clusters as A and the population of counter-rotating clusters as B. From the previous argument that the *in-situ* clusters are only found in co-rotating orbits, we can conclude that all counter-rotating clusters are captured. Additionally, globular clusters that have been tidally stripped away from dwarf galaxies and captured by the M31 have orbital-axes that are isotropically distributed thus one should find an equal number of co-rotating and counter-rotating clusters in this population. The total number of captured clusters should therefore be $2 \cdot$ B. The *in-situ* population will be the co-rotating, A, minus the co-rotating in the captured population (which by the previosly mention agrument will be the same as the number of counter-rotating clusters). In conclusion this can be written:

$$\mathrm{A} + \mathrm{B} = \underbrace{2 \cdot \mathrm{B}}_{\text{captured}} + \underbrace{\mathrm{A} - \mathrm{B}}_{in-situ} \tag{5.1}$$

In Table 5.1 I have listed the number of clusters in each of these two populations in the regions marked by the black ellipses.

In Table 5.1 I find the following regarding the population of accreted clusters and the population of *in-situ* clusters. In the outermost region there are a significantly larger

number of accreted clusters. The number of co-rotating clusters and counter-rotating clusters are well within one standard deviation of each other, assuming Poisson noise to be reason for the error. Taking the large error into consideration, we even find that it is possible that there could very will be no *in-situ* cluster in the total outer population. In addition to this one could think that in each encounter there would be a few clusters that are tidally stripped away and donated, especially if the encounters have dwarfs that come very close to the major galaxy. If this is the case then the clusters that are donated would obtain similar orbital properties. Since there is only a few tens of clusters, only a small number of encounters could give the observed population.

In contrast to this I find significantly more clusters on co-rotating orbits in the innermost region. By applying my analysis to this population of clusters I find that at approximately 50% of clusters have formed *in-situ*. This is a significant increase compared to the outermost population. Due to the large number of clusters found in this region of M31 the statistical errors is much smaller. For the region in between 15 kpc and 50 kpc there are a larger number of accreted clusters compared to those formed *in-situ*. Nevertheless, it is interesting that our model suggests that there is a significant fraction of *in-situ* even out to large distances from the centre.

1. The direction of the orbital axis is isotropically distributed, which implies that the accreted cluster population has as many clusters that orbit in counter-rotation with their host rotation curve as it has clusters that orbit in co-rotation. If assuming that clusters formed *in-situ* have orbits which are preferably in co-rotation with the galaxy, then one can separate the population of accreted clusters and *in-situ* clusters based on radial velocity measurements alone.

2. By applying this analysis to the observed globular cluster population in M31 I find that the outer population consists of mainly accreted clusters ($\gtrsim 80\%$), the inner population consists of roughly equal numbers accreted and *in-situ*, and the region in-between is a mix of the two.

5.2 Encounters in which the dwarf galaxy would have been disrupted

For all the simulations in this work we neglected any tidal effect on the dwarf galaxy. Moreover, there are simulated encounters in which the dwarf galaxy goes deep enough in the M31 potential that we would expect the dwarf to take damage due to tidal forces. Therefore, I devote this section to investigate the effects that tidal forces would have on the dwarf galaxy itself, focusing especially on encounters where the dwarf galaxy comes close to the M31 centre.

5.2.1 Numerical test of the analytic tidal radius

In Chapter 2.4 I showed how to derive an analytical formula for the tidal radius, following the method presented in Read et al. (2006). This radius gives a hint as to where our encounters would fail to produce MGC1 due to tidal disruption of the dwarf galaxy. Since preserving the structure dwarf galaxy and later hide it in our encounters is a constraint placed on the simulations due to the absence of tidal features around the observed MGC1 cluster (Mackey et al., 2010a), it is worthwhile to investigate this further. To do so I simulated encounters where I deliberately let the dwarf go deep enough in the M31 potential so that tidal disruption is bound to occur. For the simulations I used a dwarf potential model with $M_s = 10^9\,\mathrm{M}_\odot$ and $r_s = 0.6\,\mathrm{kpc}$.

In order to probe how the dwarf galaxy shape becomes distorted during the encounter I monitored it via tracer particles. For each simulation I used 500 tracer particles which were homogeneously distributed in a sphere centred on the dwarf galaxy potential. The radius of this sphere should cover the luminous structure of the dwarf galaxy. For all simulations used in this section I used a luminous radius, $r_{\mathrm{lum}} = 3\,\mathrm{kpc}$, which is in rough agreement with observed dwarf galaxies, see e.g., Mateo (1998). The velocity of all tracer particles were set in the same way as for the previous simulations, see Section 3.1. This gave the dwarf galaxy a velocity dispersion of $\sim 8.7\,\mathrm{km\,s^{-1}}$ which is in rough agreement with the observations found in similar Local Group dwarfs (see, Mateo, 1998)).

I simulated 70 encounters with dwarf galaxy trajectories that have pericentre distances ranging from $5 - 50\,\mathrm{kpc}$. To mimic the encounters in Chapter 4 I initiated the tracer particles when the dwarf galaxies were at 500 kpc from the M31 centre. All trajectories had this distance as its apocentre since these trajectories would be most likely to tidally disrupt the dwarf. I then integrated the dwarf for the same amount of time as in all previous simulations, that is for 12 Gyr after the first pericentre passage. At the end of each simulation I counted the number of tracer particles located outside $r_{\mathrm{lum}} = 3\,\mathrm{kpc}$ and compared this number to the total number of initiated tracers. This fraction gives a measure of the degree of tidal disruption.

Figure 5.3 shows the degree of tidal disruption (i.e. the fraction of tidally stripped tracer particles) as function of pericentre distance for all 70 encounters. The plot also includes a red line at $\sim 39\,\mathrm{kpc}$ which is the pericentre distance at which the tidal radius is equal to

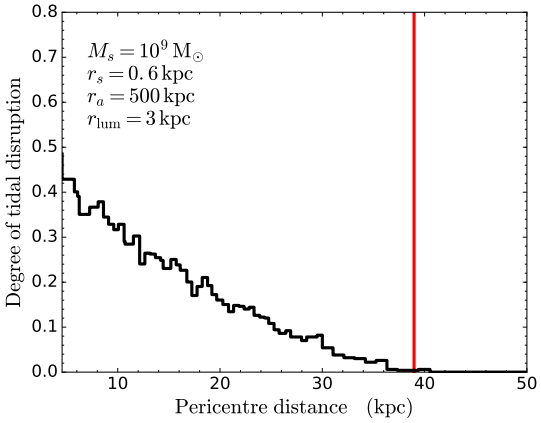

Figure 5.3: Degree of disruption, or equivalently, fraction of tracer particles stripped away from the dwarf during encounters with different pericenters. All encounters were simulated using a $10^9\,\mathrm{M}_\odot$ dwarf galaxy with an apocenter of 500 kpc, which gives the most bound orbital trajectory used in any simulation in Chapter 4. Tracer particles are meant to describe the luminous part of the dwarf galaxy and they are distributed homogeneously in a sphere with radius $r_{\mathrm{lum}} = 3\,\mathrm{kpc}$. Any tracer particle outside this radius after the 12 Gyr in the simulation was considered stripped. The red line shows the pericentre distance that gives a analytical tidal radius, $r_t = r_{\mathrm{lum}}$, using the most pessimistic parameters, $e = 0$ and $\alpha = -1$.

the luminous radius, $r_{\mathrm{lum}} = 3\,\mathrm{kpc}$ for the most pessimistic parameters ($e = 0$ and $\alpha = -1$). We see that for the encounters where the dwarf galaxy goes as deep as 5 kpc from the centre of M31 the degree of tidal disruption is almost 50%. As expected it then decreases as the trajectory pericentre is increased. I find that the pericentre distance outside which we do not expect any stripped tracer particles, calculated analytically from the tidal radius is in very good agreement with the numerical tests. The almost perfect alignment with the onset of tidally stripping tracer particles and this radius is a bit surprising, since the analytical tidal radius assumes point-mass potentials and a circular trajectory for the dwarf galaxy, both of which is not true for the numerical simulations. This gives confidence in the somewhat crude assumptions used in Chapter 2, which simplified the calculations immensely. Note that King (1962) derived an expression for the tidal radius in which these parameters were neglected. This description of the tidal radius might give a good enough approximation, at least for the encounters we investigate here.

It should be noted that the main reason for not disrupting the dwarf galaxy in my simulations is due to the absence of tidal features around the observed MGC1 cluster. However, it is not clear to what degree the dwarf needs to be tidally stripped before we could observe traces of this disruption. In order to investigate this further one would need to produce mock observations of this simulated data and compare the magnitudes of the tidal features to the magnitude limit which is set for the observations of the MGC1-like cluster. There is also the fact that a significant fraction of the MGC1-like clusters

that is produced in my simulations complete several orbits around the M31 galaxy before compared to the observed properties of MGC1. During this time there is a good chance that any tidal features would be washed out and hidden as background stars with no clear association to each other.

The second reason why I am interested in keeping the dwarf galaxy intact during the encounter is because the model used for its potential field is static in all simulations presented so far. This would not be true if there is significant distortion of the dwarf structure during the encounter. Whether this is a problem or not is investigated in the following subsection.

5.2.2 Potential field of a tidally disrupted dwarf galaxy

Here I investigate what effects changes in the potential field due to tidal disruption of the dwarf galaxy can have on the orbits of its stellar population. This is interesting because in all previous simulations the dwarf galaxy had a static potential field. This model is only valid if the shape of the dwarf remains constant throughout the simulation. As I showed previously in this section, this is not necessarily true, since very close encounters lead to significant disruption of the dwarf galaxy. In Section 3.3, where I present results for a particular encounter, we even found that the spatial distribution of the globular cluster population was distorted during closest approach (see Figure 3.3). For this particular encounter, the shape is mostly distorted in the very outer parts of the dwarf galaxy ($\gtrapprox$ 10 kpc), outside which the potential is rather weak, even for the most massive dwarf galaxy. However, this could be an issue for the encounters in which the dwarf galaxy goes very deep into the M31 potential, as this evidently leads to partial tidal disruption (see Section 5.2.1).

If the dwarf is tidally disrupted then we expect the potential field to be disrupted as well. In order to test this I tested different methods, with varying degree of complexity, that dissolved the dwarf potential during the simulations. All methods are briefly summarized in the caption of Figure 5.4. The first method, which is the simplest one is to turn off the potential field of the dwarf galaxy when it is disrupted. In practice, I did this by setting $M_s = 0$ when the dwarf galaxy was assumed to be tidally shredded. I will refer to the simulation using this method as **RUN001**. This approach is very crude since it does not take into account either the gradual stripping of material or the fact that the dwarf might not be completely dissolved during the encounter. For the second method, I took the gradual disruption into account and simply decreased the potential field strength over some amount of time. This was done by setting $M_s = f(t)M_{s,0}$, where $f(t)$ is a factor that is equal to 1 until the disruption, after which it steadily decreases with time. I tested this for two different decrease rates; one simulation f was decreased by 10^{-5} every 0.1 Myr (referred to as **RUN002**), and one simulation in which f was decreased by 10^{-7} every 0.1 Myr (referred to as **RUN003**).

For the two last methods I used somewhat more complex methods. In the simulation that I will refer to as **RUN004** I set the potential scale-length, $r_{\rm plum}$, to increase, effectively making the potential field more shallow, every time a tracer particle was stripped away from

Table 5.2: Initial conditions used for simulating the effects of tidally disrupting a dwarf galaxy. These initial conditions where estimated to describe the trajectory of the hypothesised progenitor of the Andromeda Southern Stream. Data is the same as that given in Geehan et al. (2006).

x_0 (kpc)	y_0 (kpc)	z_0 (kpc)	$v_{x,0}$ ($\mathrm{km\,s^{-1}}$)	$v_{y,0}$ ($\mathrm{km\,s^{-1}}$)	$v_{z,0}$ ($\mathrm{km\,s^{-1}}$)
14.2	−33.2	60	−50	86.02	−158

the dwarf. By keeping track of tidally stripped particles I set the program to only increase r_{plum} once for every stripped particle. This imitated how the potential field changed every time the dwarf galaxy came close to the M31, which is when tracer particles are stripped away. For each particle that was stripped away I increased r_{plum} by 0.01. In the last method I calculated the median of the distances between the dwarf galaxy and all the tracer particles, with which I scaled r_{plum}. The median should give the half-mass radius of the luminous cluster which is related to the scale-length according to $r_{\mathrm{plum}} = 1.3^{-1} r_{1/2}$. In order to give a correct scaling I included an additional constant to make the potential fit the initial potential field. This gave $r_{plum,0} = 0.6\,\mathrm{kpc} = constant \cdot 1.3^{-1} r_{1/2})$, where an initial value of $r_{1/2} = 1.5\,\mathrm{kpc}$ gave $r_{\mathrm{plum}} = 3.502 r_{1/2}\,\mathrm{kpc}$. The simulation using this method is referred to as **RUN005**.

To test this method I wanted to use a realistic encounter in which the dwarf galaxy is known to be dissolved, and therefore choose to work with the hypothesised progenitor of the Large Southern Stream in the M31 galaxy. Details for this progenitor are discussed in detail by Fardal et al. (2006). Since I am only interested in testing the effect I used simple approximated initial conditions from Font et al. (2006b) (see also Geehan et al. (2006)). These are listed in Table 5.2. In each simulation I initiated 500 tracer particles homogeneously in a sphere with 3 kpc radius, similarly to the simulations discussed in Section 5.2.1. In each simulation I integrated the trajectory of the dwarf for 12 Gyr after its first pericentre passage resulting in a total of 5 pericentre passages.

Figure 5.4 shows the time evolution of the potential field in all simulations. Note that I also include one simulation (RUN000) in which I let the potential remain static for comparison. RUN001, RUN002 and RUN003 behave as they are expected to behave given the simplicity of the method that changes their potential. More interesting are the potential fields in RUN004 and RUN005. Focusing first on RUN004, we see how the potential field reduces periodically in strength at different times. The times at which the potential field reduces corresponds to the times when the dwarf galaxy passes the pericentre in its orbit. This behaviour is what is to be expected since this is the point during the encounter when a significant fraction of the tracer particles are tidally stripped away.

Contrary to all other simulations RUN005 appears to increase at the start of the simulation and stays around the same value for the remainder of the simulation with a small scatter. The fact that it rises initially implies that the factor of 3.502 that was used to scale the scalelength did not fit the model perfectly. It stays roughly the same throughout

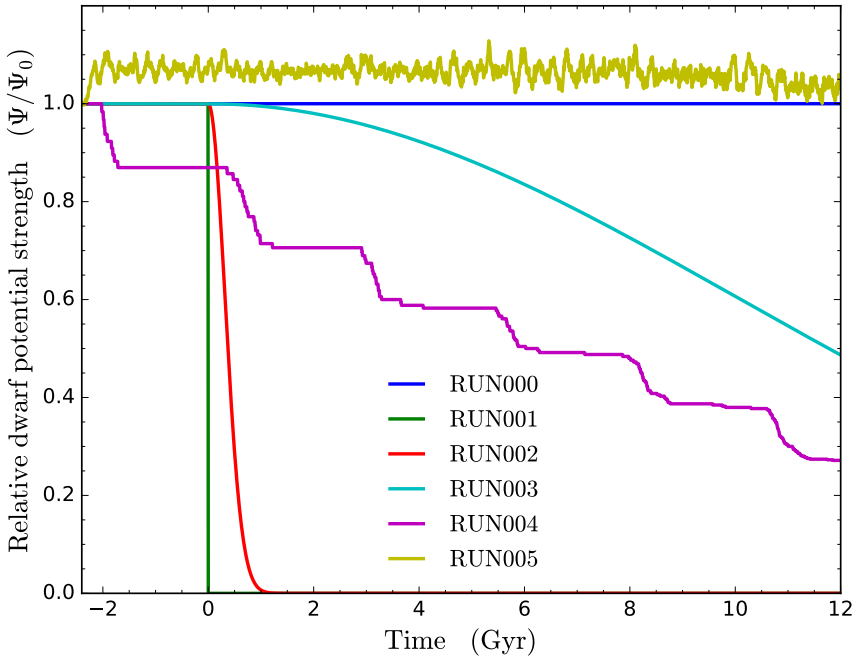

Figure 5.4: Relative potential field strength of the dwarf galaxy as function of time. Plot shows six different simulations in which the potential was dissolved with different methods to imitate a tidal disruption during the encounter. The six methods work in the following way: In RUN000, the potential remains constant; The potential in RUN001 is set to zero at $t = 0$; RUN002 has a potential that is scaled with a factor $f(t)$, which after $t = 0$ decreases with $\Delta f = 10^{-5}$ every 0.5 Myr; RUN003 is similar to RUN002, however $\Delta f = 10^{-7}$; the potential in RUN004 has a scale-length which increases with 0.01 every time a tracer particle move outside 3 kpc; RUN005 has a potential which has a scale-length that is scaled to the median distance of all tracer particles.

the simulation, although particles are tidally stripped from the dwarf. Further investigation revealed that this is because it is the outer most tracer particles that are stripped during the encounters leaving the innermost tracer particles on rather stable orbits in the dwarf galaxy. The median distance of all particles would be largely unaffected throughout the simulation given that the particle at the median distance is within the distance from the dwarf where tidal forces are too small to affect it. This is evidently the case for this simulation, giving the dwarf an almost constant potential field.

The purpose of this discussion is to investigate how the trajectories of objects initially bound to the dwarf are affected by disrupting the dwarf potential field. Because tidally stripped objects have trajectories which are primarily determined by the M31 potential the expected outcome is that objects that are stripped away have similar orbits, although the number of objects that are stripped away should change drastically.

Figure 5.5 shows SVT plots for all 6 simulations, where the grey lines show tracer particles that have been tidally stripped at some point during the encounter, i.e., they move outside the luminous radius $r_{\rm lum} = 3\,{\rm kpc}$. The blue lines show particles that are retained by the dwarf galaxy for the entire simulation. RUN001 and RUN002 which have the most abrupt diffusions of their potential fields lose all tracer particles in the simulation. This is to be expected since the gravitational force that works against the centrifugal force that the particles have due to their orbital motion in the dwarf suddenly goes to zero, throwing all particles away from the dwarf. However the trajectories of the tracer particles still follow the initial trajectory of the dwarf to a large extent. The distribution of the tracer particle has a similar width compared to the simulation with a static potential, however, the distribution is rather smooth compared to the static potential that has a large peak at the dwarf galaxy position, which of course is because a majority of the clusters are retained in this simulation.

In simulations RUN003 and RUN004 we find similar distributions at the end of the simulation. The reason for this is found in Figure 5.4, where we see that their potentials have a similar decrease, regardless of the higher complexity of the method in RUN004. It could be worthwhile to use a similar method to the one used in RUN004 to estimate the decrease of the potential field, and then use this to fit $f(t)$. Since the latter method has a significantly simpler implementation and is more efficient in a computational sense, this could be the more attractive method. Nevertheless, it should be noted that this is one specific encounter and for a more violent disruption the method used in RUN004 could prove to give more realistic results.

Finally, we focus on the last method, i.e., simulation RUN005. Since RUN005 has a potential field which is roughly constant it behaves similarly to the static potential. We find a similar distribution of tracer particles in the two cases, as can be seen if comparing the top left plot and the lower right plot in Figure 5.5. However, similarly to RUN004, this method would probably be more realistic in a more violent disruption event, where the particle at median distance is strongly affected by the tidal forces. It should also be noted that this method is the only one which in some sense is based in physical assumptions about the shape of the dwarf galaxy.

As a last comment I would like to address the fact that all potential models used here

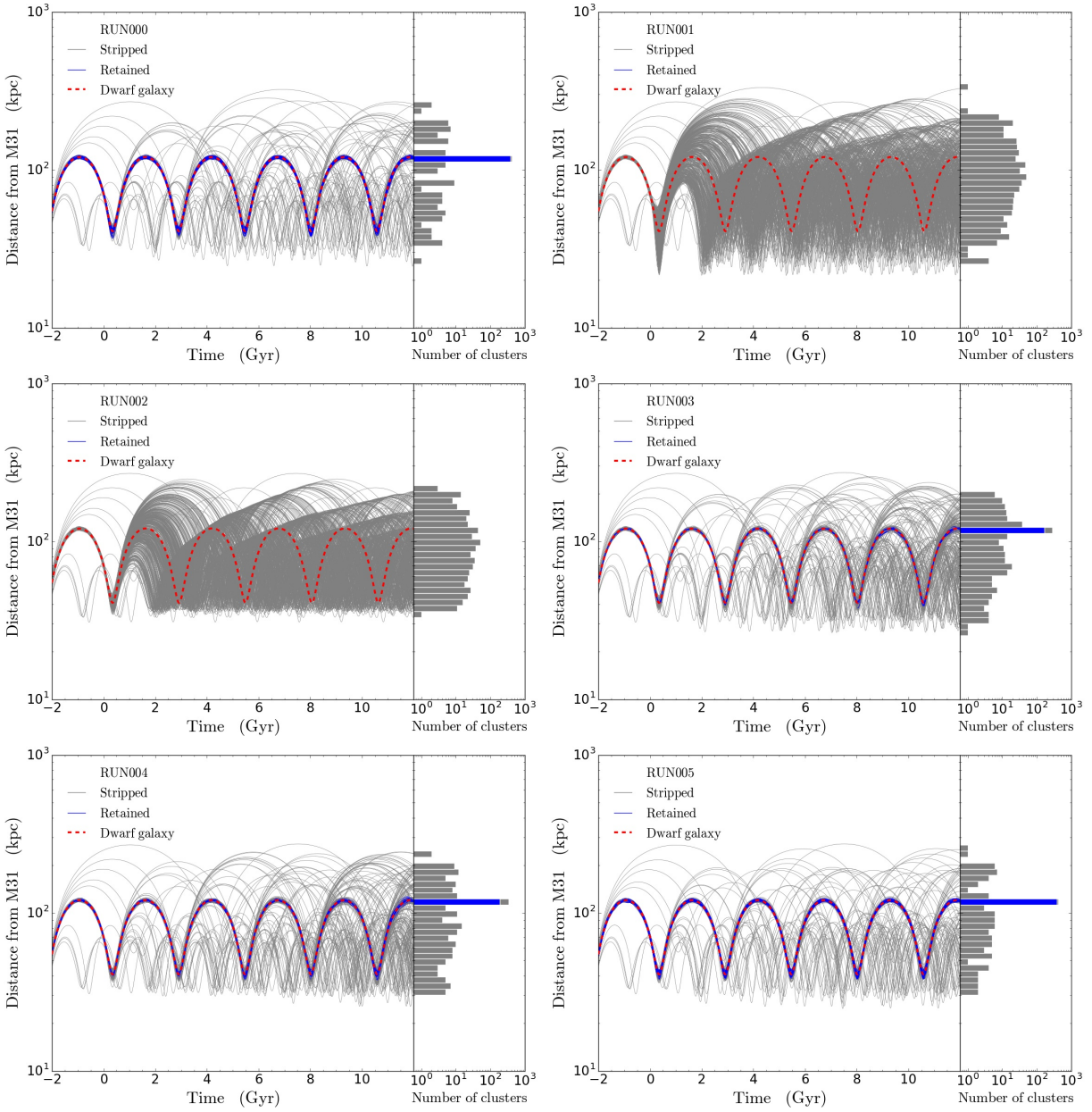

Figure 5.5: Distance from M31 as function of time (left sub-plots) and distribution at the end of the simulation (right sub-plots) for the 6 different simulations with different methods for dissolving the dwarf galaxy potential. Each sub-plot is the same as the *SVT*-plot shown in Figure 3.2, however the colour-coding differs. The dwarf trajectory is given by the red dashed line, tracer particles that have been tidally stripped away are shown by grey lines and the tracer particles that are retained in the dwarf at $t = 12\,\mathrm{Gyr}$ (end of simulation) are shown with blue lines. The methods used to dissolved the dwarf galaxy potentials are summarised in the caption of Figure 5.4. The order of the sub-plots are: RUN000 (upper left), RUN001 (upper right), RUN002 (centre left), RUN003 (centre right), RUN004 (bottom left), RUN005 (bottom right).

are spherically symmetric. Tidal forces are well known for giving the disrupted object elongated shapes, hence this assumption is not valid for most encounters where disruption is prominent. To properly investigate these kinds of effects one should resort to a pure N-body model used for both stellar matter and dark matter. Several studies where this has been the focus can be found in the literature, see e.g., Read et al. (2006); Jiang & Binney (2000); Sanders et al. (2018); Fardal et al. (2006).

1. The distance from the M31 galaxy at which tracer-particles initiated within 3 kpc of the dwarf galaxy start to be stripped away is $\sim$ 40 kpc for the most pessimistic parameters selected from the same initial conditions as in my simulations. The tidal stripping of the dwarf galaxy is only partial and does not exceed 20% until the dwarf is within $\sim$ 20 kpc.

2. Although all my simulations include static dwarf galaxy potentials, even in the cases where the dwarf is tidally stripped to some degree, additional test where the potential was varied in response to the tidal disruption shows that the trajectories of the cluster do not change significantly, although a larger number of clusters are tidally stripped away in a disrupted dwarf galaxy.

5.3 Tidal stripping away as a mechanism to populate the outer M31 system

In this section I will investigate how the data that I obtain in my simulations compare to the observed cluster population in M31. The observed globular cluster population in M31 was extensively studied by several previous works, where a main contributor has been the Pan-Andromeda Archaeological Survey[1] (PAndAS) (see, e.g., Huxor et al., 2014; McConnachie et al., 2009, 2008; Ibata et al., 2007; Martin et al., 2006, and references therein). As already mentioned, evidence suggests that a significant fraction of globular clusters in large galaxies are accreted from other galaxies. This is especially the case for the outer globular cluster population. Mackey et al. (2010b) investigated in their work spatial correlation between globular clusters and tidal features that could be distinguished in the field surrounding the M31 galaxy. They focused on objects at projected radii of $\sim$ 30 kpc from the M31 centre and found a striking association between the mentioned objects, estimating that the probability of this being due to random alignment was below 1% using Monte Carlo simulations. Although, they concluded that the implication of this study is strong evidence for a largely accreted outer globular cluster population, there are distant clusters which are seemingly isolated. One cluster in particular is MGC1, studied

[1] http://www.astro.uvic.ca/ alan/PANDAS/Home.html

by Mackey et al. (2010a), which shows no sign of tidal features. In fact, contrary to this, its extremely extended outer structure indicates that it has evolved in isolation for a large fraction of the age of the Universe.

This work has focused on simulating encounters where a dwarf galaxy has a fly-by encounter with M31, after which it leaves the system, without much interaction. If globular clusters are tidally stripped away in such encounters it provides a natural procedure to populate galaxies with isolated globular clusters, such as MGC1. Assuming that such an encounter was responsible for the donation of MGC1 I here estimate the number of fly-by encounters that M31 was likely to have throughout its history and how other clusters, especially those closer to M31 compared to MGC1, could have been left in similar encounters. It should be noted that in my simulations I consider M31 to be isolated thus neglecting any effects from other large galaxies in the Local Group, such as M33 or the Milky Way. It could very well be the case that MGC1 was produced in a major merger event and that I in this study severely over-estimate the number of dwarf galaxy fly-by encounters. I discuss this in more detail in a later section.

In order to assess the number of fly-by encounters I made some assumptions about the encounters. As was briefly mentioned in Chapter 4, it is not clear how many globular clusters a dwarf galaxy hosts (see Figure 4.10), especially in the early Universe. For this work I will make the crude assumption that every dwarf galaxy initially hosts 5 globular clusters. The lack of evidence supporting this assumption should be considered to be a serious caveat for my analysis. Further investigation would be necessary to assess the error that this could imply for my work, but for now I urge the reader to consider this issue. Furthermore, I address the fact that reproducing a cluster at exactly the orbital distance of MGC1 is very unlikely in a numerical simulation. However, I am interested in obtaining at least one cluster on an extremely wide orbit, and then see how my encounters have populated the inner regions (within 150 kpc) of M31 with tidally stripped away clusters. Therefore, I consider clusters located between $150 - 250$ kpc at the end of my simulation to be present-day MGC1-like for this analysis. Note that this is not the same definition as the one for an MGC1-like cluster in Chapter 4.

As a starting point of this analysis I estimated what number of simulated encounters I required in order to find at least one cluster located at a radial distance of $150 - 250$ kpc away from the M31 galaxy. I did this by randomly selecting encounters from all of my 2000 simulations, each of which included trajectories of 1000 globular clusters initially bound to the dwarf galaxy. For a given encounter I randomly selected 5 globular clusters and counted the number of clusters in the $150 - 250$ kpc region. I counted the total number of encounters, N, that I needed to select before I found one cluster in the mentioned region, that is a present-day MGC1-like cluster. This selection procedure is what I will refer to as a realization. To obtain a statistical estimate of N I simulated 10^5 realisations, thus obtaining the distribution of N.

The distribution of N is shown in Figure 5.6. I find that the distribution has a peak around $N = 20$. To estimate the exact maximum of this distribution I fitted it to a scaled

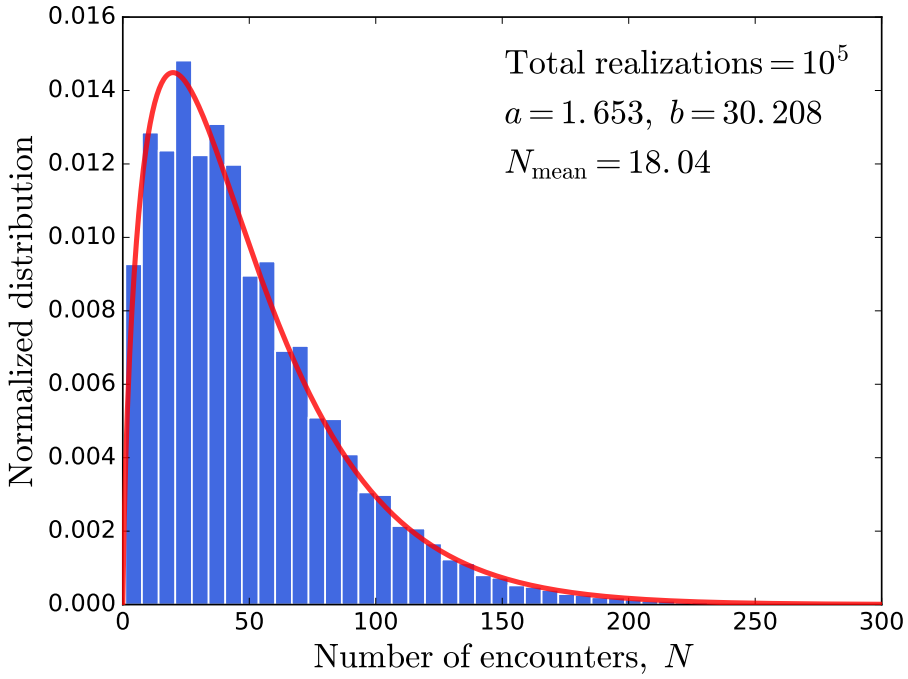

Figure 5.6: The number of fly-by encounters that we expect M31 to have had with dwarf galaxies given that they leave behind at least one globular cluster at roughly the present-day orbital distance of MGC1. The plot shows the distribution of number of encounters that I need to draw from our simulated data in order to find one globular cluster between 150 and 250 kpc, given that each dwarf galaxy hosts 5 globular clusters initially. The distribution was generated drawing 10^5 different realizations from my data. To find the maximum of the distribution I fitted a *Gamma*-distribution to the data (see Equation 5.2). The maximum was consistently found around 20 encounters.

Gamma-distribution,

$$f(x|a,b) = \frac{b^a}{\Gamma(a)} x^{a-1} \exp(-bx), \tag{5.2}$$

where $a > 0$ and $b > 0$ are fitting parameters and $\Gamma(n) = (n-1)!$ is the *Gamma*-function. The reason for choosing this specific function is because of it being very versatile in its shape. The mean if the distribution is $N_{\rm mean} \approx 20$. The distribution rises very quickly to this maximum and then decreases smoothly, going to zero at roughly $N = 200$. The fact that there is a non-zero probability of having 200 encounters without a single one producing an present-day MGC1-like clusters shows that there is a large variability in the outcome of a given encounter.

To relate $N_{\rm max} \approx 20$ to my previous results it indicates that the average likelihood of producing a present-day MGC1-like cluster in an encounter is $\sim 5\%$, compared to if I do not consider any specific time at which the cluster should have an orbital distance of 200 kpc, which gave a likelihood of finding an MGC1-like cluster ranging from $0 - 50\%$ depending on the mass of the dwarf galaxy and its total specific energy. Note that in this analysis all encounters are equally likely to be selected, thus if one is interested in a specific set of encounters, the results in Chapter 4 would be more useful. However, by investigating observations to assess how likely different encounters are to happen this analysis could be improved to give a more physically motivated estimate of the likelihood of producing MGC1-like clusters. A further improvement could be to randomly select a time at which one estimates the number of clusters in different orbital positions, which would imply that there is no preferred time in the history of the Universe when the encounter will happen.

Finally, I will look at how my simulations contribute to the M31 galaxy populations with clusters other than the ones which are MGC1-like. To do this I generated maps of the M31 cluster populations by selecting N encounters from my simulations from which I randomly selected 5 clusters. The position of these 5 clusters at $t = 12$ Gyr were plotted on the projected sky in which M31 lies, as in Figure 5.2. Figure 5.7 shows these maps for $N = 20$ (upper left), $N = 50$ (upper right), $N = 100$ (lower left) and $N = 300$ (lower right). I find that my encounters do not contribute the outer globular cluster population to any significant extent, considering the very large number of globular clusters observed there (see Figure 5.2). In fact most globular clusters are retained in the dwarf and many of those that are stripped away are placed at significantly larger distances, even outside what could be considered the vicinity of M31 (> 300 kpc). However, an interesting feature is that for each present-day MGC1-like cluster I seem to obtain at least a few clusters on orbits within 150 kpc. These clusters should, by our design, show no association to tidal features as this is one of the constraints I set on my encounters. It could be worthwhile to investigate what fraction of globular clusters in M31 lacks association to such features.

The fact that I am not able to reproduce a cluster population which resembles that of the observed outer M31 cluster population indicates that there is some assumption about my encounters which does not apply to the M31 encounters. As a first step I investigated if there is some way to select encounters in such a way that my simulations can reproduce the observations. This could hint at what the typical initial conditions would be for the

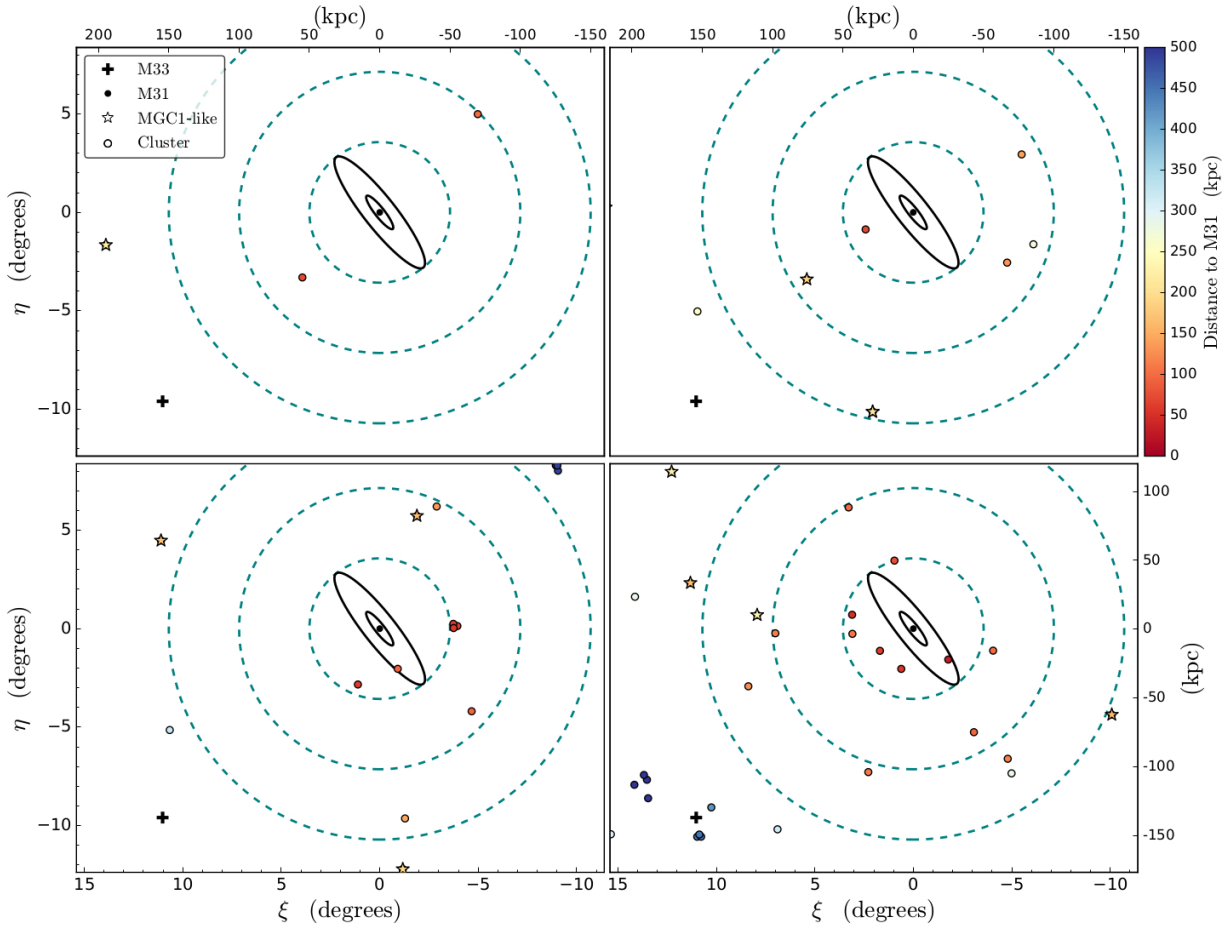

Figure 5.7: Projected spatial distribution of simulated globular clusters around the M31 galaxy. The plots have the same scale as Figure 5.2. The teal dashed lines show projected radii of 50 kpc, 100 kpc and 150 kpc. The different plots shows clusters selected from a total number of 20 (upper left), 50 (upper right), 100 (bottom left) and 300 (bottom right) encounters. The globular clusters were selected by randomly selecting 5 globular clusters from different encounters in the entire data set of the 5×10^6 simulated encounters. Each globular cluster has been colour coded according to distance from M31 in order to see whether a given cluster belongs to M31 or only appears to do so due to projection.

dwarf galaxy trajectories that have encounters with M31. I wish to remind the reader that by assuming that I can pick encounters uniformly in my entire sample implies the following assumptions:

- M31 had the same number of encounters with dwarf galaxies of mass $10^7\,M_\odot$, $10^8\,M_\odot$, $10^9\,M_\odot$ and $10^{10}\,M_\odot$.
- All encounters start 500 kpc away from the M31 galaxy with a globular cluster population which is homogeneously distributed in a shell surrounding the dwarf. The inner radius of this shell ensures that they are not tidally stripped by the dwarf galaxy, and the outer radius of the shell ensures that they are not tidally stripped away before the dwarf galaxy comes within 200 kpc of M31, thus letting them randomize before the encounter.
- The specific total orbital energy of the dwarf galaxy trajectories is uniformly distributed between 0 and the energy given by the potential field at the starting point (i.e., zero kinetic energy), with the exception of the $10^{10}\,M_\odot$ for which hyperbolic trajectories are allowed (see Figure 4.5) for range. This implies that the apocentre of the dwarf trajectory is always larger than or equal to 500 kpc.
- The dwarf galaxy trajectories have pericentres which are homogeneously distributed in a 120 kpc radius sphere centred on the M31 galaxy. This implies that the distribution of radial distances from the M31 galaxy for all pericentres scales as r^2.
- The dwarf galaxy potential is static throughout the entire encounter.
- All dwarf galaxies are at the pericentre of their trajectory at $t = 0$ after which the simulation runs for 12 Gyr.

In order to assess whether there is a selection function for my encounters that changes the aforementioned distributions in initial conditions I counted the number of clusters that each simulated encounter leaves behind in each of the bins stated in Table 5.1. I then plotted the normalized number of clusters in BIN1 versus the normalized number of clusters in BIN2, see Figure 5.8. In the same plot I also include the position of the observed clusters population in this space. I find that all my encounters are located to the bottom left of the observed mark. This implies that there is no way to select encounters from my simulations in a way that reproduces the observed population, unless I select a negative number of encounters, which would not be physical. A more rigorous description of why this is true can be found in Appendix C. In conclusion I find that there is something in my assumptions that inhibits my encounters from populating the inner region of M31 with globular clusters to the extent that is observed today. I believe that the major cause for this is that I do not allow dwarf galaxy trajectories with apocentres closer than 500 kpc of the M31 centre. Another factor that contributes to this is the lack of friction in my simulations, which would tighten the orbits of captured clusters. Nevertheless, I have found that given the assumptions about my initial conditions I am able to produce globular clusters that

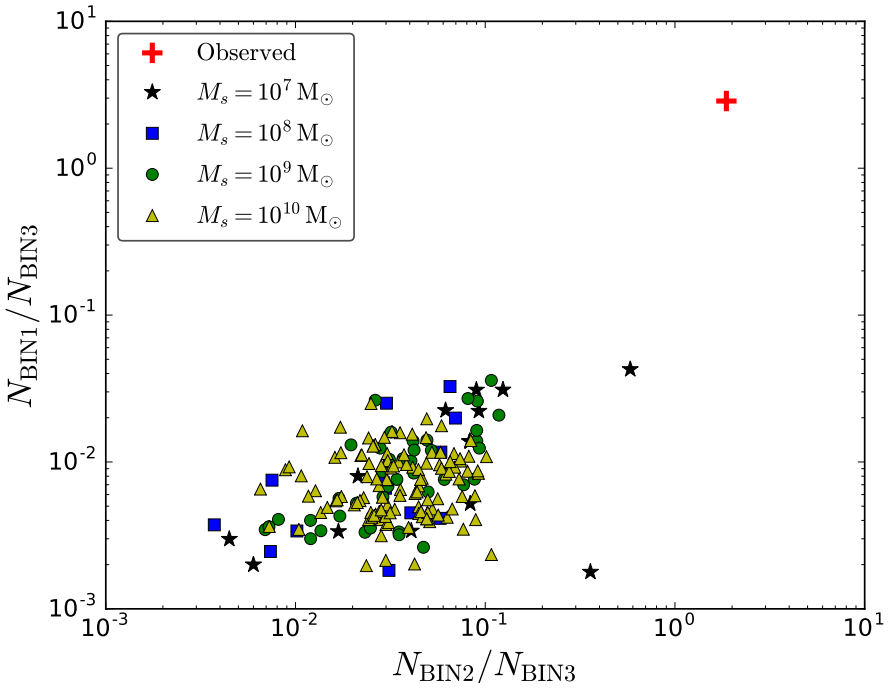

Figure 5.8: The number of clusters in BIN1 divided by the number of clusters in BIN3 versus the number of clusters in BIN2 divided by the number of clusters in BIN3 for all encounters in my simulations, marked according to figure legend. The red plus-sign marks where the quantity for the observed M31 globular cluster population lies in the space. The fact that all my encounters lie to the bottom left of the red plus-sign implies that there is no selection function that can be used to obtain the observed distribution of captured clusters in M31 from my simulated encounters.

are similar to MGC1, which has been the main focus of this work. In an upcoming work I will focus on reproducing the entire observed population of globular clusters in M31.

1. By randomly selecting 5 clusters in randomly drawn encounters from all my simulations and counting the number of clusters that are roughly located at the orbital distance of MGC1 I find that the most likely number of encounters required to obtain at least one MGC1-like cluster is ~ 20.

2. For every MGC1-like cluster that I find in my simulations I expect there to by 1-2 globular clusters with orbits inside the orbital region of MGC1. If assuming that MGC1 was produced by an encounter that resembles those in my simulations, then this implies that there should be of order a few globular clusters in the outer globular cluster population of M31 that show no signs of tidal features.

3. By comparing the globular clusters captured within three different observed regions of M31 (see black ellipses in Figure 5.2) in my simulations to the number of clusters observed in each of these regions I find that there is no way to select encounters in such a way that I reproduce the observed population.

4. From the key point above I can conclude that either my simulation miss important physics or my set of encounters is not a good representation of the encounters which produced the entire accreted globular cluster population of M31.

5.4 The Local Group

In this work I have focused solely on the M31 galaxy, assuming that it has been isolated during the simulated encounters, with the obvious exception of the incoming dwarf galaxy. However, in my simulations I consider dwarf galaxies that have orbital distances on Mpc scale, even going as far as having trajectories unbound from the M31 galaxy. Therefore, it is meaningful, and even essential for completeness, to discuss the implications of other significant objects in the Local Group. Additionally, it is also of interest to investigate the observed characteristics of Local Group dwarf galaxies, as these can help constrain both the number of encounters that M31 is likely to have had with now distant dwarf galaxies and also how the observed dwarf galaxies compare to the initial conditions used in this work.

That encounters between dwarf galaxies and large spiral galaxies occur at all is by now an established fact. Firstly, in the successful ΛCDM-cosmology regime, merger events and hierarchical assembly of large galaxies is evident, especially in the early epochs of a

galaxy's evolution, see, e.g., Bullock & Johnston (2005); Abadi et al. (2006); Font et al. (2006b). Secondly, there is a lot of observational evidence of present day mergers and encounters with dwarf galaxies; for M31 there is strong evidence from tidal streams (see, e.g., Fardal et al., 2006; Mackey et al., 2010b), and for our own Galaxy which is currently merging with the Sagittarius dwarf galaxy, (see, e.g., Ibata et al., 1995; Forbes et al., 2004, and references therein). Furthermore, several works have linked the outer globular cluster population to these type of encounters, see Searle & Zinn (1978); Mackey et al. (2010b).

Simulations of galaxy formation and evolution can provide an estimate of the merger history of galaxies like M31. Renaud et al. (2017) looked at the evolution of a Milky Way-like galaxy in a cosmological context, by investigating a simulation of a region zoomed in on the galaxy. Renaud et al. (2017) specifically investigated the origin of globular clusters, both from *in-situ* formation and accretion. Their simulation shows a rich merger history with roughly 50 mergers occurring before redshift $z = 0.5$. Most mergers that contribute significantly to the mass of the galaxy end at $z = 1$, and at this point there are several smaller galaxies orbiting the major galaxy, most of which are accreted before $z = 0.5$. This provides a significant sample of encounters from which globular clusters are accreted. Looking specifically at globular clusters Renaud et al. (2017) find that the vast majority of clusters beyond $\approx 30\,\mathrm{kpc}$ have been accreted.

Buck et al. (2018) investigated how the properties of dwarf galaxies depend on their galactic environment. They look at a population of dwarf galaxies that currently reside outside the virial radius of the host galaxy but did at some point venture inside of it. They use the term *backsplash* galaxies for this population. Through simulations they determine certain characteristics that *backsplash* galaxies would have and by comparing to observations they find that up to 50% of all isolated Local Group galaxies belong in this population. Two specific remote dwarf galaxies in their sample are And XXVIII and And XVIII, both of which are satellites of M31. Based on their analysis they find that these two galaxies have a likelihood of interactions with M31 at 91% and 38% respectively.

Finally, I would like to discuss an alternative progenitor to the MGC1 cluster and possibly major contributor to the outer globular cluster population in M31, namely the spiral galaxy M33. M33 is the third largest galaxy in the Local Group with a halo mass of $4.3 \times 10^{11}\,M_{\odot}$ (Corbelli et al., 2014), and it lies in close proximity to M31 (separation of $\approx 200\,\mathrm{kpc}$, see, e.g., Semczuk et al. (2018) or marked position in Figure 5.2. The measured radial velocity and proper motions of M33 (van der Marel et al., 2012; Brunthaler et al., 2005) not only suggest a bound orbit around M31, but also indicate a previous encounter between the two. Other authors have investigated other signs of a past encounters, e.g. a neural hydrogen bridge between the two galaxies (Lockman et al., 2012) or signs of tidally induced morphology in the M33 galaxy that can be explained by a past encounter (Semczuk et al., 2018). Cockcroft et al. (2011) conducted a search for outer globular clusters in the M33 galaxy but found a remarkable absence of such objects, especially in comparison to the globular cluster population of M31 and the Milky Way. They suggested two possible evolutionary histories that could cause this; either M33 had a dramatically less active accretion history or its outer globular cluster population was heavily stripped away in an encounter with M31. If the latter is the case then in accordance with what I

find in my simulations these clusters would obtain fairly wide orbits. This might very well be the origin of MGC1. To investigate this further one could look for chemical similarities between the two.

Chapter 6

Summary and conclusions

In this chapter I summarise the entire work of this project. The chapter starts with a very brief summary of the main idea and how I conducted the investigation of this idea. The main conclusions that I found are listed in a box following this brief summary, as a convenience for the reader. Note that some of the conclusions in this list are mentioned again in this chapter. This list serves as a quick comprehensive summary of all conclusions throughout the thesis.

Following this is a detailed summary intended for readers who are interested but does not intend to read the entire thesis. Here I go through and summarise each step of this project in more detail, as well as list the major results that led to the conclusions. In this chapter I intentionally repeat large parts of the work, and it is intended to be read by readers who have not read the entire work.

Brief summary

In this work I have investigated how captured globular clusters that have been tidally stripped away from dwarf galaxies contribute to the outer globular cluster population of the M31 galaxy. I have specifically explored whether this is a viable mechanism to produce a cluster similar to the observed cluster MGC1. MGC1 is a globular cluster which orbits the M31 galaxy at an extremely large orbital distance (200 kpc), in fact it is one of the most isolated globular clusters known in the Local Group.

To test this idea I developed a program that simulated encounters between M31 and dwarf galaxies. In these simulations I included a population of globular clusters for which I tracked the trajectories. For each encounter I determined the likelihood that a globular cluster in the dwarf galaxy ended up in one of the following groups: captured by M31, retained by the dwarf galaxy, unbound from the system and captured on an orbit similar to MGC1. Throughout the report these are referred to as Captured, Retained, Unbound and MGC1-like respectively. The program is available for download at GitHub[1] together with a README file which describes how the program is used.

[1] https://github.com/ericander/Galactic-Potential-Particle-Integrator

I find the following conclusions in my work:

1. It is possible that MGC1 was captured on a wide orbit after being tidally stripped away from a dwarf galaxy when the dwarf had an encounter with M31.

2. Furthermore, this is possible in encounters where no significant damage is caused to either the dwarf or M31. In the simulated encounters the dwarf galaxy leaves the M31 system in all practical senses, thus leaving no visible trace of the encounter. In fact, the tidal strain on the dwarf galaxy is minuscule, which should imply that any tidal features that could be associated to the captured globular cluster would be rare.

3. I find that the outcome of an encounter can vary significantly. Low mass ($10^7\,\mathrm{M}_\odot$) in-falling dwarf galaxies, with a total specific orbital energy around $-10^4\,(\mathrm{km/s})^2$, can leave as much as 50% of their cluster population on MGC1-like orbits. Larger mass galaxies can leave behind MGC1-like clusters even for hyperbolic encounters, although rarely more than 30% of their population.

4. If I select encounters uniformly from all my simulations I find that the expected number of encounters required before finding one MGC1-like cluster is approximately 20.

5. However, we should remember that 20 encounters is only a subset of all the encounters that one expects for a large spiral galaxy throughout its evolution (see, e.g., Renaud et al., 2017).

6. Although I can produce clusters that resemble MGC1, my encounters do not leave clusters on tighter orbits. In order to produce these there would have to be encounters where the dwarf has a tighter orbit, however, this is likely to tidally strip the dwarf galaxy thus leaving visible traces of the encounter.

7. This implies that the range of encounters that I simulate populate the outer regions, while the remaining encounters populate the inner regions.

8. Because the inner region hosts many more clusters I also predict that the encounters which I do not consider (e.g., mergers or tight satellite orbits) will be more numerous and/or leave many more globular clusters on tighter orbits.

Detailed summary of the simulations

In order to investigate to what extent donation of globular clusters from dwarf galaxies contribute to the overall population of globular clusters in the M31 galaxy, I used numerical simulations of encounters. In each encounter the dwarf galaxy was populated with 1000 globular clusters on random orbits. The trajectories were simulated for 12 Gyr after the first dwarf galaxy pericentre passage. At the end of the simulation the number of Captured, Retained, Unbound and MGC1-like clusters were counted and compared to the total number of clusters. This fraction was interpreted as the likelihood of placing a cluster in any of the mentioned populations for each encounter.

In order to determine the evolution of each of the simulated objects trajectories, the numerical scheme computed the acceleration at the position of a given object through the first derivative of the background potential field, see Section 2.3 for details. This background potential was given by the sum of two potentials, one for the M31 galaxy and one for the dwarf galaxy. The centre of the M31 galaxy defined the origin of the simulated space which was defined using a Cartesian coordinate system with x, y being in the plane of the M31 disc and z perpendicular to this plane.

The M31 potential was modelled as a static, axisymmetric, three-component potential field fitted to the observed data of M31. The three component model used for M31 in all simulations included a spherically symmetric Hernquist potential for the central bulge, an axisymmetric Miyamoto-Nagai potential for the galactic disc and a Navarro-Frenk-White potential for the extended halo. The model parameters that were used to approximate the observed M31 potential are listed in Table 2.1 on page 21. These parameters were estimated by Geehan et al. (2006) through a fitting procedure to the observed rotational velocity of M31. It should be noted that Geehan et al. (2006) originally used an exponential profile for their disc model, whereas I used a Miyamoto-Nagai model which was fitted to their model parameters. The reason for this is that the Miyamoto-Nagai is more efficiently calculated numerically. A comparison between the two is found in Figure 2.1 on page 22. *Note that in Chapter 2.1 I describe two potential models, although I only use one of the models in my simulations. Both these potentials are however implemented in the program as a convenience for the potential user.*

For the dwarf galaxy I used a spherically symmetric potential modelled with the Plummer model. This model is easily modified to fit dwarf galaxies of different mass and core-size, which was a crucial quality since different dwarf galaxies were to be simulated and compared to each other. The position of the dwarf galaxy defined the origin of its potential field. The model parameters I chose to work with were selected based on observed Local Group dwarf galaxies. I tested four different dwarf galaxy sizes with masses $10^7\,M_\odot$, $10^8\,M_\odot$, $10^9\,M_\odot$ and $10^{10}\,M_\odot$. The exact parameters are listed in Table 2.1 on page 21 and can be viewed in comparison to observed data (Mateo, 1998) in Figure 4.3 on page 46.

The globular cluster population was modelled as test-particles which were integrated in the total potential field of the two galaxies included in a given simulation. I intentionally left out interactions between globular clusters in my simulations so that in each encounter

I could look at the outcome of many different globular cluster trajectories. This likelihood could afterwards be compared to the observed number of globular clusters in a given dwarf to predict the expected number of clusters that a dwarf would contribute with to the different populations in the event of an encounter.

A detailed description of how a given encounter was set up is given in Sections 4.1 (dwarf galaxy initial conditions) and 3.1 (globular clusters initial conditions). Following is a compressed summary of how a simulation was set up and how the results were interpreted.

Summary of how each encounter was investigated:

1. A dwarf galaxy was initiated by randomly selecting a position and velocity for the dwarf at its pericentre passage. The selection was done in a way that provides uniformly distributed total specific orbital energy in a given range, a spatial distribution with no preferred position (i.e., radial distribution proportional to r^2) and an isotropic distribution in orbital orientation (no preferred incoming direction).

2. After placing the dwarf galaxy at the pericentre position, the trajectory was integrated backwards to a distance of 500 kpc away from the M31 centre, after which its trajectory was reversed, and re-simulated with a population of globular clusters.

3. A sample of 1000 globular clusters was initiated with homogeneous spatial distribution and circular orbits in the dwarf galaxy.

4. The encounter was simulated until 12 Gyr has passed after first pericentre passage, providing a simulation which lasts for approximately the age of the Universe.

5. The resulting globular cluster populations were first divided into 3 different groups: clusters that where captured by M31 during the encounter (Captured); clusters that remained bound to the dwarf galaxy (Retained); clusters that escaped both M31 and the dwarf (Unbound).

6. A fourth population, which is a sub-population of Captured clusters, were defined and referred to as MGC1-like clusters. These were clusters that after the encounter crossed a radial distance of 200 kpc at least two times (the second crossing was used to ensure that they where not spatially associated to the dwarf galaxy).

7. The number of clusters in each population was compared to the total number of initiated clusters to give the likelihood for a specific encounter to place a cluster in one of the mentioned populations.

Summary of the main results

In Chapter 3 I investigate the outcome of a specific encounter in order to provide understanding of a typical encounter in the range of encounters that were analysed in Chapter 4. The encounter simulated a $10^9\,M_\odot$ dwarf galaxy trajectory with a pericentre distance of $\sim 80\,\mathrm{kpc}$ and apocentre distance of $\sim 800\,\mathrm{kpc}$. For this encounter I find that roughly 20% of the cluster population end up on MGC1-like orbits. That this fraction is significantly larger than zero, and the encounter is distant enough to ensure no visible damage to the luminous structure of either the dwarf or M31, provides evidence for the main hypothesis of this work. Thus I can answer the question posed in the introduction:

It is possible that MGC1 is a cluster that was tidally stripped away from a dwarf galaxy during an encounter and captured on a wide orbit around M31, in such a way that the encounter does not tidally strip the dwarf galaxy or cause visible damage to the M31 galaxy.

In addition to proving the main hypothesis I find the following for a specific encounter: the captured clusters have a tendency to be on prograde orbits in the dwarf galaxy; this tendency is even clearer for clusters that are captured on orbits that significantly differ from the trajectory of the dwarf galaxy.

To expand the investigation I looked for general trends among encounter properties and the likelihood of contributing to the different globular cluster populations, see Chapter 4. In this chapter I divided a large sample of simulations into sets of encounters. In each set of encounters the mass of the dwarf galaxy was kept constant and the specific total orbital energy was constrained to a certain range, see Table 4.2 on page 48. Additionally, for a given set of encounters all initial globular cluster populations are identical, however, each dwarf galaxy trajectory was unique. A list of assumptions that were used for all the simulations can be found on page 77.

I find the the following trends in my sets of encounters: For all sets of encounters I find a clear correlation between total specific energy and fraction of MGC1-like clusters. The main result showing this can be found in Figure 4.4 on page 50 (see also Figure 4.5 in page 51 for additional encounters with $10^{10}\,M_\odot$ dwarf galaxies on hyperbolic trajectories). If looking at a specific set of encounters, i.e., encounter with a specific mass and given range of total specific energies, I find a linear relationship between MGC1-like fraction and pericentre distance, see Figures 4.6 and 4.7, on pages 53 and 54. This relationship can be tied to the linear relationship between pericentre distance and tidal radius in its analytical expression (see Equation 2.44 on page 29).

Lastly, I find that for all my encounters the fraction of MGC1-like clusters has no dependence on orbital direction of the dwarf trajectory, see Figure 4.9 on page 57, although the potential is not spherically symmetric. Additionally, the orbits of the captured clusters

do not seem to organise themselves in any systematic way due to the non-spherical shape of the potential. This is believed to be because of the large pericentre distances of the cluster orbits, compared to the extent of the disc.

The main result of the thesis is shown in Figures 4.11 and 4.12 on page 59. These plots show the number of MGC1-like clusters that one expects to find per encounter for all sets of encounters that were simulated for this work, based on assumptions about the average number of globular cluster hosted by the dwarf before the encounter. Figure 4.11 assumes that the number of clusters can be determined from the average mass of a globular cluster ($10^5\,\mathrm{M}_\odot$) and the fraction of mass expected to find in globular clusters; a relation derived empirically from observations, see Equation 2.14 on page 19. The results based on this globular cluster distribution show the following:

1. The contribution to MGC1-like clusters is strongly dominated by donation from dwarf galaxies with a mass of $10^{10}\,\mathrm{M}_\odot$.

2. For this mass, the number of clusters does not vary significantly for different total specific energy bins, with the exception of a steep decrease at total specific energies larger than $\sim 4 \times 10^3\,(\mathrm{km/s})^2$ (this would correspond to a velocity at infinity of $\sim 63\,\mathrm{km/s}$, i.e, a hyperbolic trajectory).

3. I find that each encounter contributes roughly one MGC1-like cluster per encounter.

There is a well known discrepancy in the cluster mass and galaxy mass relation for dwarf galaxies. This discrepancy has been controversial in the literature (see Renaud, 2018, for a review) and is also clear if looking at Local Group galaxies, see Figure 4.10 on page 57. To take this into account I included a plot (see Figure 4.12 on page 59) similar to the plot mentioned above but instead assuming 5 globular clusters per dwarf galaxy. This assumption is a very crude estimate based on what I find in the Local Group. From this I find the following:

1. MGC1 most likely originates from a low mass dwarf galaxy with a specific total energy of $\sim -9 \times 10^3\,(\mathrm{km/s})^2$ (corresponding to a maximum apocentre distance of $\sim 500\,\mathrm{kpc}$).

2. For these encounters one could expect as many as a few MGC1-like clusters per encounter.

Scientific implications, shortcomings and future work

Based on the results found, I did an investigation into some of the scientific implications of my work. The first implication that I find is based on the result that the fraction of MGC1-like cluster does not depend on dwarf galaxy orbital orientation. By following up on

this I found that the orbital orientation of the captured clusters is isotropically distributed, even after several billion years of evolution. This implies an equal number of co-rotating and counter-rotating clusters in an accreted population, see Figure 5.1 on page 61. If assuming that the clusters that form *in-situ* have orbits that are preferably oriented in the rotational direction of the galaxy, that is they are co-rotating, one can in a simple manner separate accreted and *in-situ* clusters in a large galaxy by radial velocity and positional measurements alone, see Equation 5.1. I applied this method to the observed clusters in M31 and found that the outermost globular clusters consist of $\sim 80\%$ accreted clusters (up to 100% to within approximately one sigma), see Table 5.1 on page 63. The innermost cluster population consists of an equal number of accreted versus *in-situ* clusters, while the region in between is a mix of the two.

In an analysis where I investigated the problem with having a static dwarf galaxy, I implemented various methods that dissolved the dwarf galaxy potential in the event of a tidal disruption. By investigating the trajectories of tracer particles in an encounter where I intentionally disrupted dwarf galaxies, I found that although significantly more particles were tidally stripped away from a disrupted dwarf (especially from extremely violent disruptions), the width of their radial distribution did not change significantly. The details of this analysis can be found in Section 5.2.

Lastly, I investigated the likely number of the presented types of encounters that M31 would have had in the past given that we observe only one MGC1-like cluster today. Note that an additional assumption for this analysis is that MGC1 was in fact produced in one of the encounters I simulated. Figure 5.6 on page 74 shows the main result of this analysis in which we find that M31 likely had ~ 20 encounters, assuming that MGC1 came from one of them.

Following up on this I investigated how my encounter contributed to the overall population of globular clusters in M31. I find that my simulation significantly underestimates the number of globular clusters on orbits interior to that of MGC1, in fact for every present-day MGC1-like cluster I contribute with only a few other clusters to the M31 globular cluster population. This is in strong disagreement with the observed cluster population, compare Figures 5.7 and Figure 5.2 on pages 76 and 62. Furthermore, I find that no selection function can be applied to my simulations that would relieve this issue, see Figure 5.8 on page 78.

The major shortcoming of this work is the lack of clusters on orbits tighter than that of MGC1, which is where the majority of accreted clusters reside, it implies that the set of encounters that were simulated is not a good representation of all the encounters that we expect M31 to have had in the past. This mainly arises because I do not allow my dwarf galaxies to be tidally stripped. I will elaborate on this in the following paragraph.

Firstly, I do not consider any encounters where the dwarf galaxy is either accreted by M31 or left on a tight orbit around M31. This is in conflict with the observations of the satellite galaxies in M31. I therefore urge the reader to remember that this work only looks at the outcome of a specific set of dwarf galaxy encounters. Secondly, I do not consider

any dissipation for any of my cluster orbits, which could lead to tighter orbits after the several billion years of evolution. Dynamical friction is one effect that has been known to cause dissipation of orbital energy in globular clusters moving in a field of stars, see e.g., Chandrasekhar & von Neumann (1942). Lastly, I assume that the M31 galaxy evolved in isolation. This is not true if for example M33 had a close encounter with M31 in the past, which would like stir up the outer globular cluster population and it could even have donated some fraction of its globular cluster population to M31.

In a planned follow up work on this project, I will consider solutions to all the aforementioned shortcomings. The first focus of this would be to change the initial conditions to allow for a broader range of encounters, especially focusing on trying to reproduce the entire globular cluster population by including dwarf galaxies on tighter orbits.

Acknowledgements

First and foremost I wish to express my gratitude to my supervisor Melvyn B. Davies. It has been a pleasure to work with him and the help he has provided exceeded my every expectation. I believe that I have learned something new from every conversation that I have had with him these past years.

I would also like to thank Vassily Kornienko, both for help with peer-review and interesting conversations that has helped me develop my skills at communicating my work. Conversations with him always brings new ideas and questions to be pondered.

I wish to thank Neige Frankel, with whom I shared office with during the first part of my MSc work. I have met no one who rivals her enthusiasm for science and I believe our early morning conversation has contributed a lot to this work.

I want to acknowledge Oscar Agertz and Louise Howes for making corrections to this work, as well as contributing with ideas for future work related to this project.

Lastly, I wish to thank everyone working at Lund Observatory, especially those I have had regular conversations with. Many of these conversations has led to improvements of my thesis. It also made my time here at the department interesting and very pleasant. This led me to dedicate lots of effort into successfully pursuing a PhD position at Lund Observatory, which has given me the chance to stay here at least another four years.

Bibliography

Abadi, M. G., Navarro, J. F., & Steinmetz, M. 2006, MNRAS, 365, 747

Alves-Brito, A., Forbes, D. A., Mendel, J. T., Hau, G. K. T., & Murphy, M. T. 2009, MNRAS, 395, L34

Bajkova, A. & Bobylev, V. 2017, Open Astronomy, 26, 72

Baumgardt, H., Parmentier, G., Gieles, M., & Vesperini, E. 2010, MNRAS, 401, 1832

Bekki, K., Couch, W. J., Drinkwater, M. J., & Gregg, M. D. 2001, ApJ, 557, L39

Binney, J. 1981, MNRAS, 196, 455

Binney, J. & Tremaine, S. 1987, Galactic dynamics

Braun, R. 1991, ApJ, 372, 54

Brodie, J. P. & Strader, J. 2006, ARA&A, 44, 193

Broeils, A. H. 1992, A&A, 256, 19

Brunthaler, A., Reid, M. J., Falcke, H., Greenhill, L. J., & Henkel, C. 2005, Science, 307, 1440

Buck, T., Macciò, A. V., Dutton, A. A., Obreja, A., & Frings, J. 2018, ArXiv e-prints [arXiv:1804.04667]

Bullock, J. S. & Johnston, K. V. 2005, ApJ, 635, 931

Cash, J. R. & Karp, A. H. 1990, ACM Trans. Math. Softw., 16, 201

Chandrasekhar, S. & von Neumann, J. 1942, ApJ, 95, 489

Chapman, S. C., Peñarrubia, J., Ibata, R., et al. 2007, ApJ, 662, L79

Cockcroft, R., Harris, W. E., Ferguson, A. M. N., et al. 2011, ApJ, 730, 112

Colucci, J. E. & Bernstein, R. A. 2011, in EAS Publications Series, Vol. 48, EAS Publications Series, ed. M. Koleva, P. Prugniel, & I. Vauglin, 275–278

Corbelli, E., Thilker, D., Zibetti, S., Giovanardi, C., & Salucci, P. 2014, A&A, 572, A23

Côté, P., Marzke, R. O., & West, M. J. 1998, ApJ, 501, 554

de Swart, J. G., Bertone, G., & van Dongen, J. 2017, Nature Astronomy, 1, 0059

de Vaucouleurs, G. 1948, Annales d'Astrophysique, 11, 247

di Tullio Zinn, G. & Zinn, R. 2013, AJ, 145, 50

Eggleton, P. P. 1983, ApJ, 268, 368

Euler, L. 1769, Institutionum calculi integralis, Institutionum calculi integralis No. v. 2 (imp. Acad. imp. Saènt.)

Evans, N. W., Wilkinson, M. I., Guhathakurta, P., Grebel, E. K., & Vogt, S. S. 2000, ApJ, 540, L9

Fardal, M. A., Babul, A., Geehan, J. J., & Guhathakurta, P. 2006, MNRAS, 366, 1012

Font, A. S., Johnston, K. V., Bullock, J. S., & Robertson, B. E. 2006a, ApJ, 638, 585

Font, A. S., Johnston, K. V., Guhathakurta, P., Majewski, S. R., & Rich, R. M. 2006b, AJ, 131, 1436

Forbes, D. A., Pastorello, N., Romanowsky, A. J., et al. 2015, MNRAS, 452, 1045

Forbes, D. A., Strader, J., & Brodie, J. P. 2004, AJ, 127, 3394

Freeman, K. C. 1970, ApJ, 160, 811

Galleti, S., Bellazzini, M., Federici, L., Buzzoni, A., & Fusi Pecci, F. 2007, A&A, 471, 127

Galleti, S., Federici, L., Bellazzini, M., Buzzoni, A., & Fusi Pecci, F. 2006, A&A, 456, 985

Galleti, S., Federici, L., Bellazzini, M., et al. 2014, VizieR Online Data Catalog, 5143

Geehan, J. J., Fardal, M. A., Babul, A., & Guhathakurta, P. 2006, MNRAS, 366, 996

Genina, A., Benítez-Llambay, A., Frenk, C. S., et al. 2018, MNRAS, 474, 1398

Harris, W. E. 1996, AJ, 112, 1487

Harris, W. E., Blakeslee, J. P., & Harris, G. L. H. 2017, ApJ, 836, 67

Hernquist, L. 1990, ApJ, 356, 359

Huxor, A. P., Mackey, A. D., Ferguson, A. M. N., et al. 2014, MNRAS, 442, 2165

Ibata, R., Martin, N. F., Irwin, M., et al. 2007, ApJ, 671, 1591

Ibata, R. A., Gilmore, G., & Irwin, M. J. 1995, MNRAS, 277, 781

Jiang, I.-G. & Binney, J. 2000, MNRAS, 314, 468

Kent, S. M. 1989, PASP, 101, 489

King, I. 1962, AJ, 67, 471

Kochanek, C. S. 1996, ApJ, 457, 228

Laevens, B. P. M., Martin, N. F., Sesar, B., et al. 2014, ApJ, 786, L3

Lane, H. J. 1870, American Journal of Science, 50, 57

Layden, A. C. & Sarajedini, A. 2000, AJ, 119, 1760

Leaman, R., VandenBerg, D. A., & Mendel, J. T. 2013, MNRAS, 436, 122

Little, B. & Tremaine, S. 1987, ApJ, 320, 493

Lockman, F. J., Free, N. L., & Shields, J. C. 2012, AJ, 144, 52

Mackey, A. D., Ferguson, A. M. N., Irwin, M. J., et al. 2010a, MNRAS, 401, 533

Mackey, A. D., Huxor, A. P., Ferguson, A. M. N., et al. 2010b, ApJ, 717, L11

Martin, N. F., Ibata, R. A., Irwin, M. J., et al. 2006, MNRAS, 371, 1983

Mateo, M. L. 1998, ARA&A, 36, 435

McConnachie, A. W., Huxor, A., Martin, N. F., et al. 2008, ApJ, 688

McConnachie, A. W., Irwin, M. J., Ferguson, A. M. N., et al. 2005, MNRAS, 356, 979

McConnachie, A. W., Irwin, M. J., Ibata, R. A., et al. 2009, Nature, 461, 66

Miyamoto, M. & Nagai, R. 1975, PASJ, 27, 533

Muller, M. E. 1959, Commun. ACM, 2, 19

Navarro, J. F., Frenk, C. S., & White, S. D. M. 1996, ApJ, 462, 563

Plummer, H. C. 1911, MNRAS, 71, 460

Read, J. I., Wilkinson, M. I., Evans, N. W., Gilmore, G., & Kleyna, J. T. 2006, MNRAS, 366, 429

Renaud, F. 2018, ArXiv e-prints [arXiv:1801.04278]

Renaud, F., Agertz, O., & Gieles, M. 2017, MNRAS, 465, 3622

Rubin, V. C., Ford, Jr., W. K., & Thonnard, N. 1980, ApJ, 238, 471

Runge, C. 1895, Mathematische Annalen, 46, 167

Sanders, J. L., Evans, N. W., & Dehnen, W. 2018, ArXiv e-prints [arXiv:1802.09537]

Searle, L. & Zinn, R. 1978, ApJ, 225, 357

Semczuk, M., Lokas, E. L., Salomon, J.-B., Athanassoula, E., & D'Onghia, E. 2018, ArXiv e-prints [arXiv:1804.04536]

Siegel, M. H., Dotter, A., Majewski, S. R., et al. 2007, ApJ, 667, L57

Simien, F., Pellet, A., Monnet, G., et al. 1978, A&A, 67, 73

Spitler, L. R. & Forbes, D. A. 2009, MNRAS, 392, L1

Springel, V., Frenk, C. S., & White, S. D. M. 2006, Nature, 440, 1137

Strader, J., Smith, G. H., Larsen, S., Brodie, J. P., & Huchra, J. P. 2009, AJ, 138, 547

Tonini, C. 2013, ApJ, 762, 39

van den Bergh, S. 2006, AJ, 131, 304

van der Marel, R. P., Fardal, M., Besla, G., et al. 2012, ApJ, 753, 8

Walterbos, R. A. M. & Kennicutt, Jr., R. C. 1987, A&AS, 69, 311

Watkins, L. L., Evans, N. W., & An, J. H. 2010, MNRAS, 406, 264

Wilkinson, M. I. & Evans, N. W. 1999, MNRAS, 310, 645

Zepf, S. E. & Ashman, K. M. 1993, MNRAS, 264, 611

Appendix A

Equation of motion in a rotating frame

We are interested in finding the equation of motion for a body in a coordinate system which rotates at angular velocity $\boldsymbol{\Omega}(t)$. This is most easily attained using Lagrangian mechanics (see, e.g., Binney & Tremaine, 1987). Consider a body located at Cartesian coordinates $\boldsymbol{x}$ in a rotating frame such that the inertial velocity $\boldsymbol{v}_i$ of the body is

$$\boldsymbol{v}_i = \frac{\mathrm{d}\boldsymbol{x}}{\mathrm{d}t} + \boldsymbol{\Omega} \times \boldsymbol{x}. \tag{1}$$

Note that this is completely analogues with the system described in Figure 2.2. The Lagrangian, per unit mass, for such a body is given by

$$\mathcal{L} \equiv \frac{1}{2}\boldsymbol{v}_i^2 - \Phi(\boldsymbol{x}) = \frac{1}{2}(\dot{\boldsymbol{x}} + \boldsymbol{\Omega} \times \boldsymbol{x})^2 - \Phi(\boldsymbol{x}) = \frac{1}{2}\sum_{i=1}^{3}(\dot{x}_i + e_{ijk}\Omega_j x_k)^2 - \Phi(x_i), \tag{2}$$

where $\Omega(\boldsymbol{x})$ is the potential field at $\boldsymbol{x}$ and indexing represents Cartesian coordinate with directions given by e. Using the Lagrange equation,

$$\frac{\mathrm{d}}{\mathrm{d}t}\left(\frac{\partial \mathcal{L}}{\partial \dot{x_\alpha}}\right) - \frac{\partial \mathcal{L}}{\partial x_\alpha} = 0, \tag{3}$$

we can find the equation of motion as

$$\frac{\mathrm{d}}{\mathrm{d}t}\left(\dot{x}_i + e_{ijk}\Omega_j x_k\right)\delta_{i\alpha} - (\dot{x}_i + e_{ijk}\Omega_j x_k)e_{ipq}\Omega_p\delta_{q\alpha} - \frac{\partial}{\partial x_\alpha}\Phi(x_i) = 0, \tag{4}$$

where δ is the Dirac delta function. Writing this in vector form gives a clearer interpretation of the equation,

$$\ddot{\boldsymbol{x}} + \dot{\boldsymbol{\Omega}} \times \boldsymbol{x} + 2\boldsymbol{\Omega} \times \dot{x} + \boldsymbol{\Omega} \times (\boldsymbol{\Omega} \times \boldsymbol{x}) + \nabla\Phi(\boldsymbol{x}) = 0. \tag{5}$$

We see that the equation of motion consists three terms plus a term for acceleration. The physical interpretations of these three terms are inertial force of rotation, Coriolis force and centrifugal force respectively.

Appendix B

The Cash-Karp Runge-Kutta scheme

The Cash-Karp method belongs to a family of so called adaptive Runge-Kutta methods. Similarly to plain Runge-Kutta, these methods solve ordinary differential equations by single-step evaluation of the function at a later state. Runge-Kutta methods are characteristic for evaluating the function at intermediate steps in a way that increases the precision of the final step. The general form of the explicit Runge-Kutta for a first-order ordinary differential equation, $f(x, y) = y$, with an initial condition $y(x_0) = y_0$, is given by

$$y_{n+1} = y_n + \mathrm{d}x \cdot \sum_{i=1}^{s} b_i k_i, \tag{6}$$

where

$$\begin{aligned} k_1 &= f(x_n, y_n), \\ k_2 &= f(x + c_2 \mathrm{d}x, y_n + \mathrm{d}x(a_{21} k_1)), \\ k_3 &= f(x + c_3 \mathrm{d}x, y_n + \mathrm{d}x(a_{31} k_1 + a_{32} k_2)) \\ &\vdots \\ k_s &= f(x + c_s \mathrm{d}x, y_n + \mathrm{d}x(a_{s1} k_1 + a_{s2} k_2 + \cdots + a_{s,s-1} k_{s-1})). \end{aligned}$$

The number of stages of any particular Runge-Kutta method is denoted by the index s and each method will have its own specific set of constants a, b, c for which values must be provided. These needs to be given according to a_{ij} for $1 \leq j \leq i \leq s$, while b_i for $i = 1, 2, .., s$ and

$$c_i = \sum_{j_1}^{i-1} a_{ij}, \quad i = 2, ..., s. \tag{7}$$

The value for step-size, $\mathrm{d}x$, will decide the local truncation error of the evaluation depending on the order, p, for any particular Runge-Kutta according to $\mathcal{O}(\mathrm{d}x^{p+1})$. For order up to $p = 4$ the value for s is the same as the order. The Runge-Kutta is considered an open problem, yet many known methods already exist, where the most common are the Euler method (Euler, 1769) and the fourth-order Runge-Kutta (also referred to as RK4)(Runge, 1895).

The Cash-Karp method is a special Runge-Kutta in which the function is evaluated both with an 4th order and a 5th order method. The two estimates are then compared with each other to provide a precise estimate of the evaluation error, according to

$$e_{n+1} = y_{n+1} - y^*_{n+1} = \mathrm{d}x \sum_{i=1}^{s} (b_i - b^*_i) k_i, \tag{8}$$

where the function and constants marked with the $*$ are those of the lower order evaluation. Since the $\mathcal{O}$ term provide the scaling of the local truncation error we can readily obtain

an estimate of how the error would change if we changed the step-size. If we take a step with step-size $\mathrm{d}x_0$ and this gives an error Δ_0 then the step-size which would yield a desired error Δ_1 is given by

$$\mathrm{d}x_1 = \mathrm{d}x_0 \left| \frac{\Delta_1}{\Delta_0} \right|^{0.2}. \tag{9}$$

This formula can thus be used to either decrease the step-size to increase the accuracy, or to increase the step-size if the accuracy is larger then required. This can then be used to adapt the step-size given a desired accuracy.

This step-size evaluation is used by any adaptive Runge-Kutta method. Cash & Karp (1990) developed a method of this kind which successfully evaluates a fourth and fifth order evaluation through only 6 function evaluations. The method is readily available from Equation 6 by using these constants:

$$\begin{array}{c|ccccc} 0 & & & & & \\ c_2 & a_{21} & & & & \\ c_3 & a_{31} & a_{32} & & & \\ \vdots & & \ddots & & & \\ c_s & a_{s1} & a_{s2} & \cdots & a_{s,s-1} & \\ \hline & b_1 & b_2 & \cdots & b_{s-1} & b_s \\ & b_1^* & b_2^* & \cdots & b_{s-1}^* & b_s^* \end{array}$$

$$=$$

$$\begin{array}{c|cccccc} 0 & & & & & & \\ 1/5 & 1/5 & & & & & \\ 3/10 & 3/40 & 9/40 & & & & \\ 3/5 & 3/10 & -9/10 & 6/5 & & & \\ 1 & -11/54 & 5/2 & -70/27 & 35/27 & & \\ 7/8 & 1631/55296 & 175/512 & 575/13824 & 44275/110592 & 253/4096 & \\ \hline & 37/378 & 0 & 250/621 & 125/594 & 0 & 512/1771 \\ & 2825/27648 & 0 & 18575/48384 & 13525/55296 & 277/14336 & 1/4 \end{array}$$

Appendix C

Proof that selection functions cannot alleviate the issue with reproducing the observed globular cluster population of M31

Consider the following set of variables:

A_i is the number of captured clusters in BIN1 for encounter i
B_i is the number of captured clusters in BIN2 for encounter i
C_i is the number of captured clusters in BIN3 for encounter i
A_{obs} is the observed number of clusters in BIN1
B_{obs} is the observed number of clusters in BIN2
C_{obs} is the observed number of clusters in BIN3

where the bins, denoted BIN1, BIN2 and BIN3, are the same as in Figure 5.2.

We assume that the observed population was produced by a set of encounters, i.e. the numbers A_{obs}, B_{obs} and C_{obs} are sums of A_i, B_i and C_i for a specific set of encounters i. Now assume that there exists selection function a and b such that I can select different encounters i, from the entire set of simulations executed for this work. We can scale the number of clusters in each bin against each other to find the two dimensional space in which all possible configurations can be placed, see Figure 5.8. Taking this into consideration we can write the following expression:

$$\sum_{i=0}^{N} a\frac{A_i}{C_i} + \sum_{i=0}^{N} b\frac{B_i}{C_i} = \frac{A_{\text{obs}}}{C_{\text{obs}}} + \frac{B_{\text{obs}}}{C_{\text{obs}}}, \tag{10}$$

where N is the total number of simulations that we can select from.

For physical reasons we cannot contribute with a negative number of clusters for any encounter, i.e., A_i, B_i, C_i, A_{obs}, B_{obs} and C_{obs} are all positive numbers. Additionally we cannot allow for the selection of a negative number of encounters with our selection functions, i.e, a and b must be positive or zero for all encounters. From these constraint we can derive the following conditions from Equation 10:

$$\sum_{i=0}^{N} a\frac{A_i}{C_i} - \frac{A_{\text{obs}}}{C_{\text{obs}}} + \sum_{i=0}^{N} b\frac{B_i}{C_i} - \frac{B_{\text{obs}}}{C_{\text{obs}}} = 0$$
$$\Leftrightarrow$$
$$\begin{aligned} \sum_{i=0}^{N} a\frac{A_i}{C_i} - \frac{A_{\text{obs}}}{C_{\text{obs}}} &\geq 0 \\ \sum_{i=0}^{N} a\frac{B_i}{C_i} - \frac{B_{\text{obs}}}{C_{\text{obs}}} &\geq 0 \end{aligned} \tag{11}$$

Furthermore this implies that for at least some encounters i we require

$$\begin{aligned} \frac{A_i}{C_i} &\geq \frac{A_{\rm obs}}{C_{\rm obs}} \\ \frac{B_i}{C_i} &\geq \frac{B_{\rm obs}}{C_{\rm obs}} \end{aligned} \tag{12}$$

However, in Figure 5.8 we find that this is not true, thus I have proved that clever selection of encounters will not produce a population of globular clusters which resembles that which is observed in M31.